DEVELOPMENT AND CHARACTERIZATION OF BISPECIFIC PROTEINS FOR TARGETED DRUG AND GENE DELIVERY SYSTEMS

Christina L. Parker

A dissertation submitted to the faculty at the University of North Carolina at Chapel Hill in partial fulfillment of the requirements for the degree of Doctor of Philosophy in the Department of Pharmaceutical Sciences in the School of Pharmacy.

Chapel Hill
2019

Approved by:

Samuel K. Lai

Shawn Hingtgen

Michael Jay

Brian Kuhlman

Rihe Liu

ABSTRACT

Christina L. Parker: Development and characterization of bispecific proteins for targeted drug and gene delivery systems
(Under the direction of Samuel K. Lai)

Active targeting, based on antibodies and molecules that direct effector molecules and carriers to specific cells and tissues, have been extensively investigated in various therapeutic applications including cancer and gene therapy. Indeed, antibodies or antibody fragments are often covalently coupled onto the surface of nanoparticles or viral vectors. However, their conjugation frequently results in premature clearance of the drug and gene carriers as well as reduced vector titers and stability, thereby greatly limiting efficacy. To address these challenges, I explored the use of bispecific fusion proteins (BFP) and bispecific antibodies (bsAb) to enhance cell-specific delivery of drug and gene carriers to tumor cells *in vitro* and *in vivo*. In this dissertation, I first explored a two-step targeting approach termed pretargeting that *decouples* targeting specificity from carrier circulation kinetics and stability. Specifically, pretargeting relies on bsAb or BFP that can bind both selected epitopes on target cells and subsequently administered effector molecules (ie. nanoparticles and lentiviruses). I utilized quantitative approaches and systematic analyses to (1) evaluate interactions between pretargeting BFP and nanoparticles on the cell surface that maximizes internalization of nanoparticles into target cells, and (2) determine the bsAb format that enhances tumor accumulation of pretargeted PEGylated nanoparticles. I also investigated (3) the use of bsAb coupled with engineered lentiviral vectors

for efficient targeted gene delivery capable of facilitating long-term gene integration of the therapeutic genes of interest. My results indicated that density of BFP on the cell surface can effectively limit internalization of pretargeted nanoparticles, underscoring the need to carefully tune BFP dosing for intracellular delivery. I also found that multivalency and elimination of FcRn recycling are both critical in maximizing pretargeting efficiency of PEGylated nanoparticles. Finally, I showed that the specificity of targeted viral gene delivery was enhanced by decreasing binding to off-target cells and coupling the lentiviral vectors with bsAb for selective targeting. The methodologies and overall findings described here inform future studies of antibody-cell receptor interactions and effective nanoparticle and viral vector targeting strategies.

ACKNOWLEDGEMENTS

Completion of this work was made possible through the contributions and support of many people. First, I would like to thank my advisor, Dr. Samuel Lai, who began mentoring me as an undergraduate researcher during a summer internship in 2012. Dr. Lai has offered a balanced mixture of freedom and guidance as I pursued my Ph.D., and has nurtured me as an independent scientist. I would also like to thank my committee members Dr. Shawn Hingtgen, Dr. Michael Jay, Dr. Brian Kuhlman, and Dr. Rihe Liu for their time, advice, and feedback. Special thanks to the UNC animal services cores, flow cytometry, and small animal imaging, as well as labs in DPMP and the School of Dentistry for letting me use their instruments and reagents. A major thank you to the funding sources that have made my studies possible, especially the Graduate Student Research Fellowship from the National Sciences Foundation, GlaxoSmithKline Fellowship from UNC Eshelman School of Pharmacy Foundation, and Initiative for Maximizing Diversity Excellence Fellowship from UNC Chapel Hill.

My time in graduate school has been enriched by all of the past and present members of the Lai Lab: Dr. Angela Yang, Dr. Tim Jacobs, Dr. Holly Schroeder, Morgan McSweeney, Justin McCallen, Kennetta Nunn, Dr. Dimple Harit, Jasmine Edelstein, among others. I would also like to thank Felix Nwogbo, Ugonna Ohiri, Korine Duval Ohiri, and Sasha Philius for their genuine friendship, supporting me throughout college and graduate school, and getting me out of the lab for fun. I owe so much to my parents and family for their unconditional love and support. Finally, I would to thank the STEM programs that I am so honored to have participated in from

elementary school through college: Saturday College Program at the University of Illinois at Chicago, Physician Scientists Training Program at Temple University, and Meyerhoff Scholars Program and MARC U*STAR Training Program at University of Maryland, Baltimore County.

TABLE OF CONTENTS

LIST OF TABLES

LIST OF FIGURES

LIST OF ABBREVIATIONS

Ab	antibody
ANOVA	analysis of variance
BFP	bispecific fusion protein
bsAb	bispecific antibody
BsPs	bispecific proteins
CA	clearing agent
COOH	carboxyl
DSPE	1,2-distearoyl-*sn*-glycero-3-phosphoethanolamine
EDC	1-ethyl-3-(3-dimethylaminopropyl)carbodiimide
ELISA	enzyme-linked immunosorbent assay
Env	envelope
EPR	enhanced permeability and retention
FP	fusion protein
HRP	horseradish peroxidase
ID/g	injected dose per gram
IHC	immunohistochemistry
i.v.	intravenous
LV	lentivirus, lentiviral
MAb	monoclonal antibody
MPS	mononuclear phagocytic system
mSindbis	mutated Sindbis envelope

MW	molecular weight
NH_2	amine
NP	nanoparticles
PDAM	1-pyrenylyldiazomethane
PEG	polyethylene glycol
PEGb	biotin-polyethylene glycol
PK	pharmacokinetics
PLD	PEGylated liposomal doxorubicin
PRIT	pretargeted radioimmunotherapy
PS	polystyrene
RIT	radioimmunotherapy
SA	streptavidin
scFv	single-chain variable fragment
TCO	*trans*-cyclooctene
TMB	3,3',5,5'-tetramethylbenzidine
Tz	tetrazine
V_D	volume of distribution

CHAPTER 1: INTRODUCTION

1.1 Bispecific antibodies are useful therapeutic modalities

The development of monoclonal antibodies (mAb) has profoundly impacted medicine, in particular cancer and gene therapy.[1–3] Despite clinical success in several cancers and good tolerability, the monospecificity of mAbs often limits their effectiveness in complex, heterogeneous diseases like cancer.[4] Advances in protein engineering technologies spurred the development of bispecific antibodies (bsAb) that combine the binding domains from two mAbs into one dual-targeting molecule for enhanced potency and multiple functionalities. Three bsAb have received regulatory approval (catumaxomab, blinatumomab, and emicizumab-kxwh), and many more are in clinical development.[5,6] In addition to their dual specificity, bsAb are also engineered with various characteristics, including molecular weight, specificity, affinity, valency, flexibility, stability, shape, and Fc modifications, for desired pharmacokinetics, biodistribution, and tumor penetration and retention.[7–10] BsAb are broadly separated into two major classes: IgG-like bsAb that include Fc region and therefore retain Fc-mediated effector functions and FcRn-mediated recycling for longer serum half-life, and non-IgG like bsAb fragments or fusion proteins that lack Fc domain. The Fc region is often removed from bsAb to avoid nonspecific crosslinking and activation of immune effector functions for undesired toxicity. However, Fc removal reduces size, eliminates FcRn recycling, and shortens half-life, sometimes requiring continuous infusion or repeated administration of bsAb to achieve desired exposure.

Bispecific antibodies are useful in therapeutic, imaging, and diagnostic applications.[9] In cancer therapy, bsAb function through three main mechanisms of actions: retargeting immune effector cells to tumor cells for killing, crosslinking proteins, and simultaneously interfering with two signaling cascades via receptor or ligand inactivation.[5,6,10,11] For example, FDA approved blinatumomab (Blincyto®) retargets cytotoxic T cells to tumor B lymphocytes via binding to CD3 receptors on T cells and CD19 protein on B cells, resulting in effector cell activation and cancer cell death. Emicizumab-kxwh (Hemlibra®) crosslinks factors IXa and X to activate the natural coagulation cascade and restore the blood clotting process in patients with hemophilia A. Bispecific fusion proteins (BFP) have also improved radiotherapy by changing treatment strategy from one step to a two-step system, called pretargeted radiotherapy (PRIT). PRIT was initially tested for the treatment of hematological malignancies, and demonstrated improved imaging contrast tumor suppression, and reduced radioactivity in healthy organs.[12] Given its dual targeting capability, we were interested in coupling bsAb with delivery carriers for targeted drug and gene delivery to tumors.

1.2 Challenges to targeted drug and gene delivery

Targeted drug delivery aims to maximize the therapeutic dose of anti-cancer or imaging agents at target cells while minimizing exposure and toxicity to healthy, non-targeted tissues. Anti-cancer agents are often encapsulated in nanoparticle formulations because these formulations can significantly improve the drug's bioavailability, biodistribution, and pharmacokinetics and reduce toxicity compared to free drug.[13] A major biological barrier to nanoparticles injected into the systemic circulation is rapid clearance by mononuclear phagocyte system (MPS) cells, which results in a smaller fraction of administered nanocarriers that

extravasate and accumulate at target site.[14] "Stealth" polymers often coat nanoparticles (ie. passive targeting) to minimize opsonin absorption and avoid MPS, thereby extending nanoparticle circulation half-life for increased particle accumulation in tumors. However, coating polymers also limit binding and subsequent endocytosis into target cells, another barrier to particle delivery.

To increase particle uptake, antibodies or antibody fragments that target overexpressed cellular epitopes on malignant cells relative to healthy cells are covalently attached to the surface of nanoparticles (ie. active targeting). However, this results in premature clearance of targeted drug carriers, thereby greatly limiting efficacy.[15–18] Exceeding antibody grafting thresholds actually reduces targeting efficiency *in vivo*, likely because high antibody densities compromise the "stealth" properties of coating polymers. As a result, a smaller fraction of administered nanocarriers extravasate and accumulate at target site.

Specific, long-term gene expression is a major challenge of targeted gene delivery. Unmodified lentiviral vectors possess broad tropism, which currently restricts their use to *ex vivo* transduction and subsequent reinfusion of infected cells into patients. Similar to nanoparticles, antibodies and antibody fragments are often covalently incorporated onto the surface of viral vectors to provide cell and tissue specificity. However, this results in reduced vector titers and stability, thereby limiting efficacy.[19–22] Moreover, this targeting approach necessitates generating new viral envelopes for each cellular target. To overcome these challenges, I decided to investigate the use of third-party bispecific antibodies (bsAb) or fusion proteins (BFP) to enhance specific targeting of drug and gene carriers to select cells/tissues while avoiding non-targeted, healthy tissues.

1.3 Targeted delivery using pretargeting strategy

By *decoupling* targeting from delivery, I can readily tune carrier specificity to target cells while maximizing carrier circulation kinetics and stability. Pretargeting is a two-step that relies on the use of bispecific pretargeting molecules that can bind both cellular epitopes and subsequently administered effector molecules, such as drug-loaded nanoparticles and gene carriers. First, pretargeting molecules are administered with the expectation that they will extravasate from circulation and accumulate on the surface of target cells, or be quickly eliminated from the circulation. Drug-loaded carriers are then administered, and a fraction of the extravasated carriers will bind to cell-bound pretargeting molecules and internalize into target cells. This strategy aims to simultaneously preserve prolonged circulation of coated nanoparticles and facilitate targeting to specific cells. I used the pretargeting strategy to target drug carriers to tumor cells. For gene carriers, I coupled carriers and bsAb with a simple pre-incubation step to generate targeted gene carriers without complex coupling chemistries or incorporating Ab fragments onto the lentiviral surface.

1.4 Thesis overview

In this thesis, my goal is to provide a blueprint for the engineering of bispecific antibody formats that can enhance nanoparticle and viral vector targeting and uptake into target tumor cells for improved efficacy and safety. This goal is divided into three aims in the following chapters:

Chapter 3: Elucidate interactions between bispecific antibodies and cell receptors for efficient intracellular delivery of pretargeted nanoparticles. Using *E. coli* as protein factories, I expressed and purified streptavidin-based BFP that recognize TAG-72 overexpressed on T-

leukemia cells and biotin on the surface of biotin-functionalized nanoparticles. I synthesized densely PEGylated model polymeric nanoparticles with a range of surface biotin groups. Using flow cytometry and confocal microscopy, I explored the efficiency of intracellular delivery by pretargeting BFP that bind to slowly- or non-internalizing epitopes.

Chapter 4: Investigate bispecific antibody formats for improved accumulation of pretargeted PEGylated nanoparticles in tumors. Using mammalian cells, I engineered BFP of varying size, valency, and inclusion or exclusion of Fc domain; BFP bound both HER2 overexpressed on breast cancer cells and polyethylene glycol (PEG) on PEGylated polymeric nanoparticles and PEGylated liposomal doxorubicin (PLD). I quantified BFP affinity to each target using ELISAs, and evaluated the influence of Fab valency on pretargeted nanoparticle uptake by target $HER2^+$ human breast cancer cells and off-target $HER2^-$ human cells using flow cytometry. I also evaluated how bsAb formats with and without Fc domain impacted pretargeting efficiency of PLD in tumor-bearing mice by first dosing bsAb followed by PLD, and measured doxorubicin concentration in target and off-target organs using HPLC.

Chapter 5: Evaluate the use of targeted lentiviral system using mutated lentiviral vectors and bispecific antibodies for gene delivery to tumor cells. I mutated Sindbis pseudotyped lentivirus to ablate native receptor binding and reduce binding to off-target cells without altering endosomal fusion and escape. Using mammalian cells, I engineered bsAb that bound both HER2 on target cells and two separate Sindbis envelope glycoproteins. I tested the transduction efficiency and selectivity of bsAb coupled with Sindbis lentivirus (wildtype or mutated) in target $HER2^+$ human cells, off-target $HER2^-$ human cells, and co-culture of $HER2^+$ and $HER2^-$ cells using flow cytometry.

REFERENCES

1. Scott, A. M., Wolchok, J. D. & Old, L. J. Antibody-based therapy for cancer. *Nat. Rev. Cancer* **12,** 278–287 (2012).

2. Sliwkowski, M. X. & Mellman, I. Antibody therapeutics in cancer. *Science.* **341,** 1192–1198 (2013).

3. Weiner, G. J. Building better monoclonal antibody-based therapeutics. *Nat. Rev. Cancer* **15,** 361–370 (2015).

4. Runcie, K., Budman, D. R., John, V. & Seetharamu, N. Bi-specific and tri-specific antibodies- the next big thing in solid tumor therapeutics. *Mol. Med.* **24,** (2018).

5. Kontermann, R. E. & Brinkmann, U. Bispecific antibodies. *Drug Discov. Today* **20,** 838–847 (2015).

6. Husain, B. & Ellerman, D. Expanding the Boundaries of Biotherapeutics with Bispecific Antibodies. *BioDrugs* **32,** 441–464 (2018).

7. Cuesta, Á. M., Sainz-Pastor, N., Bonet, J., Oliva, B. & Álvarez-Vallina, L. Multivalent antibodies: When design surpasses evolution. *Trends Biotechnol.* **28,** 355–362 (2010).

8. Nuñez-Prado, N. *et al.* The coming of age of engineered multivalent antibodies. *Drug Discov. Today* **20,** 588–594 (2015).

9. Brinkmann, U. & Kontermann, R. E. The making of bispecific antibodies. *MAbs* **9,** 182–212 (2017).

10. Schmid, A. S. & Neri, D. Advances in antibody engineering for rheumatic diseases. *Nat. Rev. Rheumatol.* **15,** 197–207 (2019).

11. Kontermann, R. E. Dual targeting strategies with bispecific antibodies. *MAbs* **4,** 182–197 (2012).

12. Larson, S. M., Carrasquillo, J. A., Cheung, N.-K. V & Press, O. W. Radioimmunotherapy of human tumours. *Nat. Rev. Cancer* **15,** 347–360 (2015).

13. Allen, T. M. & Cullis, P. R. Drug Delivery Systems : Entering the Mainstream. *Science (80-.).* **303,** 1818–1822 (2004).

14. Blanco, E., Shen, H. & Ferrari, M. Principles of nanoparticle design for overcoming biological barriers to drug delivery. *Nat. Biotechnol.* **33,** 941–951 (2015).

15. Bertrand, N., Wu, J., Xu, X., Kamaly, N. & Farokhzad, O. C. Cancer nanotechnology: The impact of passive and active targeting in the era of modern cancer biology. *Adv. Drug Deliv. Rev.* **66,** 2–25 (2014).

16. Torchilin, V. P. in *Handbook of Experimental Pharmacology* 3–53 (Springer, Berlin, Heidelberg, 2010). doi:10.1007/978-3-642-00477-3_1

17. Bazak, R., Houri, M., El Achy, S., Kamel, S. & Refaat, T. Cancer active targeting by nanoparticles: a comprehensive review of literature. *J. Cancer Res. Clin. Oncol.* **141,** 769–784 (2015).

18. Allen, T. M. Ligand-targeted therapeutics in anticancer therapy. *Nat. Rev. Cancer* **2,** 750–763 (2002).

19. Anliker, B. *et al.* Specific gene transfer to neurons, endothelial cells and hematopoietic progenitors with lentiviral vectors. *Nat. Methods* **7,** 929–935 (2010).

20. Dreja, H. & Piechaczyk, M. The effects of N-terminal insertion into VSV-G of an scFv peptide. *Virol. J.* **3,** 69 (2006).

21. Cronin, J., Zhang, X.-Y. & Reiser, J. Altering the tropism of lentiviral vectors through pseudotyping. *Curr. Gene Ther.* **5,** 387–398 (2005).

22. Sinn, P. L., Sauter, S. L. & McCray, P. B. Gene Therapy Progress and Prospects: Development of improved lentiviral and retroviral vectors – design, biosafety and production. *Gene Ther.* **12,** 1089–1098 (2005).

CHAPTER 2: BACKGROUND ON HETEROGENEOUS TUMOR TREATMENT AND BISPECIFIC PROTEIN-MEDIATED PRETARGETED DRUG DELIVERY[1]

2.1 Introduction

Targeted drug delivery for cancer offers the potential to significantly improve the therapeutic index of anticancer agents by increasing drug concentration at tumor sites while reducing side effects and toxicity in non-targeted tissues. A long-standing approach in the field has been to exploit the leaky tumor vasculature in tumor tissues by encapsulating therapeutic cargo into nanoparticles that remain sufficiently stable when introduced to the systemic circulation in order to reach and extravasate into cancer tissues. To further facilitate selective delivery into cancer cells, many researchers have functionalized nanoparticles with ligands that bind specific receptors on cancer cells, a strategy commonly referred to as "active" targeting.[1] Unfortunately, the accumulation of both ligand-free and ligand-conjugated systems in tumors is generally modest at best, limiting the efficacy of various therapies against cancer.[2,3]

Due to advances in the genetic and phenotypic analysis of tumors, tumor heterogeneity has recently emerged as yet another biological barrier that could limit efficient distribution, retention, and uptake of ligand-conjugated nanoparticles at tumor sites.[2,4,5] Tumor heterogeneity also encompasses the highly variable expression of target receptors, both intertumorally between patients or different tumors and intratumorally within a given tumor, and has been reported for a wide range of human tumors.[6,7] Due to the absence or suboptimal expression of their target

[1]This chapter previously appeared in the Journal of Controlled Release. The original citation is as follows: Yang Q, Parker CL, McCallen JD, Lai SK. "Addressing challenges of heterogenous tumor treatment through bispecific protein-mediated pretargeted drug delivery." *J Control Release*. **2015**, *220*(Pt B): 715-726.

receptor on many tumor cell subpopulations, actively targeted drug carriers, which typically consist of single-ligand nanoparticles, are unable to effectively bind and internalize into the full spectrum of tumor cells present in any particular tumor. As noted by Bae *et al*., "aiming at cancer cells with a single surface marker results in aiming at a single population among mixed populations which are constantly changing and moving."[2] Inadequate drug delivery to all cancer cell subpopulations typically results in only partial suppression of the cancer and eventually leads to tumor regrowth and/or the emergence of therapy-refractory tumor cell populations.[8–10] Thus, targeting strategies that can directly address the challenges associated with tumor heterogeneity and enable effective delivery of nanoparticles are sorely needed.

One promising targeting strategy is to decouple molecular homing and delivery of therapeutics into two separate steps. This approach involves first introducing bispecific proteins (BsPs) that can specifically bind (i.e., "pretarget") cancer cells, followed by the administration of a drug-carrying effector such as a nanoparticle that can be captured by the BsPs accumulated on the surface of tumor cells (Figure 1). By introducing multiple distinct BsPs, a single effector nanoparticle could in theory bind with molecular specificity to the full diversity of cancer cells present in any particular tumor. In this review, we will discuss the concept of, important considerations for, and key challenges associated with exploiting the pretargeted strategy to enhance the delivery of therapeutics to heterogeneous tumors.

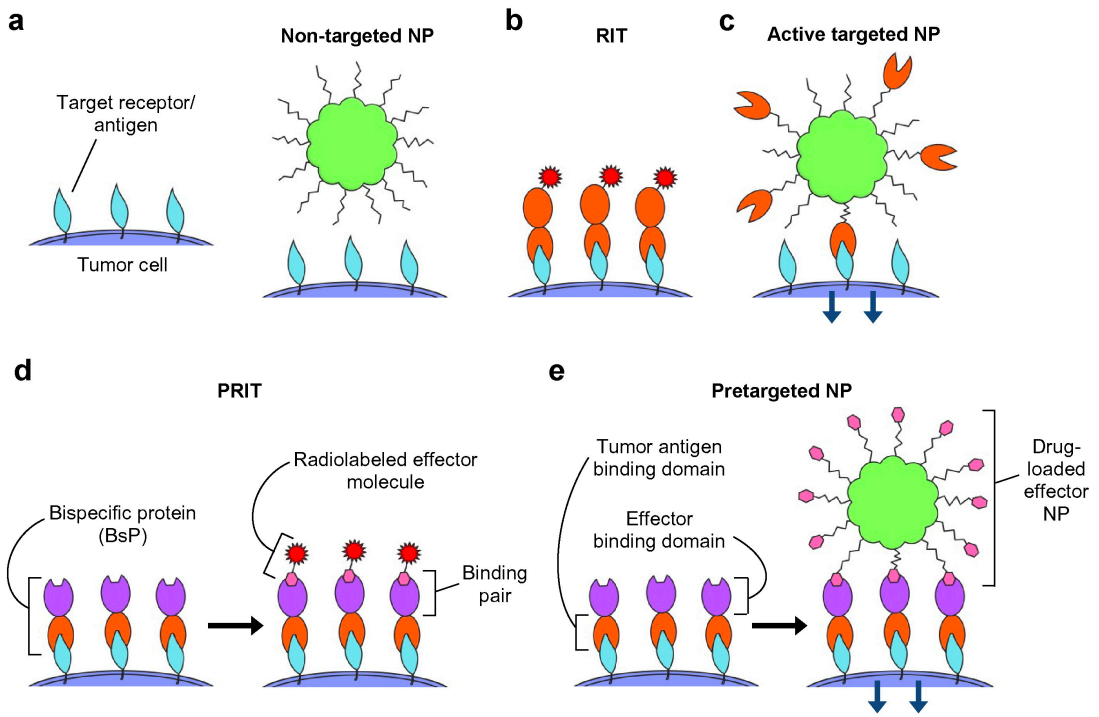

Figure 2.1. Strategies for the delivery of nanoparticle drug carriers and/or radioisotopes to tumor cells. Strategies include **a**) non-targeted, **b** & **c**) directly targeted (1-step), and **d** & **e**) pretargeted (multistep) approaches. **a**) Passively targeted nanoparticles coated solely with stealth polymers typically do not exhibit specific interactions with tumor cells. **b**) Radioimmunotherapy (RIT) uses radiolabeled tumor receptor-specific antibodies to deliver therapeutic doses of radiation to target cells. **c**) Modification with receptor-specific ligands allows the active targeting of nanoparticles (NPs) to tumor cells, which commonly induces receptor-dependent internalization. **d**) Pretargeted radioimmunotherapy (PRIT) splits tumor targeting and radioisotope delivery into sequential steps: 1) binding of bispecific proteins (BsPs) to target receptors and 2) binding of radiolabeled effector molecules to the BsPs. **e**) For pretargeted drug delivery systems, 1) bispecific proteins (BsPs) bind target receptors, and 2) a drug-loaded effector nanoparticle binds to the BsPs, which should ideally result in internalization.

2.2 Conventional cancer targeting strategies: passive targeting

In 1986, Matsumura and Maeda discovered that macromolecules can preferentially accumulate in tumors due to anatomical and pathophysiological differences between solid tumors and healthy tissue.[11–13] Specifically, tumors initiate extensive angiogenesis to maintain their rapid growth, but the newly formed blood vessels display abnormal architecture including fenestrated endothelial lining of vessel walls.[12–14] The more permeable tumor vasculature then allows macromolecules and nanoparticles to extravasate from the bloodstream and accumulate in

the tumor.[13,14] Presumably poor lymphatic drainage further permits enhanced retention of drug delivery systems within tumors.[12,14] The combination of leaky tumor vasculature and impaired lymphatic drainage constitute the phenomenon termed the enhanced permeability and retention (EPR) effect.

Harnessing the EPR phenomenon simply requires nanoparticles to (i) fall within an appropriate size range and (ii) evade rapid elimination by the mononuclear phagocytic system (MPS). While smaller nanoparticles can naturally extravasate more efficiently than larger nanoparticles, most studies suggest the tumor vasculature in mouse xenografts can permit extravasation of nanoparticles ranging from 10 to 200 nm in diameter,[13,15–17] with some studies reporting EPR of particles up to 500 nm in diameter.[14,18] In addition to size, prolonged circulation kinetics also directly improve the extent of nanoparticle extravasation through leaky tumor blood vessels by maximizing the number of times a nanoparticle will pass through the tumor vasculature.[12,18] Polyethylene glycol (PEG) was among the first "stealth" polymers used to extend liposome and other nanoparticle circulation times by minimizing opsonin adsorption and nanoparticle elimination by MPS cells, and PEGylation is the most widely adopted strategy to enhance nanoparticle tumor uptake via EPR.[12–14,18] Other coating polymers used to improve particle circulation profiles, and thereby exploit the EPR effect, include flexible, hydrophilic polysaccharides such as dextran, hyaluronic acid, and chitosan[19,20]; synthetic polymers such as polyvinyl alcohol[21] and polyvinylpyrrolidone[22]; zwitterionic polymers[23,24]; and polyoxazolines.[25] Indeed, dextran-, hyaluronic acid-, chitosan-, and N-(2-hydroxylpropyl) methylacrylamide (HPMA)-coated particles all exhibited improved EPR-mediated tumor accumulation due to prolonged circulation.[26–29] Because nanoparticles of the appropriate size and with MPS-resistant surface chemistry can naturally achieve a low to moderate level of tumor targeting without using

specific ligands, these non-molecularly targeted systems are frequently classified as *passively targeted*.

It is important to note that the EPR effect is highly variable and may not be readily exploitable for all tumors.[30] For example, hepatocellular and renal cell carcinomas are characterized by high vascular density and exhibit increased EPR effects compared to low vascular density pancreatic and prostate cancers that demonstrate diminished EPR effects.[30,31] Additionally, EPR of drug carriers is not observed homogenously throughout individual tumors, as the central foci of tumors tend to be characterized by necrotic,[30,32] hypoxic,[30,33] and hypovascular areas[12] that do not display the EPR effect.[11,34,35] EPR heterogeneity may also vary between primary tumor and metastases.[1] Therefore, harnessing EPR to enhance therapeutic responses in the clinic requires an improved understanding of how tumor heterogeneity impacts the EPR effect both within and between tumors.[1,13,30,36,37]

2.3 Conventional cancer targeting strategies: active targeting

To further improve nanoparticle-based delivery to cancer cells, numerous investigators have developed nanoparticles decorated with ligands specific to receptors overexpressed on cancer cells, an approach generally termed *active targeting*.[1] Ligands on actively targeted systems are typically grafted to the distal end of polymer chains that are used to coat the particles and provide prolong circulation kinetics.[18] These systems are presumed to effectively extravasate from the tumor vasculature based on the underlying stealth polymer coating, while the presence of ligands can facilitate nanoparticle binding to and subsequent internalization into specific tumor cells expressing the corresponding receptor,[18,38] thus directly addressing the shortcoming of inefficient cellular uptake of passively targeted systems.[14,18] Numerous targeting ligands have

been utilized to actively target nanoparticles to cancer cells, including antibodies and antibody fragments,[39,40] aptamers,[41] peptides,[42] proteins, sugars,[43] and low molecular weight ligands such as folate.[44] For excellent reviews of the features and design of actively targeted systems, please refer to[1,18,38,45].

Unfortunately, active targeting systems face several challenges that may limit their efficacy in practice. The target cell surface receptors must be highly overexpressed or selectively expressed solely on malignant cells, as opposed to healthy cells, to maximize tumor-specific delivery.[45–47] Additionally, the choice and density of ligand are critical to optimizing the effect of the targeting moiety. Greater ligand density was previously assumed to enhance nanoparticle targeting to tumors *in vivo* due to generally observed improvements in cancer cell uptake *in vitro*.[46] Nevertheless, an increasingly number of studies have shown that maximal accumulation of nanoparticles in tumors *in vivo* is typically achieved with an intermediate ligand density.[46,48–51] For example, increasing the surface aptamer density on polymeric nanoparticles actually resulted in reduced tumor accumulation and increased particle distribution in the liver.[48] The poor *in vivo* performance of particles with high ligand densities was attributed to ligand shielding or adulteration of the underlying stealth polymer coat, leading to rapid MPS clearance and a reduction in the fraction of particles that can reach and extravasate into tumors.[46,47]

2.4 Tumor heterogeneity and implications for targeted drug delivery systems

Variations in accumulated genetic mutations, which can be further exacerbated by alterations in the local tumor microenvironment, frequently lead to genomically distinct subclonal populations within the same tumor or between tumor lesions. This in turn creates a phenomenon termed tumor heterogeneity, which describes the functional and phenotypic profile

differences between cancer cells such as cellular morphology, gene expression, metabolism, motility, proliferation, level of drug resistance, and metastatic potential. Additionally, the highly variable presence of stromal cell populations such as fibroblasts, immune cells, and endothelial cells within tumors is critical in shaping the tumor microenvironment.[52,53] Interactions between the non-tumor cell populations and tumor cells contribute to different tumor phenotypes, impact tumor response to various therapies, and influence disease progression.[54,55]

Tumor heterogeneity (Figure 2.1) encompasses both (i) intertumoral heterogeneity, which describes differences between tumors in an individual patient as well as clinical response differences between patients with the same tumor subtype, and (ii) intratumoral heterogeneity, which refers to the genetic, epigenetic, and phenotypic features that vary within malignant cell populations of the same tumor mass.[56] Intratumoral heterogeneity is further classified into spatial heterogeneity, which refers to differences between distinct anatomical regions or individual cells within a tumor, and temporal heterogeneity, which refers to changes in a tumor's molecular profile and receptor expression over time. An example of intratumoral spatial heterogeneity is the highly discordant HER2 expression observed in different areas within a single biopsy from HER2-positive metastatic breast cancer patients (Figure 2.3a).[57] Temporal heterogeneity can be observed for relapsed lesions that exhibit a disparate molecular profile, compared to their original tumor.

In addition to morphological and spatiotemporal variations within the same tumor or between primary tumors, tumor heterogeneity can also directly result from metastasis. Metastatic heterogeneity (Figure 2.2) has been observed to include (i) discordant biomarker or receptor expression between metastases arising from distinct subclonal populations in the primary tumor ("intermetastatic" heterogeneity) and (ii) heterogeneity within individual metastases

("intrametastatic" heterogeneity), which may have a substantial impact on therapeutic outcome.[7,52,56,58,59] For example, Gerlinger *et al*. reported a case of intrametastatic heterogeneity in which significant changes in the mutational profiles of spatially separated biopsy samples from primary renal-cell carcinomas and metastases were identified using next-generation sequencing.[60] Additionally, Albino *et al*. observed intermetastatic heterogeneity in a melanoma patient whose multiple metastases displayed contrasting morphologies and surface antigen expression.[59] Other studies have also investigated variable estrogen, progesterone, and HER2 receptor expression between primary breast tumors and metastases, with discordance rates that varied greatly from 18% to 54%.[52,61,62] Additional types of heterogeneity include non-genetic phenotypic and functional heterogeneity[62] and tumor microenvironment heterogeneity.[52,53] Because tumor cells interact with their environment, tumor microenvironment heterogeneity exerts a crucial influence on disease progression. For example, the heterogeneous distribution of stromal cells, extracellular matrix organization, and especially hypoxic regions within the tumor microenvironment may promote metastasis and development of drug resistance.[51]

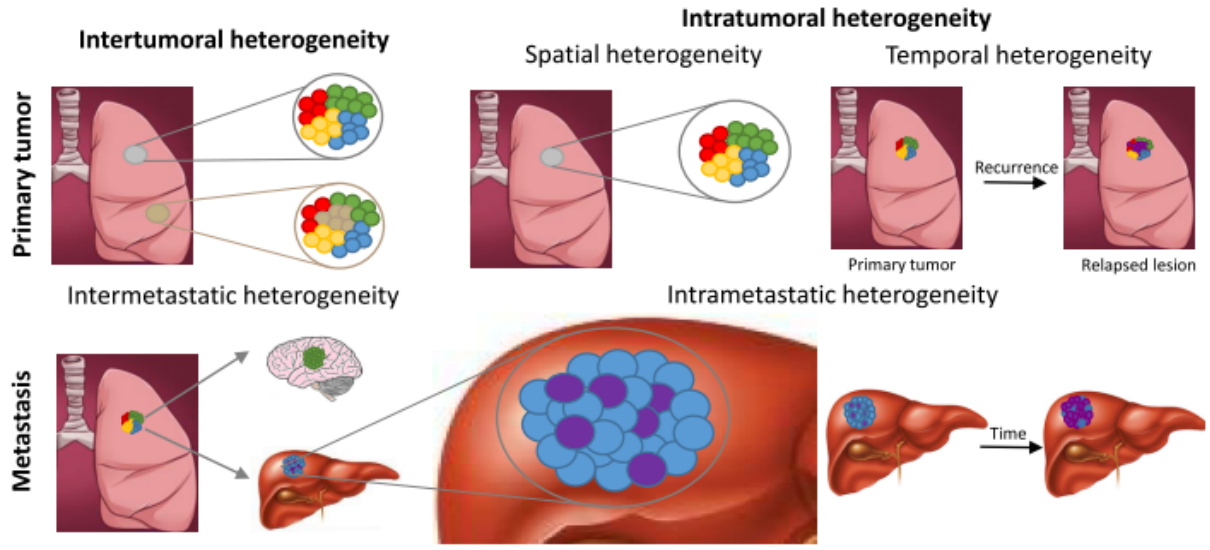

Figure 2.2. Different types of tumor heterogeneity. Spatial heterogeneity refers to differences between distinct anatomical regions or individual cells within a tumor, while temporal heterogeneity illustrates changes in a tumor's molecular profile over time. Intermetastatic heterogeneity arises from distinct subclonal populations in the primary tumor, and intrametastatic heterogeneity reflects the discordant molecular profiles of cells within individual metastases.

Tumor heterogeneity has been reported in a wide range of human tumors such as breast,[52,57] non-small cell lung,[63,64] ovarian,[52,65–67] prostate,[52,68] and lymphoma[69] and poses a significant challenge for diagnosis, prognosis, and efficacy of molecularly-targeted therapies (Figure 3b).[65,70] The presence of heterogeneous cancer cell populations within tumors will likely limit the efficacy of any therapeutics targeted against any single tumor-associated receptor, leading to poor/varied outcomes, including cancer recurrence and therapeutic resistance.[6,56] For example, the heterogeneous expression of programmed death 1 (PD-1) was reported in two distinct T-cell subxpopulations and differentially impacted survival in patients with follicular lymphoma.[69] Similarly, heterogeneous HER2 expression in breast cancer has prompted treatment stratification in the clinic based on receptor expression.[52] Indeed, intratumoral HER2 heterogeneity, both genetic and spatial, affected the trastuzumab treatment responses and survival of patients with HER2-positive metastatic breast cancer.[57] Only a small fraction of

trastuzumab-treated patients achieved complete disease eradication, and the majority of patients developed relapsed tumors that were resistant to trastuzumab therapy due to the proliferation of HER2-negative breast cancer cells.

In addition to therapy with monoclonal antibodies such as trastuzumab, variable target receptor expression in heterogeneous tumors also presents a critical bottleneck for actively targeted drug delivery systems. The common active targeting approach, in which drug-loaded particles are surface modified with a single ligand group, cannot target and facilitate intracellular delivery to the full diversity of malignant cells. One potential strategy is the administration of a cocktail of single-ligand particles. Unfortunately, this would pose considerable challenges and substantial cost burden in the context of particle formulation and complexity in clinical evaluation,[47] which has generally limited particles to one or two distinct targeting ligand groups. More importantly, a single universal targeted nanoparticle cocktail for all patients is unlikely to succeed due to interpatient heterogeneity; inadequate levels or the complete lack of corresponding target cells for a significant fraction of the ligand-modified particles could lead to increased hepatic and splenic biodistribution and, correspondingly, reduced tumor accumulation. Alternatively, multiple different targeting ligands could be theoretically conjugated onto the surface of a single nanoparticle. However, as discussed above, increased density of ligands beyond a particular threshold will likely trigger rapid MPS clearance of the particles.

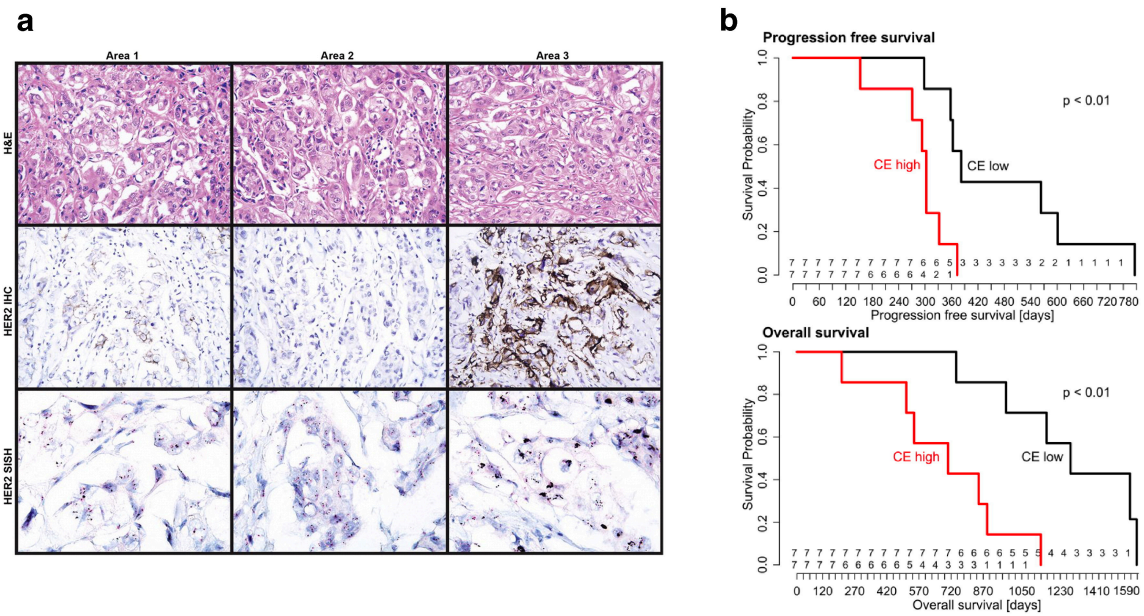

Figure 2.3. Tumor heterogeneity observed in the clinic. **a**) Spatial heterogeneity in HER2 expression between three different areas of an invasive ductal carcinoma biopsy sample. HER2 amplification was confirmed using immunohistochemistry (IHC) and silver in situ hybridization (SISH). H&E, ×200; IHC, ×200; SISH, ×400. Reprinted with permission from Lee *et al.*[57] **b**) Progression free survival (top) and overall survival (bottom) of high-grade serous ovarian cancer patients treated with platinum-based chemotherapy and surgery, stratified by degree of clonal expansion (CE). CE reflects the accumulation of mutations that promote cell expansion into varying subclonal populations from the original cell. Higher CE is correlated with divergent subclonal populations and thus greater tumor heterogeneity. Reprinted with permission from Schwarz *et al*.[65]

2.5 Pretargeted radioimmunotherapy (PRIT)

The discovery that human tumor-associated antigens could be used as targets for antibodies to differentiate tumors from normal tissue helped spawn the field of monoclonal antibody (MAb)-based immunotherapy of cancer. The multiple applications of cancer immunotherapy include radioimmunotherapy (RIT) (Figure 2.1b), which uses radioisotope-conjugated Mabs to treat radiosensitive tumors such as non-Hodgkin's lymphoma (NHL).[71] Unfortunately, the therapeutic efficacy of RIT is limited by the long circulatory half-life of many MAbs, as well as high non-specific deposition of the MAbs in normal organs, resulting in low tumor-specific delivery of radiation and significant toxicity.[72]

To overcome the shortcomings of radioimmunotherapy (RIT), many researchers have adopted a multistep approach (Figure 1d) to more specifically deliver radionuclides to tumor cells by first injecting BsPs that contain a tumor cell binding domain and an effector binding domain. Subsequently, radiolabeled effector molecules are introduced and interact with BsPs bound on the surface of tumor cells. Such an approach has been termed pretargeted radioimmunotherapy (PRIT).[73,74] Because the BsPs are non-radioactive and the radiolabeled effector molecules typically consist of modified small molecule metal chelators that can be rapidly cleared, PRIT can significantly improve the therapeutic index of radioisotope treatment compared to RIT,[72,75,76] as well as increase the maximum tolerated dose for radionuclides.[74] Pagel *et al*. demonstrated that anti-CD45 PRIT improved the specificity of radiation delivery to leukemia in a rodent model, delivering twice as much radiation to bone marrow and five times more activity to the spleen than conventional RIT.[77,78] *In vivo* PRIT was able to mediate broad tumor growth suppression and prolonged survival with the use of BsPs against receptors expressed at different levels on lymphoma cells, with CD20 and HLA-DR proving to be superior targets compared to CD22.[79,80] CD38-specific PRIT achieved tumor-to-blood ratios as high as 638:1 after 24 hours for a multiple myeloma model, compared to a ratio of ~1:1 with conventional RIT.[81] Subbiah *et al*. reported that treating athymic mice bearing Ramos human Burkitt's lymphoma xenografts with a pretargeted system consisting of anti-CD20 scFv-conjugated streptavidin (SA) and ^{90}Y-DOTA-biotin cured 100% of mice with allowable toxicity, whereas conventional RIT with ^{90}Y-1F5 at the same dose produced no cures, generated profound pancytopenia, and was lethal to all mice.[82] Zhang *et al*. demonstrated that both ^{90}Y-DOTA-biotin and ^{213}Bi-DOTA-biotin could both be used in combination with anti-CD25 scFv-conjugated SA

for PRIT of a murine T-cell lymphoma xenograft model, with the beta-emitter ^{90}Y curing 10 of 10 mice and alpha-emitter ^{213}Bi curing 7 of 10 mice.[83]

These encouraging results with PRIT studies in animal models led to clinical studies of PRIT, which have yielded promising results with reasonable tumor response rates and limited toxicity.[84] Forero *et al*. evaluated the pharmacokinetics and immunogenicity of an anti-CD20 scFv-SA conjugate in 15 patients with NHL.[85] Although the complete remission rate was low (2 of 15), the majority (12/15) patients exhibited no signs of hematologic toxicity, suggesting that the dose of radionuclide could be further increased. Another phase I/II PRIT clinical trial was performed using a chimeric anti-CD20 IgG-SA in combination with ^{90}Y-DOTA-biotin. Six of seven NHL patients demonstrated significant tumor regression, with an estimated tumor-to-whole body dose ratio of 38:1. While six of the ten patients developed humoral responses to streptavidin, the transient nature of the responses appeared to result in no significant long-term effects.[86,87] Kraeber-Bodere *et al*. evaluated the therapeutic efficacy of PRIT using a bispecific monoclonal antibody that binds to carcinoembryonic antigen (CEA) and to a ^{131}I-labeled effector molecule for PRIT of medullary thyroid cancer. Of the 17 patients treated, 4 reported pain relief, 5 demonstrated minor tumor responses, and 4 achieved biological responses (decrease in thyrocalcitonin); however, 9 patients also generated human anti-mouse antibodies.[88–90]

While PRIT has led the way in preclinical and clinical studies of pretargeting, it is important to note that the applications for pretargeted strategies extend far beyond radiotherapy. For example, solid cancers, which will account for more than 90% of all newly diagnosed cancer cases and deaths in the United States in 2015,[91] are significantly more resistant to radioimmunotherapy compared to hematological malignancies such as NHL. To date, little is known about whether the pretargeting approach can enhance the delivery of other therapeutic

agents such as nanoparticle drug carriers that can encapsulate and slowly release chemodrugs to solid tumors.

2.6 Pretargeted drug delivery to heterogeneous tumors

The growing interest in precision/personalized medicine, coupled with the incomplete treatment of heterogeneous cancers using common passively or single-ligand targeted therapies that can give rise to recurrent, more aggressive, and/or drug-resistant tumors,[7,56] highlights the need for alternative nanoparticle targeting strategies to improve treatment responses. The modular nature of pretargeted systems is particularly useful in addressing the challenge of and many barriers to effective drug delivery to heterogeneous tumors[52] because it enables pretargeted systems to be targeted to new or different tumor antigens by simply modifying the tumor binding domain of BsPs, as opposed to direct, ligand-based targeting systems that would require the formulation of a new nanoparticle system. This flexibility is expected to markedly reduce the production costs and complexity, as well as the potential regulatory burden, for pretargeted nanoparticles. Another equally appealing feature of pretargeting is the ability to pretarget multiple receptors simultaneously. The administration of a cocktail of pretargeting BsPs that can all bind to the same drug carrier could in theory enable the delivery of a drug carrier to the full spectrum of a patient's cancer cells (Figure 2.4). Drug cocktails containing mixtures of different MAbs have already been applied to cancer therapy, with one combination of pertuzumab, trastuzumab, and docetaxel significantly improving the overall survival of patients with HER2-positive breast cancer.[92] Antibody mixtures have also been used for *in vitro* and *in vivo* imaging and diagnosis of tumors.[93,94] Additionally, pretargeting with individual or mixed BsPs was able to differentially label a range of human tumor cell lines *in vitro* (Figure 2.5a).[95,96] To our

knowledge, no studies have been published on the simultaneous use of multiple pretargeting BsPs to enhance nanoparticle delivery to date, although Khaw *et al.* did report the receptor-dependent efficacy of doxorubicin nanoparticles pretargeted with anti-HER2 affibody-based BsPs in a dual tumor model.[97] In that study, tumor growth inhibition was achieved for HER2-positive BT-474 breast cancer tumors, while the HER2-negative BT-20 breast cancer tumors were simultaneously unresponsive to the treatment, further emphasizing the opportunity for improved cancer treatment through appropriate targeting of all tumor cell populations.

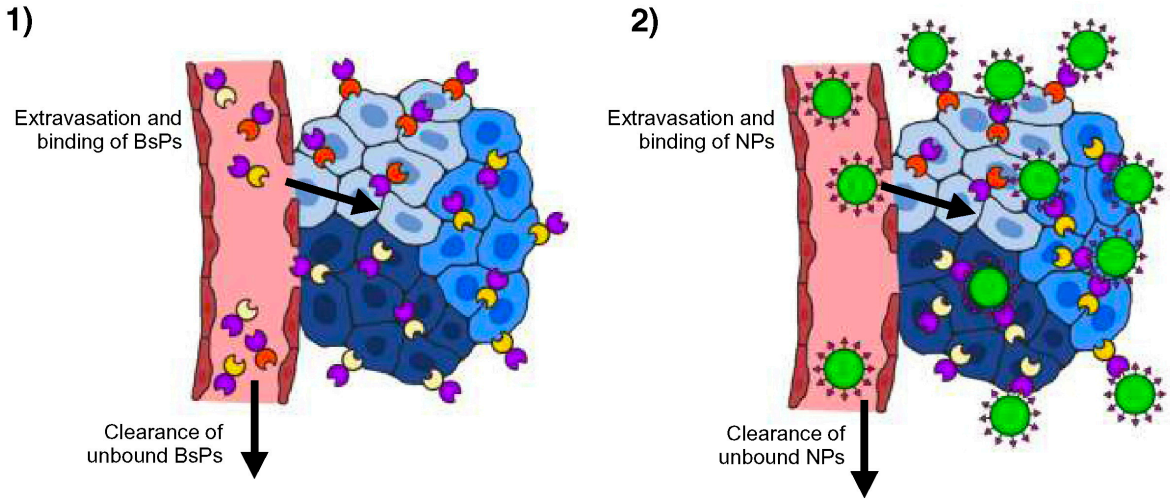

Figure 2.4. Pretargeted delivery of nanoparticles (NPs) to heterogeneous tumors. 1) A cocktail of bispecific proteins (BsPs) is administered and allowed to fully clear from systemic circulation prior to 2) dosing with nanoparticles that can be captured by BsPs on the tumor cell surface. To enable effective targeting of multiple tumor cell subpopulations using a single nanoparticle, the tumor antigen-binding domain (Figure 2.1e) of the BsPs can be modified to reflect the full diversity of tumor cells, while the effector (NP)-binding domain remains the same for all BsPs.

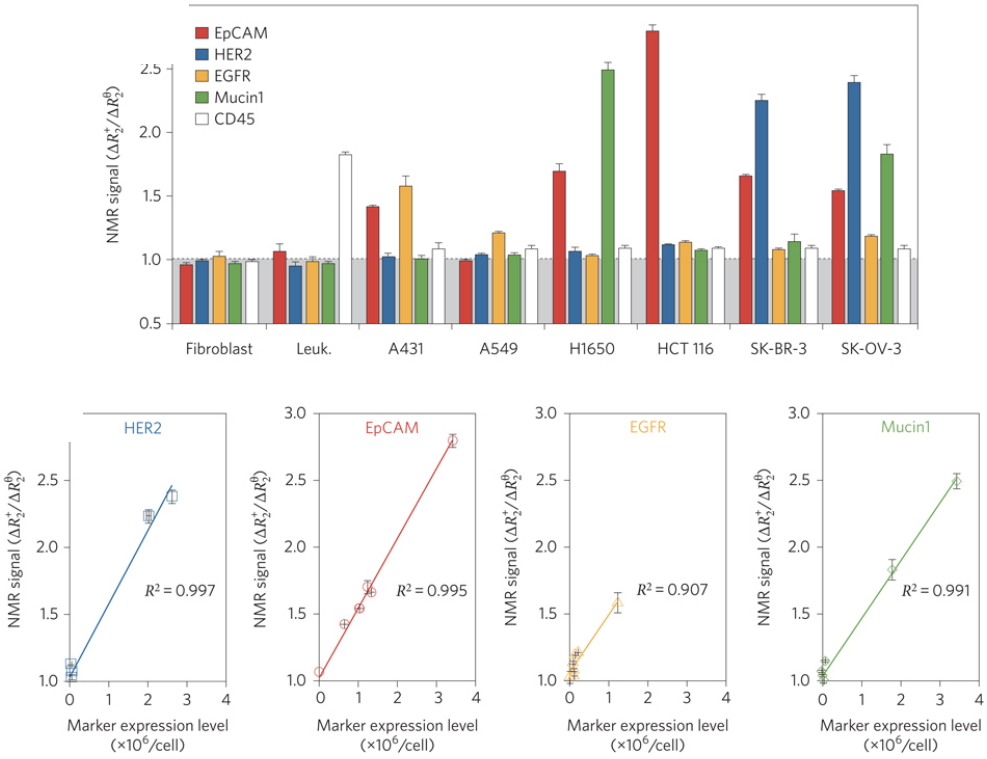

Figure 2.5. Diagnostic magnetic resonance profiling of human tumor cell lines, fibroblasts, and leukocytes using a pretargeted approach *in vitro*. The cells were labeled using various *trans*-cyclooctene (TCO)-conjugated antibodies followed by tetrazine-modified magneto-fluorescent nanoparticles (Tz-MFNPs) prior to the measurement of the transverse relaxation rate (R_2). Figure reprinted with permission from Haun *et al*.[95]

2.7 Biological and pharmaceutical aspects and considerations of pretargeted drug delivery

As multicomponent systems, the potential arsenal of pretargeted therapies is sizeable and highly diverse. Thus, many features (e.g., choice of target receptor/antigen, binding pair technology, and drug carrier) must be taken into account when developing a pretargeted drug delivery system to maximize transport of drug cargo to target cells and overall therapeutic efficacy. Because only a few publications have evaluated the use of pretargeting for nanoparticle delivery, the majority of the current knowledge about optimal pretargeted conditions have been gleaned from *in vivo* PRIT studies, but, due to the overlap of components for multistep targeting

approaches (Figure 2.1d & e), many of the lessons learned from PRIT likely apply to pretargeted nanocarriers.

2.7.1Binding pairs

A key consideration of any pretargeted delivery approach is the binding interaction between the pretargeting BsP and nanoparticle effector, as the affinity of the binding pair directly influences the capture and retention of the drug carrier at the tumor site. In addition, the immunogenicity of the BsP and its interactions with endogenous ligands can also alter the efficacy of pretargeted therapies.[71]

The first binding pairs used in pretargeted systems were based on antibody-hapten interactions. In 1985, Reardan *et al*. reported the development of antibodies against indium chelates of EDTA, and suggested the possibility of bispecific antibodies that can simultaneously recognize target antigens and metal chelates.[72,98] Soon afterwards, Goodwin *et al*. developed an early pretargeted imaging approach using a murine tumor model through the injection of anti-chelate antibodies, followed by the administration of a radiolabel.[99] Since then, a number of antibodies against various haptens have been utilized for binding to effector molecules, including anti-DTPA complex,[100,101] anti-peptide,[102–104] anti-methotrexate,[105] and anti-cotinine antibodies.[106] In addition to bispecific antibodies,[101,102,107] a range of antibody fragments and derivatives have been developed as pretargeting BsPs.[71,106,108] Most antibodies, including those used to capture radioisotope-carrying effector molecules in PRIT, exhibit nanomolar to high picomolar affinity (K_D ~10^{-7}-10^{-10} M) for the antigen target on the surface of cancer cells.[98,105,109] Because PRIT typically uses single radionuclide-loaded agents, the improvement of antibody-hapten binding through multivalency can significantly enhance the specificity of radioisotope

localization and retention in tumor sites.[102,108,109] For example, the application of pretargeted bivalent haptens, termed the affinity enhancement system (AES), was able to improve the tumor biodistribution of bivalent ^{111}In-diDTPA by more than 7-fold compared to monovalent ^{111}In-DTPA (tumor biodistribution: 52.9% vs. 7.6% ID/g at 1 h and 92.5% vs. 0.9% ID/g at 72 h, respectively).[110]

As a binding pair with one of the strongest noncovalent binding affinities (K_D ~10^{-14}-10^{-15} M), the streptavidin (SA)-biotin system was quickly adopted by the pretargeting field.[111,112] Additionally, SA is a tetravalent protein and could enable the capture of multiple biotinylated drug molecules. SA and biotin can be attached to tumor-specific pretargeting proteins and/or effector molecules through a variety of methods, including direct conjugation,[82,113,114] genetic engineering of fusion proteins,[115–117] and enzymatic conjugation.[118] While SA-based PRIT systems have demonstrated increased tumor specificity and higher therapeutic indices relative to directly targeted systems[82,117] and have even been evaluated in clinical trials,[85,114,119] the immunogenic nature of SA, a bacterial protein, represents a major challenge to widespread clinical use of SA-biotin binding pairs.[85,87] The immunogenicity of SA can be reduced through site-specific mutations,[120,122] although it remains unclear whether these SA mutants will be sufficiently hypoimmunogenic to allow for repeated dosing in humans. The problem of interference from endogenous biotin,[123] which necessitates the use of biotin-free feed for *in vivo* studies, could also be potentially addressed by SA mutants that selectively bind bis-biotin instead of biotin.[121,124] Other proteins that naturally bind to specific substrates (e.g., enzymes) can also be modified to bind to exogenous molecules for use in pretargeting, although only a few such systems have been reported in the literature.[125,126]

The majority of published pretargeted and multistep targeting systems utilize antibody-hapten or protein-ligand interactions, but research in areas such as complementary synthetic nucleic acids and peptides and bioorthogonal chemistry continues to generate novel classes of binding pairs. Morpholinos (MORFs) are the most popular class of synthetic nucleic acid analogs for pretargeting using complementary nucleic acids and have been evaluated preclinically in combination with tumor-specific pretargeting antibodies and a variety of radionuclides.[127–131] In addition to relatively low immunogenicity, optimized complementary morpholinos exhibit high specificity and binding affinity,[132] and the use of bivalent MORFs may further enhance affinity.[133] Bioorthogonal chemistry comprises reactions that can rapidly occur in a living system with high selectivity and without any off-target reactions or toxicity. These properties enable pretargeting using small molecule binding pairs with low immunogenicity, although the relative merits of different bioorthogonal chemistries vary based on reaction kinetics, complexity of synthesis, and stability of the resulting conjugate (see refs [71,134,135]). Rossin *et al*. demonstrated the feasibility of using "click" chemistry for pretargeting of radioisotopes *in vivo* by treating tumor-bearing mice with an anti-TAG72 antibody (CC49) modified with *trans*-cyclooctene (TCO), which then reacted with ^{111}In-tetrazine (^{111}In-Tz) administered 24 h later.[136] The CC49-TCO predosed mice exhibited a tumor uptake of 4.2% ID/g and tumor-to-muscle (T/M) ratio of 13.1, compared to tumor uptake and T/M ratios of 0.3% ID/g and 0.5 and 1% ID/g and 2.1 for unmodified CC49 and control Ab-TCO groups, respectively. Further preclinical studies have confirmed the utility of TCO-tetrazine and other bioorthogonal chemistries for tumor imaging and treatment.[71,137–139]

While all of the aforementioned classes of binding pairs have also been used in the pretargeting of nanoparticles and other potential drug carriers,[95,140–142] the ability of pretargeted

systems to actually deliver therapeutics to tumor cells has only been evaluated in a few studies.[97,143–145] Pretargeted poly-lysine polymers,[146] liposomes,[147] and carbon nanotubes[148] have been used to deliver higher doses of encapsulated or conjugated radionuclides to both solid tumor and hematologic cancer cells, suggesting that the application of nanocarriers could further improve the efficacy of PRIT. In the context of cancer chemotherapy, pretargeted biotinylated polymeric nanoparticles loaded with pactilaxel (PTX) increased the *in vitro* cell killing of glioma and breast cancer cells, relative to free drug or Taxol and nontargeted nanoparticles.[143,144] The injection of an anti-HER2 affibody-anti-DTPA Fab complex (BAAC) 8 h prior to the administration of ^{99m}Tc-DTPA-succinylated polylysine enabled the specific labeling of tumors (5.3% ID/g vs. 0.5% ID/g for anti-DTPA Fab-pretargeted particles).[97] BAAC pretargeting of doxorubicin- and DTPA-conjugated polyglutamic acid produced tumor growth inhibition results that were similar to those of free doxorubicin, but pretargeting through the combination of BAAC and polymer-drug conjugate minimized weight loss in mice relative to the free drug treatment,[97] underscoring the ability of pretargeting to improve the therapeutic index of chemotherapeutics *in vivo*.

Although BsP considerations such as immunogenicity and competition with endogenous ligands apply to both PRIT and pretargeted nanoparticles, other features and characteristics of binding pairs required for pretargeted drug delivery systems may differ from those for pretargeting based on small molecule effectors. Nanoparticles are inherently highly multivalent due to their large surface area, which allows the grafting of tens to possibly thousands of a given binding partner moiety. Thus, BsPs with lower affinity to a hapten may still be able to capture hapten-coated nanoparticles with high avidity compared to individual radiolabeled haptens. However, as is the case with actively targeted systems, the incorporation of peptides, nucleic

acids, proteins and other macromolecular components onto drug carrier particles could negatively impact their circulation kinetics and efficiency of extravasation into tumors. For highly asymmetric binding pairs that consist of a large protein and a smaller moiety (e.g., SA-biotin, antibody-hapten), the smaller, the more immunologically inert moiety should be assigned to the effector nanoparticle, rather than the BsP, to minimize MPS clearance. Steric considerations may further support the modification of drug carriers with smaller BsP-binding components. For instance, Haun *et al*. reported that, in addition to providing a 10- to 15-fold increase in cell binding relative to directly targeted iron oxide nanoparticles, a pretargeted antibody-TCO/Tz-NP system demonstrated significantly higher fluorescent labeling of various tumor cell lines, compared to an antibody-biotin/avidin-NP system.[95] The authors attributed this difference to the large footprint of avidin (~67 kDa) on the particles, which likely resulted in the reduced accessibility and valency of biotin-binding sites. The use of a PEG spacer for TCO-antibody modification also improved the pretargeting of quantum dots by reducing masking of reactive groups.[149]

2.7.2 Target antigen(s)

A diverse array of receptors and other antigens overexpressed on tumor cells have been exploited for active targeting of nanoparticles and for RIT.[1,150] In contrast, the number of target cancer antigens/receptors suitable for pretargeted approaches is certainly more limited. The multistep nature of pretargeting requires that the tumor cell-binding BsP must remain on the tumor cell surface to capture subsequently injected effector drug carriers. Indeed, the majority of PRIT studies to date utilize BsPs that target epitopes generally considered to be non-internalizing, including CD20, CD45, TAG72, and CEA.[75,85,115,133,142,145,148] However, Liu *et al*.

observed the fairly rapid internalization of radiolabeled anti-TAG72 and anti-CEA antibodies, with about 60% of the antibodies internalized by LS174T colon carcinoma cells after 5 h.[128] Similarly, although HER2 is thought to be an internalizing epitope, pretargeting using bispecific antibodies against HER2 mediated enhanced tumor accumulation *in vivo*.[97,106,151] Whether these apparently counterintuitive results are due to differences in antibody internalization kinetics between *in vitro* and *in vivo* conditions (e.g., differences in receptor density, receptor turnover rates, and/or endocytosis and cell signaling pathways), dosing of the pretargeting molecules at sufficiently high levels that compensate for loss due to antigen/BsP internalization, or other factors remains unknown.

While the pretargeting molecule should initially remain non-internalized, many therapeutics require intracellular delivery to be effective and/or exhibit maximal potency; thus, the ideal pretargeted nanoparticle must be internalized only after binding of the drug carrier (Figure 2.1). Although internalization mediated by a non-internalizing pretargeting molecule may appear paradoxical, cellular entry could be achieved by relying on the eventual endocytosis of bound receptors or, more preferably, through multivalent nanoparticle binding effects such as crosslinking of receptors. Mulvey *et al*. observed that anti-A33-MORF conjugates remained stably on the surface of LS174T cells for up to 24 h, and that the addition of complementary MORF-modified carbon nanotubes resulted intracellular punctate staining indicative of internalization (Figure 2.6).[148] In contrast, free complementary MORFs failed to induce internalization (Figure 2.6). Gunn *et al*. similarly reported that iron oxide nanoparticles pretargeted to CD20-expressing cells were found in endosomes, as visualized by transmission electron microscopy.[140] These results suggest that BsPs that bind non-internalizing epitopes can still facilitate pretargeted intracellular delivery of nanocarriers.

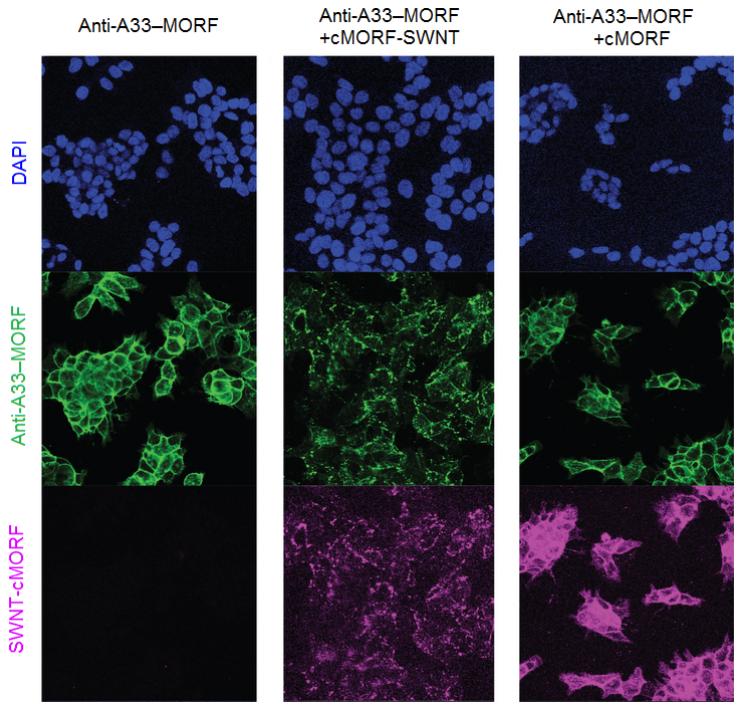

Figure 2.6. Internalization of pretargeted single-walled carbon nanotubes (SWNTs). LS174T (A33-positive) colon carcinoma cells were preincubated anti-A33 antibodies conjugated to morpholino oligonucleotide (anti-A33-MORFs) for 4 h prior to washing and further incubation with complementary MORF (cMORF)-SWNT-AlexaFluor 647 or free cMORF-AlexaFluor 647. Figure reprinted with permission from Mulvey *et al*.[148]

2.7.3 Pharmacokinetics and biodistribution

The theoretical improvements in the therapeutic index of drug delivery systems that can be achieved using pretargeting are based on the decoupling of the tumor targeting vs. drug-carrying functions. This in turn implies that the efficacy of a given pretargeted system is dependent on the pharmacokinetics and biodistribution of each component. One of the most important requirements is that the pretargeting BsPs are maximally cleared from systemic circulation prior to the administration of the drug carrier, particularly for pretargeted systems based on high affinity binding pairs such as SA-biotin. Indeed, SA-coated liposomes were detectable in circulation for at least 24 h after i.v. administration in mice, whereas SA-coated liposomes premixed with biotinylated anti-Thy1.2 antibodies prior to dosing were rapidly cleared

within 4 h,[145] illustrating the potential problem of circulating BsP binding to effector nanoparticles before the particles can extravasate into the tumor. Correspondingly, Karacay *et al*. found that, while an anti-CEA IgG x anti-DTPA Fab' conjugate demonstrated superior tumor labeling relative to $F(ab')_2$ x Fab' and Fab' x Fab' constructs, the $F(ab')_2$ x Fab' conjugate provided better pretargeting of a divalent DTPA peptide due to the high residual blood concentration of IgG x Fab' even 6 days after administration.[100] In order to simultaneously optimize tumor distribution and retention along with systemic clearance, a variety of techniques have been used to modify the size, valency, and composition of pretargeting BsPs, including the "dock-and-lock" method[152,153] and fusion protein engineering.[85,115,125]

An alternative approach to ensure elimination of residual pretargeting molecules from the systemic circulation is the use of clearing agents (CAs) prior to the dosing of nanoparticles or therapeutic effector molecules. These multivalent agents are generally designed to bind tightly to the pretargeting molecules and are sufficiently large enough to be rapidly cleared from the systemic circulation without extravasating into tumors. Previously reported CAs include secondary antibodies[154] and avidin,[155] as well as biotinylated and galactosylated human serum albumin[156] and dendrimers.[78,115] The use of a CA can effectively purge circulating BsP molecules (reducing blood concentrations by up to 10-fold) without affecting the tumor accumulation of pretargeting molecules.[115,155,157] The potential drawback of CA use is the addition of yet another dose and wait step to the course of therapy. For example, the use of CAs with the sequential combination of biotinylated antibodies, SA, and finally biotinylated radionuclide resulted in a *5-step* PRIT strategy (biotinylated MAb/avidin CA/streptavidin/biotinylated CA/biotinylated radiolabeled chelate).[158,159] Although the radioimmunotherapy was well-tolerated and effective in glioma patients, with a median survival of 33.5 months (compared to 8 months for untreated

control patients) in a nonrandomized phase I/II study, the need for several parenteral injections to deliver a single dose of radiation or drug not only introduces a high degree of complexity but also increases the cost of therapy. A simpler 2-step approach is likely far more preferable, particularly when using antibody-hapten binding pairs. These pretargeted systems appear to better tolerate the presence of minute amounts of uncleared pretargeting BsP, possibly due to the lower affinity and the dissociation of BsP-effector complexes formed in the blood.[160]

The pharmacokinetics of the pretargeted drug carrier must also be taken into consideration. Because the commonly utilized pretargeting molecules are generally much smaller than nanoparticle drug carriers, the overall tumor distribution and accumulation of pretargeted systems is therefore limited by the circulation and extravasation kinetics of the drug carrier. To minimize premature elimination from the circulation and maximize tumor accumulation, drug carriers should be effectively coated with stealth polymers, whereas the use of bulky, charged, and/or hydrophobic moieties to facilitate particle binding to the pretargeting molecule should be avoided if possible. As noted in the previous section, this latter requirement may affect the choice of binding pair technology for pretargeted nanoparticle systems, as well as the assignment of binding pair components to the BsP and effector particle. For example, if using a SA-biotin binding system, the nanoparticle should be biotinylated, with the SA component in the pretargeting molecule, rather than vice versa.

2.8 Challenges and unknowns

The combination of a bispecific pretargeting cocktail with nanoparticle drug carriers is a promising but vastly underexplored approach to targeting nanoparticles to heterogeneous tumors.

Thus, many aspects of this proposed strategy must be rigorously evaluated to confirm its suitability for clinical applications.

One of the major challenges is that a greater dose of pretargeting BsP could potentially reduce nanoparticle binding and accumulation to tumor cells. Because tumor receptor expression varies both spatially and temporally, and receptor testing is typically performed on primary tumor biopsies obtained close to the time of diagnosis, "personalized" pretargeting cocktails based on those patient biopsy results is unlikely to capture the full heterogeneity of cancer cells in a patient over time, particularly for relapsed and/or highly metastatic tumors.[6] Thus, truly personalized pretargeted therapy would greatly benefit from improvements in noninvasive molecular profiling of cancers.[56,161] As an alternative to the fine-tuning of individual pretargeting cocktails, the properties of BsPs could be optimized to allow rapid elimination of non-binding BsPs from the circulation. The mechanism, rate, and extent of pretargeting BsP clearance with and without the use of clearing agents must be carefully investigated, particularly since Pagel and colleagues observed that the administration of high doses of MAb-SA conjugates specific to receptors poorly expressed on certain lymphoma tumors overloaded the capacity of mice to hepatically clear MAb-SA/CA complexes, resulting in low tumor-to-normal organ biodistribution ratios and toxicity.[79,162] The increased doses of total protein required for a cocktail pretargeting approach may also affect the immunogenicity of the pretargeting BsPs used.

Additionally, the limited number of appropriate target receptor/antibody combinations that have been evaluated for pretargeting to date may hinder the development of useful pretargeting cocktails. The main driving forces behind the discovery of novel tumor-specific receptors and their corresponding ligands/antibodies are diagnostic biomarkers, imaging

applications and targeted drug and MAb therapy. Unfortunately, few of these studies focus on *non-internalizing* antibodies, a critical requirement of pretargeting. However, the use of (pre)clinically validated ligands and therapeutic MAbs could lead to fortuitous combinations for pretargeting. For example, anti-CD20 MAbs can induce apoptosis clinically,[163] and anti-CD20 Fab' fragments linked to MORFs have been found to also induce apoptosis of B-cell lymphomas *in vitro* and inhibit development of diffuse tumors *in vivo* upon crosslinking by cMORF-modified polymers.[141] The use of antibodies with inherent therapeutic efficacy for pretargeting of drug carriers could allow for synergistic treatment effects. Improvements in the generation of diverse bispecific proteins and antibodies will also certainly expand the diversity of available pretargeting molecules.[152,153,164]

Other concerns regarding the application of pretargeted drug delivery systems include the clinical feasibility of multistep parenteral injections and the poor tumor accumulation of many drug carriers in patient tumors. Similar to passively and actively targeted nanoparticles, the tumor accumulation of pretargeted drug carriers would still rely on the EPR effect,[145] which has been found to be highly variable.[36]

2.9 Conclusion

Despite marked advances in biotechnology, nanotechnology and drug delivery, effective therapy for cancer remains exceedingly challenging, with few treatment options that can provide durable suppression or elimination of the tumor without resulting in eventual recurrence and/or the development of drug-resistant tumors. Emerging insights into tumor physiology have underscored tumor heterogeneity as one of the key bottlenecks to targeted therapy. The concept of pretargeting using a cocktail of bispecific pretargeting proteins combines the strengths of

precision medicine and personalized medicine by offering the potential to deliver nanoparticle therapeutics to diverse cell populations while avoiding the pharmacokinetic pitfalls typically associated with actively targeted nanoparticles. Although the radioimmunotherapy field has offered substantial evidence supporting the pretargeting strategy, its application for enhancing targeted delivery of nanoparticle therapeutics remains underexplored to date. We believe further rigorous evaluation of pretargeted NP systems is both warranted and needed to confirm whether pretargeting can indeed prove superior to current passive and active targeting approaches.

REFERENCES

1. Bertrand N, Wu J, Xu X, Kamaly N, Farokhzad OC. Cancer nanotechnology: The impact of passive and active targeting in the era of modern cancer biology. *Adv Drug Deliv Rev*. 2014;66:2-25.

2. Bae YH, Park K. Targeted drug delivery to tumors: Myths, reality and possibility. *J Control Release*. 2011;153(3):198-205.

3. Venditto VJ, Szoka Jr FC. Cancer nanomedicines: So many papers and so few drugs! *Adv Drug Deliv Rev*. 2013;65:80-88.

4. Stapleton S, Milosevic M, Tannock IF, Allen C, Jaffray DA. The intra-tumoral relationship between microcirculation, interstitial fluid pressure and liposome accumulation. *J Control Release*. 2015;211:163-170.

5. Yuan F, Leunig M, Huang SK, Berk DA, Papahadjopoulos D, Jain RK. Microvascular permeability and interstitial penetration of sterically stabilized (stealth) liposomes in a human tumor xenograft. *Cancer Res*. 1994;54:3352-3356.

6. Janku F. Tumor heterogeneity in the clinic: is it a real problem? *Ther Adv Med Oncol*. 2014;6(2):43-51.

7. Bedard PL, Hansen AR, Ratain MJ, Siu LL. Tumour heterogeneity in the clinic. *Nature*. 2013;501(7467):355-364.

8. Ding L, Ley TJ, Larson DE, et al. Clonal evolution in relapsed acute myeloid leukaemia revealed by whole-genome sequencing. *Nature*. 2012;481:506-510.

9. Blatter S, Rottenberg S. Minimal residual disease in cancer therapy – Small things make all the difference. *Drug Resist Updat*. 2015.

10. Fu F, Nowak MA, Bonhoeffer S. Spatial Heterogeneity in Drug Concentrations Can Facilitate the Emergence of Resistance to Cancer Therapy. *PLoS Comput Biol*. 2015;11:e1004142.

11. Matsumura Y, Maeda H. A new concept for macromolecular therapeutics in cancer chemotherapy: mechanism of tumoritropic accumulation of proteins and the antitumor agent smancs. *Cancer Res*. 1986;46:6387-6392.

12. Fang J, Nakamura H, Maeda H. The EPR effect: Unique features of tumor blood vessels for drug delivery, factors involved, and limitations and augmentation of the effect. *Adv Drug Deliv Rev*. 2011;63(3):136-151.

13. Kobayashi H, Watanabe R, Choyke PL. Improving conventional enhanced permeability and retention (EPR) effects; what is the appropriate target? *Theranostics*. 2013;4:81-89.

14. Torchilin V. Tumor delivery of macromolecular drugs based on the EPR effect. *Adv Drug Deliv Rev*. 2011;63(3):131-135.

15. Toy R, Peiris PM, Ghaghada KB, Karathanasis E. Shaping cancer nanomedicine: the effect of particle shape on the in vivo journey of nanoparticles. *Nanomedicine (Lond)*. 2014;9:121-134.

16. Banerjee D, Harfouche R, Sengupta S. Nanotechnology-mediated targeting of tumor angiogenesis. *Vasc Cell*. 2011;3:3.

17. Phillips MA, Gran ML, Peppas NA. Targeted Nanodelivery of Drugs and Diagnostics. *Nano Today*. 2010;5:143-159.

18. Torchilin VP. Passive and active drug targeting: drug delivery to tumors as an example. *Handb Exp Pharmacol*. 2010:3-53.

19. Amoozgar Z, Park J, Lin Q, Yeo Y. Low Molecular-Weight Chitosan as a pH-Sensitive Stealth Coating for Tumor-Specific Drug Delivery. *Mol Pharm*. 2012;9:1262-1270.

20. Passirani C, Barratt G, Devissaguet JP, Labarre D. Long-circulating nanoparticles bearing heparin or dextran covalently bound to poly(methyl methacrylate). *Pharm Res*. 1998;15:1046-1050.

21. Takeuchi H, Kojima H, Yamamoto H, Kawashima Y. Evaluation of circulation profiles of liposomes coated with hydrophilic polymers having different molecular weights in rats. *J Control Release*. 2001;75:83-91.

22. Torchilin VP, Trubetskoy VS, Whiteman KR, Caliceti P, Ferruti P, Veronese FM. New synthetic amphiphilic polymers for steric protection of liposomes in vivo. *J Pharm Sci*. 1995;84:1049-1053.

23. Cao Z, Zhang L, Jiang S. Superhydrophilic zwitterionic polymers stabilize liposomes. *Langmuir*. 2012;28:11625-11632.

24. Salmaso S, Caliceti P. Stealth properties to improve therapeutic efficacy of drug nanocarriers. *J Drug Deliv*. 2013;2013:374252.

25. Zalipsky S, Hansen CB, Oaks JM, Allen TM. Evaluation of blood clearance rates and biodistribution of poly(2-oxazoline)-grafted liposomes. *J Pharm Sci*. 1996;85:133-137.

26. Amoozgar Z, Yeo Y. Recent advances in stealth coating of nanoparticle drug delivery systems. *Wiley Interdiscip Rev Nanomed Nanobiotechnol*. 2012;4:219-233.

27. Kopecek J, Kopeckova P. HPMA copolymers: origins, early developments, present, and future. *Adv Drug Deliv Rev*. 2010;62:122-149.

28. Jäger E, Jäger A, Chytil P, et al. Combination chemotherapy using core-shell nanoparticles through the self-assembly of HPMA-based copolymers and degradable polyester. *J Control Release*. 2013;165:153-161.

29. Choi KY, Min KH, Na JH, et al. Self-assembled hyaluronic acid nanoparticles as a potential drug carrier for cancer therapy: synthesis, characterization, and in vivo biodistribution. *J Mater Chem*. 2009;19:4102-4107.

30. Maeda H. Toward a full understanding of the EPR effect in primary and metastatic tumors as well as issues related to its heterogeneity. *Adv Drug Deliv Rev*. 2015.

31. Konno TT, Maeda H, Iwai K, et al. Selective targeting of anti-cancer drug and simultaneous image enhancement in solid tumors by arterially administered lipid contrast medium. *Cancer*. 1984;54:2367-2374.

32. Fenton BM, Paoni SF, Beauchamp BK, Ding I. Zonal image analysis of tumour vascular perfusion, hypoxia, and necrosis. *Br J Cancer*. 2002;86:1831-1836.

33. Jiang L, Greenwood TR, Artemov D, et al. Localized hypoxia results in spatially heterogeneous metabolic signatures in breast tumor models. *Neoplasia*. 2012;14:732-741.

34. Ekdawi SN, Stewart JM, Dunne M, et al. Spatial and temporal mapping of heterogeneity in liposome uptake and microvascular distribution in an orthotopic tumor xenograft model. *J Control Release*. 2015;207:101-111.

35. Stapleton S, Allen C, Pintilie M, Jaffray DA. Tumor perfusion imaging predicts the intra-tumoral accumulation of liposomes. *J Control Release*. 2013;172:351-357.

36. Huynh E, Zheng G. Cancer nanomedicine: addressing the dark side of the enhanced permeability and retention effect. *Nanomedicine (Lond)*. 2015:1-3.

37. Prabhakar U, Maeda H, Jain RK, et al. Challenges and key considerations of the enhanced permeability and retention effect for nanomedicine drug delivery in oncology. *Cancer Res*. 2013;73:2412-2417.

38. Bazak R, Houri M, El Achy S, Kamel S, Refaat T. Cancer active targeting by nanoparticles: a comprehensive review of literature. *J Cancer Res Clin Oncol*. 2015;141:769-784.

39. Fiandra L, Mazzucchelli S, De Palma C, et al. Assessing the in vivo targeting efficiency of multifunctional nanoconstructs bearing antibody-derived ligands. *ACS Nano*. 2013;7:6092-6102.

40. Hoang B, Ekdawi SN, Reilly RM, Allen C. Active targeting of block copolymer micelles with trastuzumab Fab fragments and nuclear localization signal leads to increased tumor uptake and nuclear localization in HER2-overexpressing xenografts. *Mol Pharm*. 2013;10:4229-4241.

41. Sayari E, Dinarvand M, Amini M, et al. MUC1 aptamer conjugated to chitosan nanoparticles, an efficient targeted carrier designed for anticancer SN38 delivery. *Int J Pharm*. 2014;473:304-315.

42. Shen YA, Liu CS, Chang YH, et al. Subtype-specific binding peptides enhance the therapeutic efficacy of nanomedicine in the treatment of ovarian cancer. *Cancer Lett*. 2015;360:39-47.

43. David A, Kopeckova P, Kopecek J, Rubinstein A. The role of galactose, lactose, and galactose valency in the biorecognition of N-(2-hydroxypropyl)methacrylamide copolymers by human colon adenocarcinoma cells. *Pharm Res*. 2002;19:1114-1122..

44. Wu G, Wang Z, Bian X, Du X, Wei C. Folate-modified doxorubicin-loaded nanoparticles for tumor-targeted therapy. *Pharm Biol*. 2014;52:978-982.

45. Allen TM. Ligand-targeted therapeutics in anticancer therapy. *Nat Rev Cancer*. 2002;2:750-763.

46. Beech JR, Shin SJ, Smith JA, Kelly KA. Mechanisms for targeted delivery of nanoparticles in cancer. *Curr Pharm Des*. 2013;19:6560-6574.

47. Cheng Z, Al Zaki A, Hui JZ, Muzykantov VR, Tsourkas A. Multifunctional Nanoparticles: Cost Versus Benefit of Adding Targeting and Imaging Capabilities. *Science*. 2012;338:903-910.

48. Gu F, Zhang L, Teply BA, et al. Precise engineering of targeted nanoparticles by using self-assembled biointegrated block copolymers. *Proc Natl Acad Sci U S A*. 2008;105:2586-2591.

49. Elias DR, Poloukhtine A, Popik V, Tsourkas A. Effect of ligand density, receptor density, and nanoparticle size on cell targeting. *Nanomedicine Nanotechnology, Biol Med*. 2013;9:194-201.

50. Fakhari A, Baoum A, Siahaan TJ, Le KB, Berkland C. Controlling Ligand Surface Density Optimizes Nanoparticle Binding to ICAM-1. *J Pharm Sci*. 2011;100(3):1045-1056.

51. Moradi E, Vllasaliu D, Garnett M, Falcone F, Stolnik S. Ligand density and clustering effects on endocytosis of folate modified nanoparticles. *RSC Adv*. 2012;2(7):3025-3033.

52. Denison and You Han Bae. Cancer Targeted Drug Delivery. TA. Heterogeneity of Cancers and Its Implication for Targeted Drug Delivery. *Springer*. 2013:337-362.

53. Junttila MR, De Sauvage FJ. Influence of tumour micro-environment heterogeneity on therapeutic response. *Nature*. 2013.

54. Smith MP, Sanchez-Laorden B, O'Brien K, et al. The immune microenvironment confers resistance to MAPK pathway inhibitors through macrophage-derived TNFalpha. *Cancer Discov*. 2014;4:1214-1229.

55. Jung Y, Kim JK, Shiozawa Y, et al. Recruitment of mesenchymal stem cells into prostate tumours promotes metastasis. *Nat Commun*. 2013;4:1795.

56. Jamal-Hanjani M, Quezada SA, Larkin J, Swanton C. Translational implications of tumor heterogeneity. *Clin Cancer Res*. 2015;21:1258-1266.

57. Lee HJ, Seo AN, Kim EJ, et al. HER2 heterogeneity affects trastuzumab responses and survival in patients with HER2-positive metastatic breast cancer. *Am J Clin Pathol*. 2014;142:755-766.

58. Ding L, Ellis MJ, Li S, et al. Genome remodelling in a basal-like breast cancer metastasis and xenograft. *Nature*. 2010;464:999-1005.

59. Albino AP, Lloyd KO, Houghton AN, Oettgen HF, Old LJ. Heterogeneity in surface antigen and glycoprotein expression of cell lines derived from different melanoma metastases of the same patient. Implications for the study of tumor antigens. *J Exp Med*. 1981;154:1764-1778.

60. Gerlinger M, Rowan AJ, Horswell S, et al. Intratumor heterogeneity and branched evolution revealed by multiregion sequencing. *N Engl J Med*. 2012;366:883-892.

61. Arslan C, Sari E, Aksoy S, Altundag K. Variation in hormone receptor and HER-2 status between primary and metastatic breast cancer: review of the literature. *Expert Opin Ther Targets*. 2011;15:21-30.

62. Meacham CE, Morrison SJ. Tumour heterogeneity and cancer cell plasticity. *Nature*. 2013;501:328-337.

63. Jakobsen JN, Sorensen JB. Intratumor heterogeneity and chemotherapy-induced changes in EGFR status in non-small cell lung cancer. *Cancer Chemother Pharmacol*. 2012;69:289-299.

64. Taniguchi K, Okami J, Kodama K, Higashiyama M, Kato K. Intratumor heterogeneity of epidermal growth factor receptor mutations in lung cancer and its correlation to the response to gefitinib. *Cancer Sci*. 2008;99:929-935.

65. Schwarz RF, Ng CK, Cooke SL, et al. Spatial and temporal heterogeneity in high-grade serous ovarian cancer: a phylogenetic analysis. *PLoS Med*. 2015;12:e1001789.

66. Choi YP, Shim HS, Gao MQ, Kang S, Cho NH. Molecular portraits of intratumoral heterogeneity in human ovarian cancer. *Cancer Lett*. 2011;307:62-71.

67. Vogelstein B, Papadopoulos N, Velculescu VE, Zhou S, Diaz Jr. LA, Kinzler KW. Cancer genome landscapes. *Science*. 2013;339:1546-1558.

68. Liu J, Lau SK, Varma VA, et al. Molecular mapping of tumor heterogeneity on clinical tissue specimens with multiplexed quantum dots. *ACS Nano*. 2010;4:2755-2765.

69. Yang ZZ, Grote DM, Ziesmer SC, Xiu B, Novak AJ, Ansell SM. PD-1 expression defines two distinct T-cell sub-populations in follicular lymphoma that differentially impact patient survival. *Blood Cancer J*. 2015;5:e281.

70. Yap TA, Gerlinger M, Futreal PA, Pusztai L, Swanton C. Intratumor heterogeneity: seeing the wood for the trees. *Sci Transl Med*. 2012;4:127ps10.

71. van de Watering FC, Rijpkema M, Robillard M, Oyen WJ, Boerman OC. Pretargeted imaging and radioimmunotherapy of cancer using antibodies and bioorthogonal chemistry. *Front Med*. 2014;1:44.

72. Walter RB, Press OW, Pagel JM. Pretargeted radioimmunotherapy for hematologic and other malignancies. *Cancer Biother Radiopharm*. 2010;25(2):125-142.

73. Goldenberg DM, Chang CH, Rossi EA, J W, McBride, Sharkey RM. Pretargeted molecular imaging and radioimmunotherapy. *Theranostics*. 2012;2:523-540.

74. Green DJ, Pagel JM, Pantelias A, et al. Pretargeted radioimmunotherapy for B-cell lymphomas. *Clin Cancer Res*. 2007;13:5598s-5603s.

75. Pagel JM, Hedin N, Subbiah K, et al. Comparison of anti-CD20 and anti-CD45 antibodies for conventional and pretargeted radioimmunotherapy of B-cell lymphomas. *Blood*. 2003;101:2340-2348.

76. Green DJ, Pagel JM, Nemecek ER, et al. Pretargeting CD45 enhances the selective delivery of radiation to hematolymphoid tissues in nonhuman primates. *Blood*. 2009;114:1226-1235.

77. Pagel JM, Matthews DC, Kenoyer A, et al. Pretargeted radioimmunotherapy using anti-CD45 monoclonal antibodies to deliver radiation to murine hematolymphoid tissues and human myeloid leukemia. *Cancer Res*. 2009;69:185-192.

78. Pagel JM, Kenoyer AL, Back T, et al. Anti-CD45 pretargeted radioimmunotherapy using bismuth-213: high rates of complete remission and long-term survival in a mouse myeloid leukemia xenograft model. *Blood*. 2011;118:703-711.

79. Pagel JM, Orgun N, Hamlin DK, et al. A comparative analysis of conventional and pretargeted radioimmunotherapy of B-cell lymphomas by targeting CD20, CD22, and HLA-DR singly and in combinations. *Blood*. 2009;113:4903-4913.

80. Pagel JM, Pantelias A, Hedin N, et al. Evaluation of CD20, CD22, and HLA-DR targeting for radioimmunotherapy of B-cell lymphomas. *Cancer Res*. 2007;67:5921-5928.

81. Green DJ, Orgun NN, Jones JC, et al. A preclinical model of CD38-pretargeted radioimmunotherapy for plasma cell malignancies. *Cancer Res*. 2014;74:1179-1189.

82. Subbiah K, Hamlin DK, Pagel JM, et al. Comparison of immunoscintigraphy, efficacy, and toxicity of conventional and pretargeted radioimmunotherapy in CD20-expressing human lymphoma xenografts. *J Nucl Med*. 2003;44:437-445.

83. Zhang M, Zhang Z, Garmestani K, et al. Pretarget radiotherapy with an anti-CD25 antibody-streptavidin fusion protein was effective in therapy of leukemia/lymphoma xenografts. *Proc Natl Acad Sci U S A*. 2003;100(4):1891-1895.

84. Axworthy DB, Reno JM, Hylarides MD, et al. Cure of human carcinoma xenografts by a single dose of pretargeted yttrium-90 with negligible toxicity. *Proc Natl Acad Sci U S A*. 2000;97:1802-1807.

85. Forero A, Weiden PL, Vose JM, et al. Phase 1 trial of a novel anti-CD20 fusion protein in pretargeted radioimmunotherapy for B-cell non-Hodgkin lymphoma. *Blood*. 2004;104(1):227-236.

86. Weiden PL, Breitz HB, Press O, et al. Pretargeted radioimmunotherapy (PRIT) for treatment of non-Hodgkin's lymphoma (NHL): initial phase I/II study results. *Cancer Biother Radiopharm*. 2000;15:15-29.

87. Weiden PL, Breitz HB. Pretargeted radioimmunotherapy (PRIT) for treatment of non-Hodgkin's lymphoma (NHL). *Crit Rev Oncol Hematol*. 2001;40:37-51.

88. Kraeber-Bodere F, Bardet S, Hoefnagel CA, et al. Radioimmunotherapy in medullary thyroid cancer using bispecific antibody and iodine 131-labeled bivalent hapten: preliminary results of a phase I/II clinical trial. *Clin Cancer Res*. 1999;5:3190s-3198s.

89. Kraeber-Bodere F, Faivre-Chauvet A, Sai-Maurel C, et al. Toxicity and efficacy of radioimmunotherapy in carcinoembryonic antigen-producing medullary thyroid cancer xenograft: comparison of iodine 131-labeled F(ab')2 and pretargeted bivalent hapten and evaluation of repeated injections. *Clin Cancer Res*. 1999;5:3183s-3189s.

90. Kraeber-Bodere F, Rousseau C, Bodet-Milin C, et al. Targeting, toxicity, and efficacy of 2-step, pretargeted radioimmunotherapy using a chimeric bispecific antibody and 131I-labeled bivalent hapten in a phase I optimization clinical trial. *J Nucl Med*. 2006;47:247-255.

91. Society AC. Cancer Facts & Figures. 2015.

92. Swain SM, Kim SB, Cortes J, et al. Pertuzumab, trastuzumab, and docetaxel for HER2-positive metastatic breast cancer (CLEOPATRA study): overall survival results from a randomised, double-blind, placebo-controlled, phase 3 study. *Lancet Oncol*. 2013;14:461-471.

93. Koyama Y, Barrett T, Hama Y, Ravizzini G, Choyke PL, Kobayashi H. In vivo molecular imaging to diagnose and subtype tumors through receptor-targeted optically labeled monoclonal antibodies. *Neoplasia*. 2007;9:1021-1029.

94. Barrett T, Koyama Y, Hama Y, et al. In vivo Diagnosis of Epidermal Growth Factor Receptor Expression using Molecular Imaging with a Cocktail of Optically Labeled Monoclonal Antibodies. *Clin Cancer Res*. 2007;13:6639-6648.

95. Haun JB, Devaraj NK, Hilderbrand SA, Lee H, Weissleder R. Bioorthogonal chemistry amplifies nanoparticle binding and enhances the sensitivity of cell detection. *Nat Nanotechnol*. 2010;5:660-665.

96. Karver MR, Weissleder R, Hilderbrand SA. Bioorthogonal reaction pairs enable simultaneous, selective, multi-target imaging. *Angew Chem Int Ed Engl*. 2012;51:920-922.

97. Khaw BA, Gada KS, Patil V, et al. Bispecific antibody complex pre-targeting and targeted delivery of polymer drug conjugates for imaging and therapy in dual human mammary cancer xenografts: targeted polymer drug conjugates for cancer diagnosis and therapy. *Eur J Nucl Med Mol Imaging*. 2014;41:1603-1616.

98. Reardan DT, Meares CF, Goodwin DA, et al. Antibodies against metal chelates. *Nature*. 1985;316:265-268.

99. Goodwin DA, Meares CF, McCall MJ, McTigue M, Chaovapong W. Pre-targeted immunoscintigraphy of murine tumors with indium-111-labeled bifunctional haptens. *J Nucl Med*. 1988;29:226-234.

100. Karacay H, Sharkey RM, McBride WJ, et al. Pretargeting for Cancer Radioimmunotherapy with Bispecific Antibodies: Role of the Bispecific Antibody's Valency for the Tumor Target Antigen. *Bioconjug Chem*. 2002;13:1054-1070.

101. van Schaijk FG, Oosterwijk E, Molkenboer-Kuenen JD, et al. Pretargeting with Bispecific Anti-Renal Cell Carcinoma x Anti-DTPA(In) Antibody in 3 RCC Models. *J Nucl Med*. 2005;46:495-501.

102. Gestin JF, Loussouarn A, Bardies M, et al. Two-step targeting of xenografted colon carcinoma using a bispecific antibody and 188Re-labeled bivalent hapten: biodistribution and dosimetry studies. *J Nucl Med*. 2001;42:146-153.

103. Hillairet de Boisferon M, Raguin O, Dussaillant M, Rostène W, Barbet J, Gruaz-Guyon A. Enhanced Targeting Specificity to Tumor Cells by Simultaneous Recognition of Two Antigens. *Bioconjug Chem*. 2000;11:452-460.

104. McBride WJ, Zanzonico P, Sharkey RM, et al. Bispecific antibody pretargeting PET (immunoPET) with an 124I-labeled hapten-peptide. *J Nucl Med*. 2006;47:1678-1688.

105. Pimm M V, Robins RA, Embleton MJ, et al. A bispecific monoclonal antibody against methotrexate and a human tumour associated antigen augments cytotoxicity of methotrexate-carrier conjugate. *Br J Cancer*. 1990;61:508-513.

106. Yoon S, Kim YH, Kang SH, et al. Bispecific Her2 x cotinine antibody in combination with cotinine-(histidine)2-iodine for the pre-targeting of Her2-positive breast cancer xenografts. *J Cancer Res Clin Oncol*. 2014;140:227-233.

107. Gada KS, Patil V, Panwar R, Hatefi A, Khaw BA. Bispecific antibody complex pre-targeted delivery of polymer-drug conjugates for cancer therapy. *Drug Deliv Transl Res*. 2012;2:65-76.

108. Le Doussal JM, Martin M, Gautherot E, Delaage M, Barbet J. In vitro and in vivo targeting of radiolabeled monovalent and divalent haptens with dual specificity monoclonal antibody conjugates: enhanced divalent hapten affinity for cell-bound antibody conjugate. *J Nucl Med*. 1989;30:1358-1366.

109. Janevik-Ivanovska E, Gautherot E, Hillairet de Boisferon M, et al. Bivalent hapten-bearing peptides designed for iodine-131 pretargeted radioimmunotherapy. *Bioconjug Chem*. 1997;8:526-533.

110. Boerman OC, Kranenborg MH, Oosterwijk E, et al. Pretargeting of renal cell carcinoma: improved tumor targeting with a bivalent chelate. *Cancer Res*. 1999;59:4400-4405.

111. Lesch HP, Kaikkonen MU, Pikkarainen JT, Yla-Herttuala S. Avidin-biotin technology in targeted therapy. *Expert Opin Drug Deliv*. 2010;7:551-564.

112. Pimm M V, Fells HF, Perkins AC, Baldwin RW. Iodine-131 and indium-111 labelled avidin and streptavidin for pre-targetted immunoscintigraphy with biotinylated anti-tumour monoclonal antibody. *Nucl Med Commun*. 1988;9:931-941.

113. Newton-Northup JR, Figueroa SD, Quinn TP, Deutscher SL. Bifunctional phage-based pretargeted imaging of human prostate carcinoma. *Nucl Med Biol*. 2009;36:789-800.

114. Knox SJ, Goris ML, Tempero M, et al. Phase II trial of yttrium-90-DOTA-biotin pretargeted by NR-LU-10 antibody/streptavidin in patients with metastatic colon cancer. *Clin Cancer Res*. 2000;6:406-414.

115. Lin Y, Pagel JM, Axworthy D, Pantelias A, Hedin N, Press OW. A genetically engineered anti-CD45 single-chain antibody-streptavidin fusion protein for pretargeted radioimmunotherapy of hematologic malignancies. *Cancer Res*. 2006;66(7):3884-3892.

116. Cheung NK, Modak S, Lin Y, et al. Single-chain Fv-streptavidin substantially improved therapeutic index in multistep targeting directed at disialoganglioside GD2. *J Nucl Med*. 2004;45:867-877.

117. Pagel JM, Lin Y, Hedin N, et al. Comparison of a tetravalent single-chain antibody-streptavidin fusion protein and an antibody-streptavidin chemical conjugate for pretargeted anti-CD20 radioimmunotherapy of B-cell lymphomas. *Blood*. 2006;108(1):328-336.

118. Stachler MD, Chen I, Ting AY, Bartlett JS. Site-specific modification of AAV vector particles with biophysical probes and targeting ligands using biotin ligase. *Mol Ther*. 2008;16:1467-1473.

119. Kalofonos HP, Rusckowski M, Siebecker DA, et al. Imaging of tumor in patients with indium-111-labeled biotin and streptavidin-conjugated antibodies: preliminary communication. *J Nucl Med*. 1990;31:1791-1796.

120. Yumura K, Ui M, Doi H, et al. Mutations for decreasing the immunogenicity and maintaining the function of core streptavidin. *Protein Sci*. 2013;22:213-221.

121. Wilbur DS, Park SI, Chyan MK, et al. Design and synthesis of bis-biotin-containing reagents for applications utilizing monoclonal antibody-based pretargeting systems with streptavidin mutants. *Bioconjug Chem*. 2010;21:1225-1238.

122. Meyer DL, Schultz J, Lin Y, et al. Reduced antibody response to streptavidin through site-directed mutagenesis. *Protein Sci*. 2001;10:491-503.

123. Rusckowski M, Fogarasi M, Fritz B, Hnatowich DJ. Effect of endogenous biotin on the applications of streptavidin and biotin in mice. *Nucl Med Biol*. 1997;24:263-268.

124. Hamblett KJ, Press OW, Meyer DL, et al. Role of biotin-binding affinity in streptavidin-based pretargeted radioimmunotherapy of lymphoma. *Bioconjug Chem*. 2005;16:131-138.

125. Steiner M, Gutbrodt K, Krall N, Neri D. Tumor-targeting antibody-anticalin fusion proteins for in vivo pretargeting applications. *Bioconjug Chem*. 2013;24:234-241.

126. Knight JC, Mosley M, Stratford MR, et al. Development of an enzymatic pretargeting strategy for dual-modality imaging. *Chem Commun*. 2015;51:4055-4058.

127. Liu G, Dou S, Liu Y, Wang Y, Rusckowski M, Hnatowich DJ. 90Y labeled phosphorodiamidate morpholino oligomer for pretargeting radiotherapy. *Bioconjug Chem*. 2011;22:2539-2545.

128. Liu G, Dou S, Pretorius PH, et al. Tumor pretargeting in mice using MORF conjugated CC49 antibody and radiolabeled complimentary cMORF effector. *Q J Nucl Med Mol Imaging*. 2010;54:333-340.

129. Liu G, Liu C, Zhang S, et al. Investigations of 99mTc morpholino pretargeting in mice. *Nucl Med Commun*. 2003;24:697-705.

130. Liu G, He J, Dou S, Gupta S, Rusckowski M, Hnatowich DJ. Further investigations of morpholino pretargeting in mice--establishing quantitative relations in tumor. *Eur J Nucl Med Mol Imaging*. 2005;32:1115-1123.

131. He J, Liu G, Gupta S, Zhang Y, Rusckowski M, Hnatowich DJ. Amplification Targeting: A Modified Pretargeting Approach with Potential for Signal Amplification—Proof of a Concept. *J Nucl Med*. 2004;45:1087-1095.

132. Sharkey RM, Goldenberg DM. Cancer radioimmunotherapy. *Immunotherapy*. 2011;3:349-370.

133. He J, Wang Y, Dou S, et al. Affinity enhancement pretargeting: synthesis and testing of a 99mTc-labeled bivalent MORF. *Mol Pharm*. 2010;7:1118-1124.

134. Carroll L, Evans HL, Aboagye EO, Spivey AC. Bioorthogonal chemistry for pre-targeted molecular imaging--progress and prospects. *Org Biomol Chem*. 2013;11:5772-5781.

135. Knight JC, Cornelissen B. Bioorthogonal chemistry: implications for pretargeted nuclear (PET/SPECT) imaging and therapy. *Am J Nucl Med Mol Imaging*. 2014;4:96-113.

136. Rossin R, Verkerk Renart P, van den Bosch SM, et al. In Vivo Chemistry for Pretargeted Tumor Imaging in Live Mice. *Angew Chemie Int Ed*. 2010;49:3375-3378.

137. Rossin R, van Duijnhoven SM, Lappchen T, van den Bosch SM, Robillard MS. Trans-cyclooctene tag with improved properties for tumor pretargeting with the diels-alder reaction. *Mol Pharm*. 2014;11:3090-3096.

138. Zeglis BM, Sevak KK, Reiner T, et al. A pretargeted PET imaging strategy based on bioorthogonal Diels-Alder click chemistry. *J Nucl Med*. 2013;54:1389-1396.

139. Lee SB, Kim HL, Jeong H-J, Lim ST, Sohn M-H, Kim DW. Mesoporous Silica Nanoparticle Pretargeting for PET Imaging Based on a Rapid Bioorthogonal Reaction in a Living Body. *Angew Chemie Int Ed*. 2013;52:10549-10552.

140. Gunn J, Park SI, Veiseh O, Press OW, Zhang M. A pretargeted nanoparticle system for tumor cell labeling. *Mol Biosyst*. 2011;7:742-748.

141. Chu TW, Yang J, Zhang R, Sima M, Kopecek J. Cell surface self-assembly of hybrid nanoconjugates via oligonucleotide hybridization induces apoptosis. *ACS Nano*. 2014;8:719-730.

142. Nobs L, Buchegger F, Gurny R, Allemann E. Biodegradable nanoparticles for direct or two-step tumor immunotargeting. *Bioconjug Chem*. 2006;17:139-145.

143. Bushman J, Vaughan A, Sheihet L, Zhang Z, Costache M, Kohn J. Functionalized nanospheres for targeted delivery of paclitaxel. *J Control Release*. 2013;171:315-321.

144. PULKKINEN M, PIKKARAINEN J, WIRTH T, et al. Three-step tumor targeting of paclitaxel using biotinylated PLA-PEG nanoparticles and avidin–biotin technology: Formulation development and in vitro anticancer activity. *Eur J Pharm Biopharm*. 2008;70(1):66-74.

145. Longman SA, Cullis PR, Choi L, de Jong G, Bally MB. A two-step targeting approach for delivery of doxorubicin-loaded liposomes to tumour cells in vivo. *Cancer Chemother Pharmacol*. 1995;36:91-101.

146. Frost SH, Jensen H, Lindegren S. In vitro evaluation of avidin antibody pretargeting using 211At-labeled and biotinylated poly-L-lysine as effector molecule. *Cancer*. 2010;116:1101-1110.

147. Cao Y, Suresh MR. Bispecific MAb aided liposomal drug delivery. *J Drug Target*. 2000;8:257-266.

148. Mulvey JJ, Villa CH, McDevitt MR, Escorcia FE, Casey E, Scheinberg DA. Self-assembly of carbon nanotubes and antibodies on tumours for targeted amplified delivery. *Nat Nanotechnol*. 2013;8:763-771.

149. Rahim MK, Kota R, Haun JB. Enhancing reactivity for bioorthogonal pretargeting by unmasking antibody-conjugated trans-cyclooctenes. *Bioconjug Chem*. 2015;26:352-360.

150. Navarro-Teulon I, Lozza C, Pelegrin A, Vives E, Pouget JP. General overview of radioimmunotherapy of solid tumors. *Immunotherapy*. 2013;5:467-487.

151. Sato N, Hassan R, Axworthy DB, et al. Pretargeted radioimmunotherapy of mesothelin-expressing cancer using a tetravalent single-chain Fv-streptavidin fusion protein. *J Nucl Med*. 2005;46:1201-1209.

152. Goldenberg DM, Rossi EA, Sharkey RM, McBride WJ, Chang CH. Multifunctional antibodies by the Dock-and-Lock method for improved cancer imaging and therapy by pretargeting. *J Nucl Med*. 2008;49:158-163.

153. Sharkey RM, Karacay H, Litwin S, et al. Improved therapeutic results by pretargeted radioimmunotherapy of non-Hodgkin's lymphoma with a new recombinant, trivalent, anti-CD20, bispecific antibody. *Cancer Res*. 2008;68:5282-5290.

154. Sharkey RM, Primus FJ, Goldenberg DM. Second antibody clearance of radiolabeled antibody in cancer radioimmunodetection. *Proc Natl Acad Sci U S A*. 1984;81:2843-2846.

155. Mirallié E, Saï-Maurel C, Faivre-Chauvet A, et al. Improved pretargeted delivery of radiolabelled hapten to human tumour xenograft in mice by avidin chase of circulating bispecific antibody. *Eur J Nucl Med Mol Imaging*. 2005;32:901-909.

156. Breitz HB, Weiden PL, Beaumier PL, et al. Clinical optimization of pretargeted radioimmunotherapy with antibody-streptavidin conjugate and 90Y-DOTA-biotin. *J Nucl Med*. 2000;41:131-140.

157. Liu G, Dou S, Chen X, et al. Adding a clearing agent to pretargeting does not lower the tumor accumulation of the effector as predicted. *Cancer Biother Radiopharm*. 2010;25:757-762.

158. Paganelli G, Grana C, Chinol M, et al. Antibody-guided three-step therapy for high grade glioma with yttrium-90 biotin. *Eur J Nucl Med*. 1999;26:348-357.

159. Grana C, Chinol M, Robertson C, et al. Pretargeted adjuvant radioimmunotherapy with yttrium-90-biotin in malignant glioma patients: a pilot study. *Br J Cancer*. 2002;86:207-212.

160. Goldenberg DM, Chatal JF, Barbet J, Boerman O, Sharkey RM. Cancer Imaging and Therapy with Bispecific Antibody Pretargeting. *Updat Cancer Ther*. 2007;2:19-31.

161. Sabatier R, Goncalves A, Bertucci F. Personalized medicine: present and future of breast cancer management. *Crit Rev Oncol Hematol*. 2014;91:223-233.

162. Pantelias A, Pagel JM, Hedin N, et al. Comparative biodistributions of pretargeted radioimmunoconjugates targeting CD20, CD22, and DR molecules on human B-cell lymphomas. *Blood*. 2007;109:4980-4987.

163. Witzig TE, Gordon LI, Cabanillas F, et al. Randomized controlled trial of yttrium-90-labeled ibritumomab tiuxetan radioimmunotherapy versus rituximab immunotherapy for patients with relapsed or refractory low-grade, follicular, or transformed B-cell non-Hodgkin's lymphoma. *J Clin Oncol*. 2002;20:2453-2463.

164. Jain M, Kamal N, Batra SK. Engineering antibodies for clinical applications. *Trends Biotechnol*. 2007;25:307-316.

CHAPTER 3: EFFECT OF MULTIVALENT INTERACTIONS BETWEEN FUSION PROTEINS AND CELL RECEPTORS ON NANOPARTICLE INTERNALIZATION[2]

3.1 Introduction

The primary goal of targeted drug delivery is to maximize the dose of therapeutic molecules in target tissues while minimizing exposure and toxicity in non-target tissues. A commonly exploited strategy, often referred to as "active targeting," involves conjugating ligands onto the surface of nanoparticle drug carriers. The expectation is that these nanocarriers can circulate in the bloodstream for sufficient duration such that they can extravasate, encounter, and bind to specific receptors on the surface of target cells.[1,2] Unfortunately, actively targeted nanoparticles often possess relatively poor circulation kinetics as a result of rapid clearance by the mononuclear phagocytic system (MPS), presumably because the presence of ligands on the particle surface compromises the otherwise stealth characteristics of polymeric coatings on these nanoparticles.[1,3–5] This in turn limits the fraction of nanoparticles that can reach and extravasate at target cells/tissues.[1] Inadequate nanoparticle targeting is further exacerbated by the fact that many diseases are comprised of heterogeneous populations of cells that cannot be effectively targeted by a single ligand.[4] These potential shortcomings of active targeting have led many investigators to explore alternative strategies to deliver nanoparticles to target cells/tissues, including ultrasound,[6] magnetic or electric fields,[7–9] and cell-based delivery systems.[10,11]

[2]This chapter previously appeared as an article in Acta Biomaterialia. The original citation is as follows: Parker CL, Yang Q, Yang B, McCallen JD, Park SI, Lai SK. "Multivalent interactions between streptavidin-based pretargeting fusion proteins and cell receptors impede efficient internalization of biotinylated nanoparticles." *Acta Biomaterialia* **2017**, 63, 181-189.

A well-established strategy for enhancing delivery of effector molecules to target cells is "pretargeting," a multi-step approach that takes advantage of molecules that bind both cellular epitopes and effector molecules. Specifically, bispecific antibody or fusion protein (BFP) molecules (henceforth abbreviated BFP) are first administered, with the expectation that they can circulate, extravasate, and accumulate on the surface of target cells, or otherwise be quickly eliminated from systemic circulation. The effector molecules are subsequently administered and captured by cell-bound BFP. This approach has been extensively studied for the treatment of hematological malignancies in pretargeted radioimmunotherapy (PRIT).[12] Multiple preclinical studies have shown that PRIT can lead to greater tumor-to-background ratios and reduced radioactivity in healthy organs compared to radiolabeled monoclonal antibodies used in conventional radioimmunotherapy, thereby improving imaging contrast and tumor suppression.[12–14] Additionally, several studies have reported promising results for pretargeting in diagnostic applications like PET[15–18] and optical imaging.[19,20] Despite substantial promise of PRIT for treatment of different hematological malignancies, pretargeting remains largely underexplored for use in improving targeting of nanoparticles.

An implicit requirement for effective pretargeting is that the BFP must remain on the cell surface until nanoparticles can extravasate from the circulation and reach target cells. This implies that the ideal BFP should bind cellular epitopes that are either non-internalizing, or at minimum very slowly internalizing. A natural and obvious concern with pretargeting is whether BFP bound to non-internalizing or slowly internalizing cellular epitopes can facilitate *intracellular* delivery of nanoparticles. This is particularly important because the cellular fate of nanoparticles can directly impact the type of therapeutics that can be effectively delivered via pretargeting. To investigate this question, we sought to evaluate whether BFP based on anti-

tumor-associated glycoprotein (TAG)-72 single chain variable fragments (scFvs) conjugated to streptavidin (SA) can facilitate intracellular delivery of biotin-functionalized polymeric nanoparticles to a T-cell leukemia cell line. TAG-72, which is highly overexpressed in several cancers including T-cell leukemia,[21,22] exhibits limited internalization and shedding,[23] making it an ideal cellular target for the pretargeted approach.

3.2 Materials and Methods

3.2.1 Cell lines and bispecific fusion proteins

Jurkat T-acute lymphoblastic leukemia cell line was obtained from the University of North Carolina at Chapel Hill Tissue Culture Facility, and cultured in RPMI 1640 medium (Gibco by Thermo Fisher, Grand Island, NY, USA) supplemented with 10% fetal bovine serum (Sigma-Aldrich, St. Louis, MO, USA) and 1% penicillin streptomycin (Gibco) at 37°C and 5% CO_2. BFP comprised of streptavidin (SA) linked to four scFvs against either CD20 (αCD20-SA) or TAG-72 (αTAG-72-SA) were kind gifts received from Oliver W. Press' group at Fred Hutchinson Cancer Research Cancer (Seattle, WA).[24]

3.2.2 Nanoparticle synthesis and characterization

Carboxylate-modified green fluorescent polystyrene (PS) beads with mean diameter of 100 nm were purchased from Thermo Fisher Scientific (Grand Island, NY, USA). Methoxy polyethylene glycol (PEG) amine (mPEG-NH_2, MW 3000 g/mol) and biotin PEG amine (biotin-PEG-NH_2, MW 3244 g/mol) were purchased from JenKem Technology (Beijing, China) and Rapp Polymere (Tuebingen, Germany), respectively. mPEG-NH2 and biotin-PEG-NH2 were conjugated to PS particles at varying molar ratios (0-100% biotin) using EDC coupling to

produce PS-PEG-biotin beads, as previously described.[25] To indirectly quantify PEG density, the number of residual COOH groups remaining after PEG conjugation was measured using fluorogenic 1-pyrenyldiazomethane, as previously described.[25] Hydrodynamic size and zeta potential of synthesized particles were determined by dynamic light scattering and laser Doppler anemometry, respectively, using a Zetasizer Nano (Malvern, U.K.). Nanoparticle size distribution and concentration were also determined by Nanoparticle Tracking Analysis technology using Malvern NanoSight NS500. For Nanosight characterization, each nanoparticle sample was diluted 1:200,000 in filtered PBS and run in 5 replicates.

3.2.3 Nanoparticles uptake measured by flow cytometry

Jurkat (TAG-72$^+$) cells were seeded in 96-well plates at a density of 100,000 cells/well, and treated with no FP, 500 nM control αCD20-SA BFP or 500 nM cell-specific αTAG-72-SA BFP for 4 hr at 37°C. After washing the cells three times with cold PBS to eliminate unbound BFP, cells were incubated with fluorescent PS-particles at a ratio of 10^4 beads/cell for 12 hr at 37°C or 4°C. Next, cells were washed twice with a cold acid buffer (0.2 M glycine, 0.15 M NaCl, pH 3.0) to further remove surface bound nanoparticles followed by three cold PBS washes. Samples were kept on ice until bead uptake was quantified by flow cytometry analysis (BD FACS Canto). 10,000 cells were counted per sample and the mean fluorescence intensity was measured for each sample.

3.2.4 Nanoparticle uptake measured by imaging flow cytometry

One million Jurkat cells per well were treated with 500 nM αTAG-72-SA BFP for 4 hr at 37°C. After removing unbound BFP by washing cells thrice with ice cold PBS, PS-PEG-biotin

(PS-PEGb) 100% nanoparticles (10^3 beads/cell) incubated with cells for 12 hr at either 37°C or 4°C. Three cold acid washes followed by three cold PBS washes were performed to remove unbound and surface associated nanoparticles (NP). We added 2 μg/ml Hoechst 33342 to live cells for nuclear staining, and resuspended cells in a final volume of 50-70 μl PBS prior to transferring to siliconized tubes. Samples were kept on ice until nanoparticle internalization was evaluated by Amnis ImageStream Flow Cytometer where 10,000 cells per sample were imaged. Amnis IDEAS software (v6.1) was used to quantify the average number of punctate fluorescent spots, corresponding to green NP, per cell.

3.2.5 Labeled BFP internalization kinetics

We fluorescently labeled 500 nM αTAG-72-SA BFP with 10 ug of fluorescent biotin (Atto488-biotin, Sigma-Aldrich) by mixing and rotating at room temperature in the dark for at least 1 hr, followed by filtration through Amicon filters (MWCO 30 kDa) to remove unconjugated Atto488-biotin from the final product. To assess the internalization kinetics of BFP, cells were incubated with fluorescently labeled BFP at various time points and later washed three times with cold PBS to eliminate unbound BFP. Cells were stained with 2 μg/ml of Hoechst 33342 and 1X Cell Mask Deep Red plasma membrane dye at 37°C prior to confocal imaging.

3.2.6 Confocal imaging of nanoparticles in cells

Live cell confocal microscopy was performed to measure the colocalization of pretargeted PS-PEGb nanoparticles in Jurkat cells to different intracellular markers, including early and late endosomes, lysosomes, and acidic vesicles. Early endosomes, late endosomes, and

lysosomes were stained with CellLight Rab5a-RFP, Rab7a-RFP, and Lamp1-RFP, BacMam 2.0 (Life Technology), respectively. Briefly, we seeded 80,000 Jurkat cells per well in a 96-well plate and treated cells with 24 μl CellLight-RFP reagents (40 particles per cell) overnight at 37°C to label intracellular markers, and then incubated with 75 μl of 1X BacMam enhancer 2.0 working solution for 2 hr at 37°C to boost expression of markers in Jurkat cells. BacMam enhancer working solution was removed and replaced with fresh media. After a 4-6 hr wait at 37°C, we incubated cells with 500 nM αTAG-72-SA BFP for 4 hr at 37°C. Then, unbound BFP were removed by PBS washes and cells were incubated with green fluorescent PS-PEGb 100% nanoparticles (10^4 beads/cell) for 12 hr at 37°C. Unbound NP were removed with cold PBS washes, and nuclei were subsequently labeled with 2 ug/ml Hoechst 33342 for 30 min at 37°C. We removed excess dye with two cold PBS washes and resuspended cells in OptiMEM. Cells were transferred to 8-chambered coverglass dishes (Nunc Lab-Tek), which were previously coated in poly-ι-lysine and exposed to UV light overnight for sterilization, then imaged on Olympus FluoView FV 1200 laser scanning confocal microscope. To label acidic vesicles, such as lysosomes, we stained cells with 500 nM LysoTracker red (Life Technology) for 30 min at 37°C and removed excess dye prior to confocal imaging. After BFP and NP incubations, we labeled cells with 1X CellMask Deep Red plasma membrane stain (Life Technology) at 37°C to evaluate particle uptake relative to the plasma membrane. Cells treated with unmodified carboxylate beads (PS-COOH) were included as a control for non-specific particle internalization. Note, some cells may appear slightly oblong due to association of Jurkat cells (a suspension cell) to coverglass coated with poly-ι-lysine necessary for imaging purposes.

3.2.7 Statistical methods

All data are presented as mean ± SD. All graphs and statistical tests were performed using Graph Pad 7 software. For flow cytometry data, group comparisons were analyzed using two-way ANOVA and *post hoc* Tukey's test. A student's t-test was performed on ImageStream spot count data. A p-value <0.05 was considered to indicate statistical significance.

3.3 Results

3.3.1 Pretargeted 100 nm nanoparticles associate tightly with cells but are poorly internalized

To investigate whether pretargeting can facilitate intracellular delivery of nanoparticles, we first incubated Jurkat (T-leukemia) cells with BFP based on streptavidin linked to 4 scFvs that bind TAG-72, followed by 100 nm polystyrene nanoparticles densely coated with biotin-polyethylene glycol (PS-PEGb) (Table 1).

Sample	Size (nm)	Average Diameter (nm)[a]	ζ (mV)[b]	PEG density (#/nm^2)[c]	Approx. number of biotin per NP
PS-COOH	100	151 ± 4	-69	0	0
PS-PEG-biotin 100%	100	176 ± 4	3	2.7	84,000
PS-PEG-biotin 50%	100	155 ± 2	-2	1.4	31,000
PS-PEG-biotin 20%	100	155 ± 6	-1	1.7	11,000

[a] Measured by Nanosight NS500
[b] Measured by electrophoretic light scattering (ZetaSizer)
[c] Calculated from fluorogenic PEG quantification assay (PDAM assay) [25]

Table 3.1.Nanoparticle characterization.

By flow cytometry, we observed markedly greater association of PS-PEGb fluorescence in Jurkat cells pretargeted with αTAG-72-SA than a control BFP that binds CD20, a common receptor on B-cells (αCD20-SA), confirming the specificity of the fusion protein to its cellular target (Figures 3.1A, B). We next compared nanoparticle association to cells at 37°C versus 4°C,

a temperature that generally blocks energy-dependent internalization mechanisms[26–29]; surface-bound nanoparticles were removed with pH 3.0 acid washes prior to flow cytometry.[30] When pretargeting cells with αTAG-72-SA BFP, we observed much greater level of mean fluorescence intensity of PS-PEGb incubated at 37°C than at 4°C (Figure 3.1B; $p<0.0001$), which is consistent with the notion that BFP can specifically facilitate nanoparticle internalization into Jurkat cells (Figure 3.2). Acid washes did not substantially reduce cell-associated fluorescence of PS-PEGb pretargeted with αTAG-72-SA at 37°C, seemingly implying that the fluorescent particles were not readily exposed on the cell surface (Fig 3.1B).

We next sought to validate that 100 nm PS-PEGb were internalizing into cells by directly visualizing the distribution of fluorescent particles in individual cells using Amnis ImageStream Flow Cytometer. Similar to flow cytometry studies, we found far greater cell-associated fluorescence when pretargeted nanoparticles were incubated with cells at 37°C than 4°C (Figure 3.1D). Surprisingly, rather than finding nanoparticle fluorescence localized within cells, images from ImageStream showed that the vast majority of nanoparticles were preferentially accumulated on the cell periphery (Figure 3.1C). The images suggest that pretargeted nanoparticles either remained on the surface of the cells, or were retained at or near the cell membrane, unable to be removed with repeated acid washes.

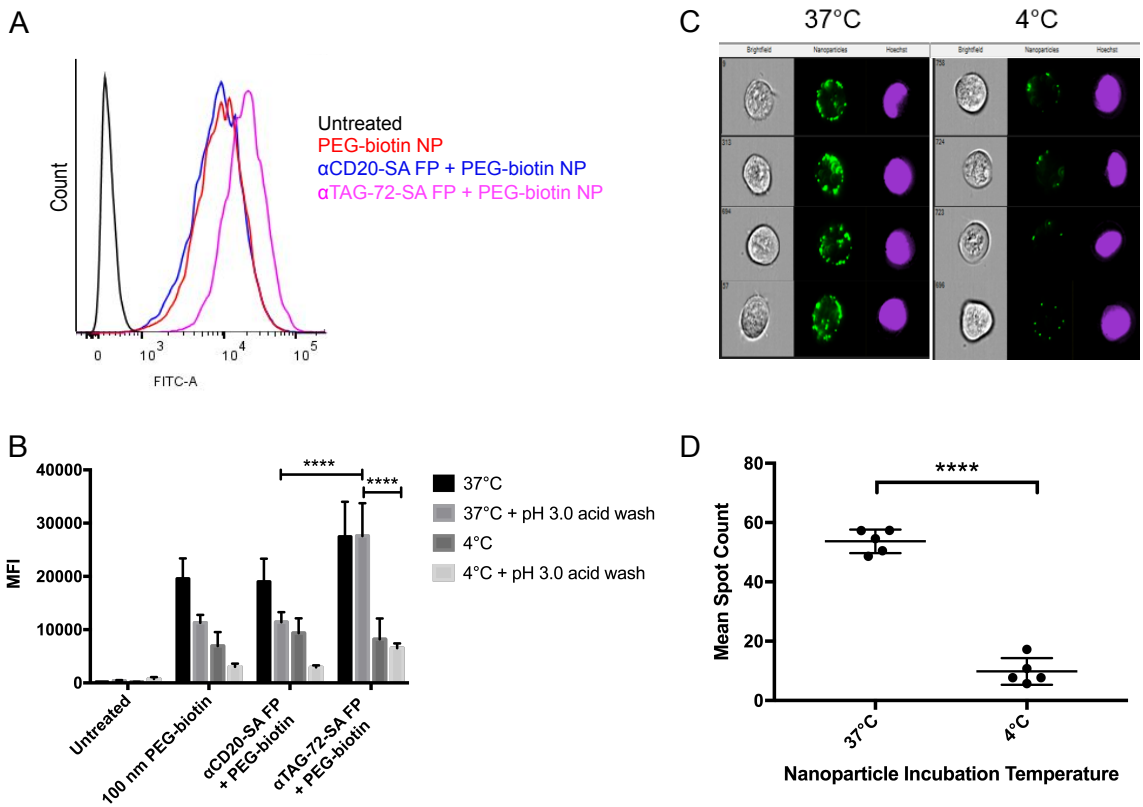

Figure 3.1. Pretargeted delivery of biotinylated, fluorescent nanoparticles (PS-PEG-biotin) to Jurkat cells. (A) Distribution of fluorescence in Jurkat cells upon incubation with different streptavidin-based bispecific proteins followed by 100 nm biotinylated, fluorescent PEG-coated polystyrene nanoparticles (PS-PEGb) measured by flow cytometry. **(B)** Mean fluorescence intensity (MFI) of fluorescent PS-PEGb nanoparticles at 37ºC vs. 4°C. Each uptake study condition represents 2 experiments in triplicate wells, and 10,000 cells counted per each well. Statistical significance difference ($p<0.0001$) between pretargeting NP with cell-specific (αTAG-72-SA) and control (αCD20-SA) pretargeting protein both at 37°C with pH 3.0 acid wash is indicated by asterisks. Statistical significance difference ($p<0.0001$) between the amount of cell-associated fluorescence for PS-PEGb nanoparticles guided by αTAG-72-SA FP at 37°C with pH 3.0 acid wash and 4°C with pH 3.0 acid wash is indicated by asterisks. **(C)** Representative Amnis ImageStream Flow Cytometer images of Jurkat cells pretreated with αTAG-72-SA FP for 4 hr at 37°C followed by incubation of PS-PEGb nanoparticles for 12 hr at either 37°C or 4°C. In each panel, left column shows bright field images of the cells, second column shows images of fluorescent PS-PEGb nanoparticles, and the third column shows nuclei staining with Hoechst. **(D)** Mean number of punctate nanoparticle fluorescent spots per cell measured by Amnis IDEAS software. Each temperature conditions represents N = 5 independent samples with 10,000 cells imaged per sample. Statistical significance difference ($p<0.0001$) between mean particle spots at 37°C and 4°C is indicated by asterisks.

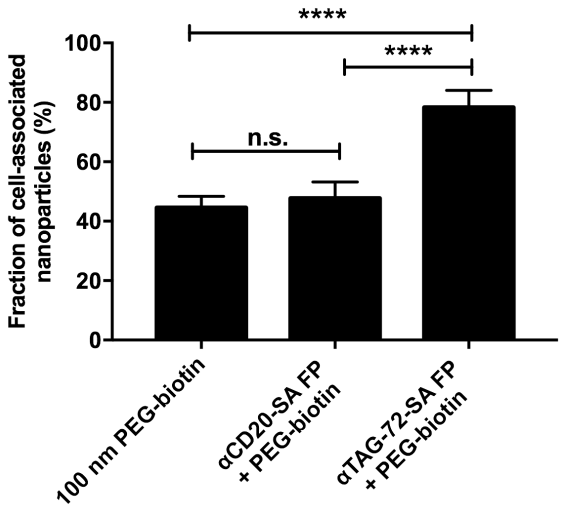

Figure 3.2. Fraction of nanoparticles associated with cells above background in the presence of acid wash. This was calculated using the following equation:

$$Fraction\ of\ cell-associated\ nanoparticles\ (\%) = \frac{37°C\ acid\ wash - 4°C\ acid\ wash 37°C}{37°C} * 100$$

Each uptake study condition represents 2 experiments in triplicate wells, and 10,000 cells counted per well. Statistical significance difference ($p<0.0001$) between pretargeting NP with cell-specific (αTAG-72-SA) and control (αCD20-SA) pretargeting protein is indicated by asterisks. Statistical significance difference ($p<0.0001$) between biotinylated nanoparticles and pretargeted NP with cell-specific (αTAG-72-SA) pretargeting protein is also indicated by asterisks. In general, the flow cytometry results agree well with the confocal images, with the lone exception that this new analysis failed to reveal limited internalization of the pretargeted 100 nm biotinylated beads.

To more carefully investigate the distribution of nanoparticles within cells, we next performed live-cell confocal microscopy. Consistent with the ImageStream data, confocal images showed that pretargeted 100 nm nanoparticles were largely found in the periphery of the cells, with only a very modest fraction found inside cells (Figure 3.3). Not surprisingly, most pretargeted 100 nm nanoparticles exhibited little colocalization with the nuclear stain or intracellular markers specific for the endo-lysosomal pathway, including Rab5a (early endosomes), Rab7a (late endosomes), Lamp1 (lysosomes) and Lysotracker (acidic vesicles)

(Figure 3.3), suggesting that the pretargeted particles did not enter into the endolysosomal trafficking pathway. To investigate whether the nanoparticles were inside cells or retained within the plasma membrane, we further performed colocalization studies using CellMask Deep Red plasma membrane stain, and observed a high degree of colocalization. Altogether, these results indicate that although a small fraction of pretargeted 100 nm nanoparticles were capable of undergoing endocytosis, the vast majority of nanoparticles were retained at or near the cell surface (Figure 3.4A); partitioned in the cell membrane in a manner that prevented the nanoparticles from dissociating from the cells despite repeated acid washes.

3.3.2 Investigating why pretargeting of 100 nm nanoparticles results in poor internalization

We first sought to confirm that the nanoparticles were not too large to be internalized into Jurkat cells by incubating the cells with comparably sized PS-COOH nanoparticles. Similar to prior studies with other cell lines, we found 100 nm PS-COOH nanoparticles readily internalized into Jurkat cells, suggesting that the nanoparticle size and its mechanical properties (rigidity) were not directly responsible for the poor internalization of our pretargeted nanoparticles (Figure 3.4B).

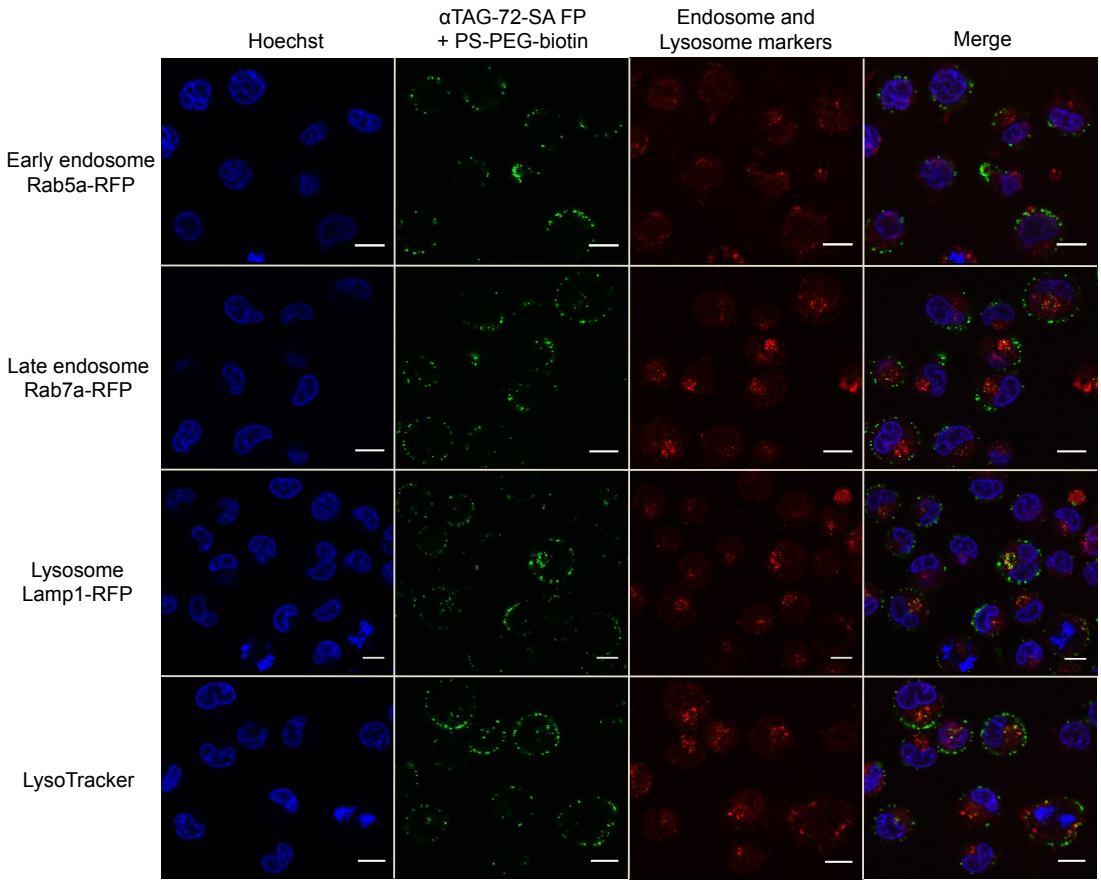

Figure 3.3. Confocal imaging of 100 nm PS-PEGb nanoparticles (green) in Jurkat cells treated with different intracellular markers (red), including early endosomes (Rab5a-RFP), late endosomes (Rab7a-RFP), lysosomes (Lamp1-RFP) and acidic vesicles (LysoTracker). Jurkat cells were first treated with αTAG-72-SA FP for 4 hr at 37°C followed by incubation of PS-PEGb nanoparticles for 12 hr at 37°C. Colocalization between nanoparticles and intracellular vesicle markers would appear as yellow and is denoted by a white arrow. Note, some cells may appear slightly oblong due to association of Jurkat cells (a suspension cell) to coverglass coated with poly-ι-lysine necessary for imaging purposes. Scale bar, 20 μm.

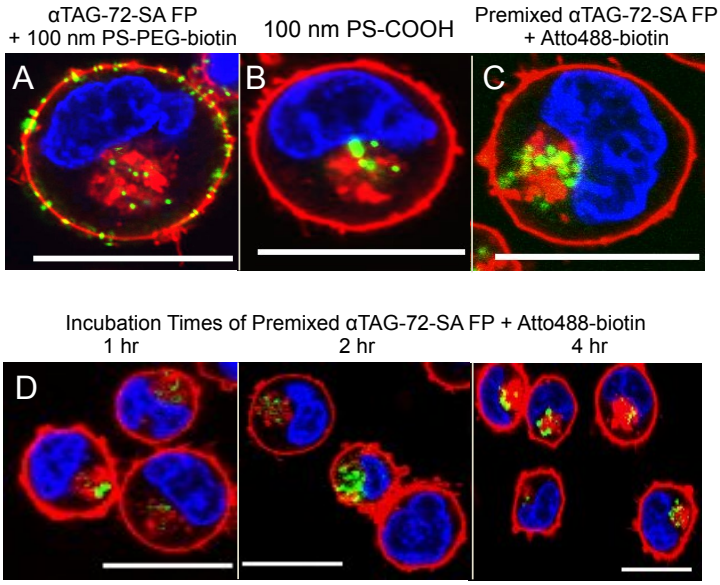

Figure 3.4. Confocal imaging of green fluorescent nanoparticles. (A) PS-PEGb nanoparticles pretargeted with αTAG-72-SA FP for 4 hr at 37°C followed by incubation of PS-PEGb nanoparticles for 12 hr at 37°C, **(B)** comparably sized carboxyl-modified latex nanoparticles incubated under identical 12 hr 37°C conditions, and **(C)** αTAG-72-SA FP incubated for 4 hr at 37°C followed by washing and incubation at 37°C for 12 hr. (A-C) Scale bar, 10 um. **(D)** *Labeled FP internalization kinetics.* Representative confocal images showing that αTAG-72-SA FP prelabeled with Atto488-biotin was internalized by Jurkat cells at shorter incubation times of 1, 2, and 4 hr at 37°C. The plasma membrane was labelled red and cell nuclei in blue for all conditions. Note, some cells may appear slightly oblong due to association of Jurkat cells (a suspension cell) to coverglass coated with poly-ι-lysine necessary for imaging purposes. Scale bar, 20 μm.

It is possible that the inefficient internalization observed with pretargeting is simply due to BFP binding to a non-internalizing cellular epitope. To investigate this possibility, we prelabeled αTAG-72-SA BFP with fluorescent biotin for at least 1 hour, removed unbound biotin by filtration, and measured the internalization of the BFP-fluorescent biotin complexes in Jurkat cells. The fluorescently labeled BFP were found inside cells after 12 hours (Figure 3.4C) similar to 100 nm PS-COOH (Figure 3.4B) nanoparticles, in stark contrast to pretargeted 100 nm nanoparticles (Figure 3.4A). We also evaluated the internalization kinetics of fluorescent BFP at shorter time intervals (1, 2, and 4 h), and observed BFP internalization at all 3 intervals (Figure

3.4D). These results are consistent with *in vitro* kinetic studies showing that approximately 60% of radiolabeled anti-mesothelin scFv$_4$-SA BFP internalized into human epidermoid cancer A431 cells within 6 h,[31] and indicate that αTAG-72-SA BFP could be internalized and thus capable of facilitating intracellular delivery.

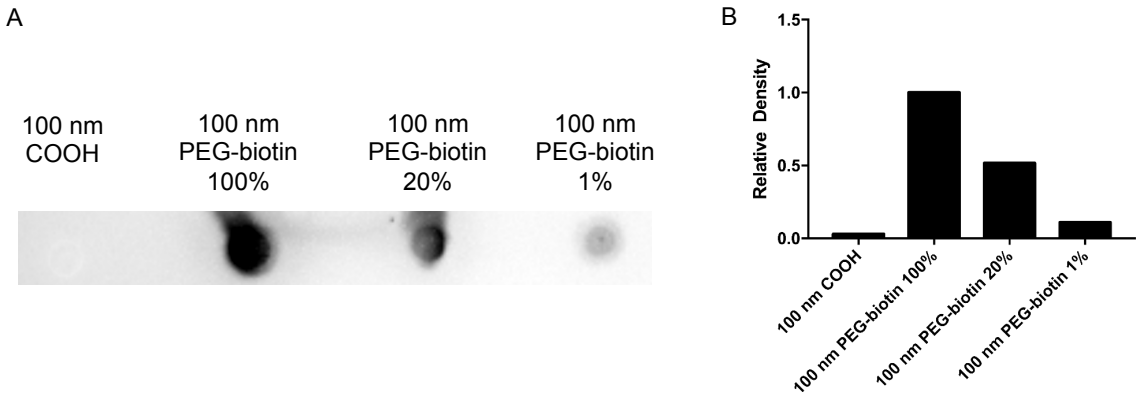

Figure 3.5. Assessment of biotin density on the surface of 100 nm polystyrene beads. Control PS-COOH and PS-PEG beads with various biotin densities were blotted onto nitrocellulose membrane. Surface biotin was detected with streptavidin-HRP (dilution 1:8,000). (A) From this dot blot image, an intensity plot was generated in ImageJ to compare the chemiluminescence signal of each nanoparticle sample. (B) Biotin density for each sample was compared relative to 100 nm PEG-biotin 100%. Unmodified beads (100 nm COOH) showed the lowest biotin density. As expected, relative biotin density decreased with the decreasing amount of PEG-biotin conjugated onto polystyrene beads.

Multivalent binding between BFP and nanoparticles can lead to an aggregation of BFP and nanoparticles on the cell surface such that the multimeric complexes cannot be readily endocytosed.[32–34] To investigate whether such multivalent binding is responsible for limited PS-PEGb internalization, we tested 100 nm PS-PEG particles with varying surface biotin densities (Figure 3.5) in Jurkat cells pretargeted with αTAG-72-SA BFP. Confocal microscopy and flow cytometry (flow data not shown) showed substantially reduced cell-associated fluorescence as the biotin density on PS-PEG-biotin nanoparticles decreased, without appreciable increase in the fraction of nanoparticle internalization (Figure 3.6A). In other words, we were not able to adequately eliminate potential polyvalent binding simply by reducing biotin density on beads

without compromising particle binding to BFP-bound cells altogether. Another approach to potentially reduce the formation of multiple beads/multiple αTAG-72-SA BFP complex is to reduce the concentration of nanoparticles, which should slow the rates of nanoparticle binding to BFP on the cell surface and consequently reduce the formation of complexes with multiple beads linked by the same BFP. However, similar to reducing the surface biotin density on PS-PEGb beads, reducing the bead to cell ratio from 10^4:1 to 10^2:1 did not increase the fraction of beads internalized, and instead again directly reduced particles associated to Jurkat cells (Figure 3.6B). Next, we evaluated reducing the multivalency on the αTAG-72-SA BFP by first incubating with slight molar excess of biotin to achieve 1-2 free biotin binding sites per SA-based FP, before incubating with cells and then 100 nm PS-PEGb nanoparticles. Unfortunately, the partially "blocked" BFP again greatly reduced PS-PEGb association to Jurkat cells without improving the fraction of nanoparticles that are internalized (Figure 3.6C).

The observations up to this point are consistent with the hypothesis that any nanoparticle-BFP complexes on the cell surface are more likely comprised of multiple BFP linked to the same particle, rather than multiple particles linked to the same BFP. We thus decided to attempt reducing the density of BFP on the cell surface by introducing a mixture of αTAG-72-SA BFP and αTAG-72 IgG_1 at different ratios to cells (Figure 3.6D). Much to our surprise, we observed a two-fold increase in the fraction of internalized nanoparticles into Jurkat cells treated with BFP:IgG mixture than cells treated with αTAG-72-SA BFP alone (Figure 3.7, $p<0.0001$). Our observations suggest there is likely an optimal surface density of TAG-72-targeted BFP that will facilitate effective intracellular delivery of pretargeted nanoparticles. Above this surface density, the same 100 nm PS-PEGb particle can likely bind to multiple BFP

simultaneously, which may make it more difficult for invaginations on the cell surface to pinch off and form vesicles for subsequent internalization into cells.

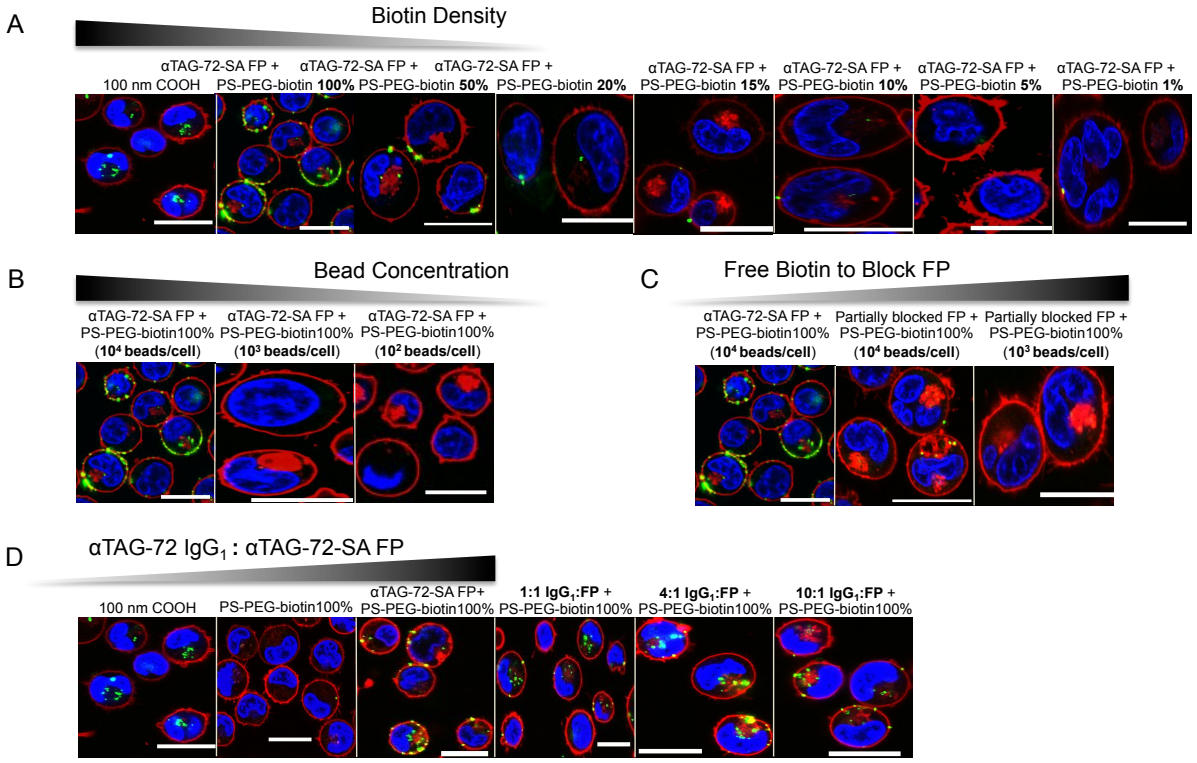

Figure 3.6. Various strategies to increase internalization of pretargeted 100 nm PS-PEGb beads. (**A**) Representative images of Jurkat cells incubated with pretargeted 100 nm PS-PEGb beads with decreasing biotin density. Scale bar, 20 μm. (**B**) Representative images showing that decreasing bead concentration of pretargeted 100 nm PS-PEGb beads did not improve internalization. Scale bar, 20 μm. (**C**) Internalization of pretargeted 100 nm PS-PEGb beads was not improved by partially blocking biotin binding sites on αTAG-72-SA FP. Scale bar, 20 μm. (**D**) αTAG-72-SA BFP was premixed with αTAG-72 IgG_1 at different molar ratios before incubating with cells then PS-PEGb NPs. For all images, nanoparticles are green, plasma membrane label is red, and Hoechst-labeled nuclei are blue. Note, some cells may appear slightly oblong due to association of Jurkat cells (a suspension cell) to coverglass coated with poly-ι-lysine necessary for imaging purposes. Scale bar, 20 μm.

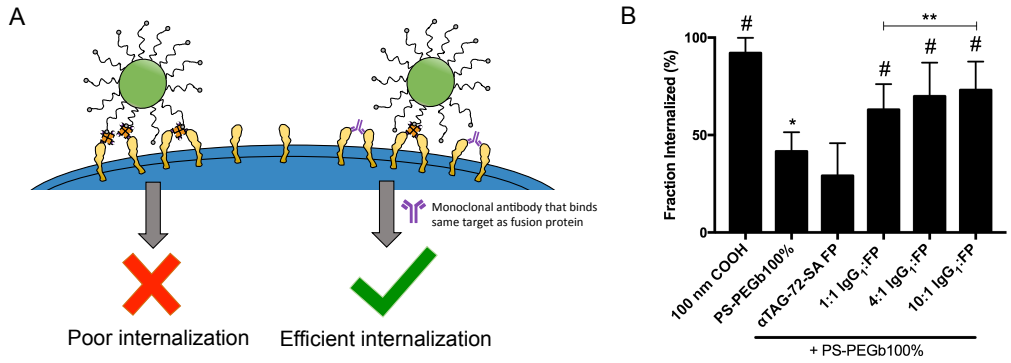

Figure 3.7. Reduction in multivalent interactions yields increased nanoparticle internalization. (**A**) Schematic illustrating efficient internalization of pretargeted nanoparticles as the density of available receptors is reduced, likely due to a reduction in the number of BFP crosslinked by nanoparticles in the presence of a monoclonal antibody. (**B**) Quantitative analysis of confocal images where αTAG-72-SA FP was premixed with αTAG-72 IgG_1 at different molar ratios before incubating with cells then PS-PEGb NPs (Figure 4D). A two-fold increase in the fraction of internalized nanoparticles was observed as the density of cell-bound fusion proteins was reduced. Statistical significance difference ($p<0.0001$) for treatment groups vs PS-PEGb beads pretargeted with αTAG-72-SA FP alone as indicated by hash sign (#). * indicates $p<0.05$ vs αTAG-72-SA FP + PS-PEGb. ** indicates $p<0.01$ for biotin beads pretargeted with 1:1 IgG_1:FP vs 10:1 IgG_1:FP. Data represents n=4 experiments with 20-50 cells analyzed per condition by ImageJ software.

3.4 Discussion

The efficiency of intracellular delivery plays a crucial role in the efficacy of specific classes of therapeutics. For example, gene therapy, gene silencing, and gene editing all require intracellular delivery of genetic materials. Since pretargeting requires the BFP molecule to be present on the cell surface when the effector molecules are introduced, an obvious question with pretargeted nanoparticle delivery is whether BFP that target non-internalizing or slowly internalizing epitopes on cells can still facilitate intracellular delivery of subsequently dosed nanoparticles. Here, by performing a series of careful confocal microscopy, we showed that pretargeting indeed could result in poor nanoparticle internalization, likely due to the formation of BFP-nanoparticle complexes with multiple BFP bound to the same nanoparticle on the cell

surface. More importantly, we found that the limited internalization can be overcome by carefully tuning the interactions between BFP and the nanoparticles. Specifically, by decreasing the density of BFP on the cell surface by reducing the number of available TAG-72 epitopes that BFP can bind to, we can markedly increase the fraction of nanoparticles internalized into target cells. Our work not only underscores the importance of carefully tuning nanoparticle-BFP interactions for pretargeted drug delivery, but also that intracellular delivery can be achieved with pretargeting.

Several groups have reported varying degrees of intracellular delivery with pretargeted nanoparticle systems. For example, Gunn *et al* observed the presence of pretargeted iron oxide nanoparticles in endosomes of $CD20^+$ Ramos cells by transmission electron microscopy.[22] However, that appears to be a relatively rare event, since confocal micrographs in the same paper showed that the majority of pretargeted nanoparticles were preferentially accumulated in the cell periphery. Mulvey *et al* reported that antibodies functionalized with morpholinos were stable on the surface of LS174T cells for up to 24 h.[35] The addition of single-walled nanotubes (SWNT) modified with complementary oligonucleotides (average length 250 nm by DLS and TEM, diameter ~1.2 nm) resulted in clustering of antibody-SWNT complexes along the cell periphery and limited internalization, in good agreement with our observations here. In contrast, Hapuarachcige *et al*[36] reported internalization of paclitaxel-loaded albumin carriers pretargeted using Trastuzumab that bind particles via bioorthorgonal chemistry. An earlier study from the same group also reported that crosslinking HER2-bound biotinylated trastuzumab via streptavidin accelerated endocytosis of otherwise poorly internalized trastuzumab.[37] These results highlight important potential differences in the internalization of different slowly internalizing or non-internalizing epitopes. Unlike with actively targeted nanoparticles where

greater receptor density of the surface of target cells is preferred, our work suggests there is likely an optimal receptor density that maximizes cellular internalization of pretargeted nanoparticles. Therefore, for applications that require intracellular or exclusively extracellular delivery, the optimal nanoparticle/BFP combination most likely needs to be carefully optimized for the specific overexpressed epitope of interest.

As a multistep process, pretargeting presents its own unique set of challenges in the clinic. For instance, receptor density on cell surface will likely play a critical role in determining whether a monoclonal antibody is needed to impede multivalent crosslinking between fusion proteins and cell receptors. Furthermore, the use of a monoclonal antibody might induce toxicity concerns because the Fc domain can mediate effector functions, such as antibody-dependent cellular cytotoxicity (ADCC), complement-dependent cytotoxicity (CDC), and antibody-dependent cellular phagocytosis (ADCP).[38,39] Antibody-bound cells can be eliminated via lysis, complement cascade, or phagocytosis prior to the binding of therapeutic nanoparticles, thereby limiting the efficacy of pretargeting. To avoid this potential toxicity, physicians may replace the monoclonal antibody with a Fab molecule that recognizes the same receptor target. The absence of the Fc will simultaneously avoid effector functions and reduce the number of available receptors on the cell surface for BFP binding. Ultimately, successful pretargeting strategies will require extensive optimization of the pharmacokinetics and biodistribution of both pretargeting molecules and therapeutic nanoparticles. In addition, for therapies that require intracellular delivery, the BFP-to-receptor ratio must be optimized. The optimum stoichiometric ratios for pretargeting molecules to specific Fab molecules would naturally differ depending on the receptor of interest and its density on the cell surface. Unfortunately, the actual optimum concentrations of the pretargeting molecules must be determined empirically, likely by both *in*

vitro and *in vivo* approaches. If there is no optimal concentration that could facilitate efficient internalization, a different receptor target on the same cells should be considered.

3.5 Conclusions

Here, we demonstrate that pretargeted nanoparticles can efficiently internalize into cells by tuning the number of available receptors on cell surface. Indeed, by mixing a monoclonal antibody and bispecific fusion protein that both recognize the same cellular epitope, we were able to achieve efficient internalization of pretargeted nanoparticles, presumably by reducing multivalent interactions between nanoparticles and fusion proteins on the cell surface. Our finding demonstrates that, despite binding to slowly internalizing epitopes on target cells, pretargeting may be extended to applications that require intracellular delivery. The combination of pretargeting with gene therapy, gene silencing or gene editing is likely to be particularly promising in applications for genetic diseases with substantial cellular and tissue heterogeneity.

REFERENCES

1. Bertrand, N., Wu, J., Xu, X., Kamaly, N. & Farokhzad, O. C. Cancer nanotechnology: the impact of passive and active targeting in the era of modern cancer biology. *Adv Drug Deliv Rev* **66,** 2–25 (2014).

2. Torchilin, V. P. Passive and active drug targeting: drug delivery to tumors as an example. *Handb Exp Pharmacol* **197,** 3–53 (2010).

3. Cheng, Z., Al Zaki, A., Hui, J. Z., Muzykantov, V. R. & Tsourkas, A. Multifunctional Nanoparticles: Cost Versus Benefit of Adding Targeting and Imaging Capabilities. *Science (80-.).* **338,** 903–910 (2012).

4. Yang, Q., Parker, C. L., McCallen, J. D. & Lai, S. K. Addressing challenges of heterogeneous tumor treatment through bispecific protein-mediated pretargeted drug delivery. *J. Control. Release* **220,** 715–726 (2015).

5. Reuter, K. G. *et al.* Targeted PRINT Hydrogels: The Role of Nanoparticle Size and Ligand Density on Cell Association, Biodistribution, and Tumor Accumulation. *Nano Lett.* **15,** 6371–6378 (2015).

6. Husseini, G. A., Pitt, W. G. & Martins, A. M. Ultrasonically triggered drug delivery: Breaking the barrier. *Colloids Surfaces B Biointerfaces* **123,** 364–386 (2014).

7. Mody, V. V. *et al.* Magnetic nanoparticle drug delivery systems for targeting tumor. *Appl. Nanosci.* **4,** 385–392 (2014).

8. Tietze, R. *et al.* Magnetic nanoparticle-based drug delivery for cancer therapy. *Biochemical and Biophysical Research Communications* **468,** 463–470 (2015).

9. Rodzinski, A. *et al.* Targeted and controlled anticancer drug delivery and release with magnetoelectric nanoparticles. *Sci. Rep.* 20867 (2016). doi:10.1038/srep20867

10. Su, Y., Xie, Z., Kim, G. B., Dong, C. & Yang, J. Design strategies and applications of circulating cell-mediated drug delivery systems. *ACS Biomater Sci Eng* **1,** 201–217 (2015).

11. McMillan, J., Batrakova, E. & Gendelman, H. E. *Cell delivery of therapeutic nanoparticles*. *Prog Mol Biol Transl Sci* **104,** (2011).

12. Larson, S. M., Carrasquillo, J. A., Cheung, N.-K. V. & Press, O. W. Radioimmunotherapy of human tumours. *Nat. Rev. Cancer* **15,** 347–360 (2015).

13. Buchsbaum, D. J. *et al.* Intraperitoneal pretarget radioimmunotherapy with CC49 fusion protein. *Clin. Cancer Res.* **11,** 8180–8185 (2005).

14. van de Watering, F. C., Rijpkema, M., Robillard, M., Oyen, W. J. & Boerman, O. C. Pretargeted imaging and radioimmunotherapy of cancer using antibodies and bioorthogonal chemistry. *Front Med* **1,** 44 (2014).

15. Lee, S. B. *et al.* Mesoporous Silica Nanoparticle Pretargeting for PET Imaging Based on a Rapid Bioorthogonal Reaction in a Living Body. *Angew. Chemie Int. Ed.* **52,** 10549–10552 (2013).

16. Kraeber-Bodéré, F. *et al.* A pretargeting system for tumor PET imaging and radioimmunotherapy. *Front. Pharmacol.* **6,** 54 (2015).

17. van Duijnhoven, S. M. J. *et al.* Diabody Pretargeting with Click Chemistry In Vivo. *J. Nucl. Med.* **56,** 1422–1428 (2015).

18. Hou, S. *et al.* Pretargeted positron emission tomography imaging that employs supramolecular nanoparticles with in vivo bioorthogonal chemistry. *ACS Nano* **10,** 1417–1424 (2016).

19. Perrault, S. D. & Chan, W. C. W. In vivo assembly of nanoparticle components to improve targeted cancer imaging. *PNAS* **107,** 11194–11199 (2010).

20. Agasti, S. S. *et al.* Supramolecular Host–Guest Interaction for Labeling and Detection of Cellular Biomarkers. *Angew Chem Int Ed Engl* **51,** 450–454 (2012).

21. Allen, T. M. Ligand-targeted therapeutics in anticancer therapy. *Nat. Rev. Cancer* **2,** 750–763 (2002).

22. Gunn, J., Park, S. I., Veiseh, O., Press, O. W. & Zhang, M. A pretargeted nanoparticle system for tumor cell labeling. *Mol Biosyst* **7,** 742–748 (2011).

23. Rossin, R. *et al.* In Vivo Chemistry for Pretargeted Tumor Imaging in Live Mice. *Angew. Chemie Int. Ed.* **49,** 3375–3378 (2010).

24. Schultz, J. *et al.* A tetravalent single-chain antibody-streptavidin fusion protein for pretargeted lymphoma therapy. *Cancer Res.* **60,** 6663–6669 (2000).

25. Yang, Q. *et al.* Evading Immune Cell Uptake and Clearance Requires PEG Grafting at Densities Substantially Exceeding the Minimum for Brush Conformation. *Mol. Pharm.* **11,** 1250–1258 (2014).

26. Kim, J. S. *et al.* Cellular uptake of magnetic nanoparticle is mediated through energy-dependent endocytosis in A549 cells. *J. Vet. Sci.* **7,** 321–326 (2006).

27. Madani, F., Lindberg, S., Langel, Ü., Futaki, S. & Gräslund, A. Mechanisms of Cellular Uptake of Cell-Penetrating Peptides. *J. Biophys.* **2011,** 414729 (2011).

28. Mohamed, B. M. *et al.* Activation of stress-related signalling pathway in human cells upon Si(O)2 nanoparticles exposure as an early indicator of cytotoxicity. *J. Nanobiotechnology* **9,** 29 (2011).

29. Kim, A. J., Boylan, N. J., Suk, J. S., Lai, S. K. & Hanes, J. Non-degradative intracellular trafficking of highly compacted polymeric DNA nanoparticles. *J. Control. Release* **158,** 102–107 (2012).

30. Kameyama, S. *et al.* Acid wash in determining cellular uptake of Fab/cell-permeating peptide conjugates. *Pept. Sci.* **88,** 98–107 (2007).

31. Sato, N. *et al.* Pretargeted radioimmunotherapy of mesothelin-expressing cancer using a tetravalent single-chain Fv-streptavidin fusion protein. *J Nucl Med* **46,** 1201–1209 (2005).

32. Monine, M. I., Posner, R. G., Savage, P. B., Faeder, J. R. & Hlavacek, W. S. Modeling multivalent ligand-receptor interactions with steric constraints on configurations of cell-surface receptor aggregates. *Biophys. J.* **98,** 48–56 (2010).

33. Hlavacek, W. S., Posner, R. G. & Perelson, A. S. Steric effects on multivalent ligand-receptor binding: Exclusion of ligand sites by bound cell surface receptors. *Biophys. J.* **76,** 3031–3043 (1999).

34. Bhatia, S., Camacho, L. C. & Haag, R. Pathogen Inhibition by Multivalent Ligand Architectures. *J Am Chem Soc* **138,** 8654–8666 (2016).

35. Mulvey, J. J. *et al.* Self-assembly of carbon nanotubes and antibodies on tumours for targeted amplified delivery. *Nat Nanotechnol* **8,** 763–771 (2013).

36. Jawa, V. *et al.* Evaluating Immunogenicity Risk Due to Host Cell Protein Impurities in Antibody-Based Biotherapeutics. doi:10.1208/s12248-016-9948-4

37. Zhu, W., Okollie, B. & Artemov, D. Controlled internalization of her-2/neu receptors by cross-linking for targeted delivery. *Cancer Biol. Ther.* **6,** 1960–1966 (2007).

38. Vidarsson, G., Dekkers, G. & Rispens, T. IgG subclasses and allotypes: From structure to effector functions. *Front. Immunol.* **5,** 520 (2014).

39. Saxena, A. & Wu, D. Advances in therapeutic Fc engineering - modulation of IgG-associated effector functions and serum half-life. *Frontiers in Immunology* (2016). doi:10.3389/fimmu.2016.00580

CHAPTER 4: PRETARGETED DELIVERY OF PEG-COATED DRUG CARRIERS TO BREAST TUMORS USING MULTIVALENT, BISPECIFIC ANTIBODY AGAINST PEG AND HER2

4.1 Introduction

In cancer therapy, targeted drug delivery aims to maximize the dose of anti-cancer or imaging agents delivered to cancer cells/tissues while minimizing exposure and toxicity to healthy, non-targeted tissues. One broadly studied approach is to encapsulate anti-cancer agents into nanocarriers coated with "stealth" polymers, such as liposomes, micelles, and polymeric nanoparticles, that can in turn accumulate in tumors due to tumors' inherent leaky vasculature (i.e. the Enhanced Permeability and Retention (EPR) effect).[1–3] Unfortunately, coating polymers that minimize opsonin absorption also limit binding and internalization into target cells. To increase particle uptake, antibodies and other moieties that target differential expression of select surface receptors on cancer cells compared to healthy cells are often attached to the nanocarriers' surface (i.e. active targeting), with the expectation that the actively targeted carriers would more effectively deliver cargo therapeutics to target cells.[4–7] Interestingly, numerous studies have found that increasing antibody grafting beyond certain thresholds actually *reduced* overall targeting efficiency *in vivo*[8–13], presumably because a high density of conjugated ligands compromised the anti-fouling nature of "stealth" polyethylene glycol (PEG) coatings. This leads to premature elimination of the carriers from circulation by the mononuclear phagocyte system (MPS)[4,8,14,15], and results in a smaller fraction of the administered nanocarriers that could extravasate and accumulate at target site. Indeed, a number of studies have reported that actively

targeted nanoparticles did not improve particle delivery to tumors compared to passively targeted nanoparticles.[16–18]

To overcome the aforementioned limitations with both active- and passive targeting, some researchers are exploring "pretargeting" as a strategy to preserve prolonged circulation of coated nanoparticles while simultaneously enabling their targeting to specific cells.[19] Pretargeting is a two-step strategy that relies on the use of bispecific pretargeting molecules that can bind both cellular epitopes and subsequently administered effector molecules. Ideal pretargeting molecules would extravasate from systemic circulation and accumulate on the surface of target cells, or be quickly eliminated from the circulation. Drug-loaded carriers are then administered, and a fraction of the extravasated carriers would be captured by cell-bound pretargeting molecules, followed by endocytosis into target cells. This approach was initially tested for the treatment of hematological malignancies in the form of pretargeted radioimmunotherapy (PRIT), which improved imaging contrast and tumor suppression as well as reduced radioactivity in healthy organs.[20] Later studies have extended the use of bispecific proteins to pretarget nanocarriers to specific cell populations.[21–24] While bsAb are commonly designed in Ig-like format with a Fc domain,[25,26] other pretargeting molecules are designed as bsAb fragments lacking a Fc domain.[21,23,27] To date, none of the studies evaluated how the design of the bsAb format may impact pretargeting efficiency of nanocarriers.

A longstanding challenge in bsAb engineering has been the proper pairing of heavy and light chains leading to high purity and yield of the final product. Here, we used a recently developed bsAb platform called OrthoMab to investigate the optimal bsAb design for pretargeted delivery of polymeric nanoparticles to tumors. By introducing orthogonal mutations pairs into heavy and light chains, the OrthoMab platform yields high fidelity pairing of the correct heavy

and light chains for functional bsAb.[28] We designed two bsAb (tandem Fab and Fab-IgG_1) that recognize both HER2 receptors overexpressed on breast cancer cells, and PEG present on PEGylated liposomal doxorubicin (PLD) and PEGylated polystyrene beads. While the bivalent tandem Fab (two Fab domains connected by a flexible linker) has one binding domain per antigen, the tetravalent Fab-IgG_1 (additional Fab covalently linked to the Fab domains of a traditional IgG molecule) has two binding domains per antigen. This allows us to evaluate the effect of Fab valency (number of binding domains per antigen) and impact of FcR-binding on targeting and distribution of pretargeted PEG nanocarriers to $HER2^+$ breast cancer cells *in vitro* and in an orthotopic xenograft breast tumor model in mouse.

4.2 Materials and methods

4.2.1 Cell lines and animals

Human SKBR3, A2780, and BT474 were purchased from the UNC-CH Tissue Culture Facility. SKBR3 cells were cultured in McCoy's medium containing 15% fetal bovine serum, and A2780 cells were cultured in RPMI 1640 containing 10% fetal bovine serum and 1% L-glutamine. BT474 cells were maintained in RPMI 1640 media with 2 g/L sodium bicarbonate and 2 mM L-glutamine, and supplemented with 10% fetal bovine serum, 4.5 g/L glucose, 10 mM HEPES, 1.0 mM sodium pyruvate, and 0.01 mg/ml human insulin. All cells were maintained at 37°C and 5% CO_2.

Female athymic nude (6-8 week old) mice were obtained from Charles River Laboratories (Wilmington, MA, USA) or bred in-house by UNC Animal Services Core (Chapel Hill, NC), and maintained in a sterile housing suite. All animal experiments were carried out in accordance with an animal use protocol approved by the University of North Carolina Animal

Care and Use Committee. Mice were randomly assigned to treatment groups and investigators were blinded to the treatments.

4.2.2 Chimeric antibody construction and characterization

Sequences for chimeric anti-PEG and anti-HER2 antibodies (Ab) were generated by combining the V_H/V_L regions of commercially available murine anti-PEG (6.3 IgG_1; IBMS Academia Sinica)[29] and humanized anti-HER2 (Trastuzumab; Genentech)[30] with the C_H1/C_L and Fc regions of human IgG_1 Ab. To generate bsAb (Fab-IgG_1 and tandem Fab) that recognized both PEG and HER2, separate orthogonal mutation sets were introduced into anti-HER2 Fab and anti-PEG Fab.[28] Orthogonal mutation sets provided high fidelity pairing of heavy and light chains; this technology was licensed through a partnership between Dualogics and the University of North Carolina at Chapel Hill (UNC-CH). Although orthogonal mutations were introduced into the anti-HER2 and anti-PEG Fab domains to ensure high fidelity pairing of the heavy and light chains in the bsAb designs, these mutations were not incorporated into the chimeric monoclonal antibodies (mAbs).

Plasmids encoding heavy and light chains were cotransfected into Expi293F cells (Thermo Fisher Scientific) and grown for 96 h. Chimeric IgG_1^{PEG}, IgG_1^{HER2}, and bispecific Fab-IgG_1 were purified from expression supernatant using protein A agarose (Thermo Fisher Scientific, Grand Island, NY). The tandem Fab was designed to include a polyhistidine tag on its C-terminus and was purified from expression supernatant using Ni-NTA agarose (Qiagen Inc, Germantown, MD). All purified antibodies were dialyzed into PBS, concentration determined using A280 (Nanodrop One/One), and assessed for size and purity by sodium dodecyl sulfate polyacrylamide gel electrophoresis (SDS-PAGE).

4.2.3 Antibody binding affinity characterization

HER2-specific ELISAs were performed to confirm binding of purified antibodies to HER2 as well as compare dissociation constants of bispecific antibodies relative to parental monoclonal control, IgG_1^{HER2}. Briefly, recombinant human ErbB2/HER2 Fc chimera protein (R&D Systems, cat no. 1129-ER, Minneapolis, MN) was coated onto high-binding half-area 96-well Costar plates (Corning) at 1 μg/ml in bicarbonate buffer overnight at 4°C. After blocking plate with 5% nonfat milk in PBS with 0.05% Tween (PBST), purified antibody samples were diluted in 1% nonfat milk in PBST at various concentrations and incubated for 1 h, followed by washes with PBST. Bound antibodies were detected using goat anti-human kappa light chain HRP (Sigma-Aldrich, cat no. A7164, 1:10,0000 dilution) for 1 h followed by 1-step Ultra TMB (Thermo Fisher Scientific). After stopping the HRP reaction with 2N sulfuric acid, the absorbance at 450 nm and 570 nm was measured using a Spectramax M2 plate reader (Molecular Devices).

To quantify PEG specific binding, PEG ELISAs were performed as previously described.[31] Bound antibodies were detected using goat anti-human kappa light chain HRP (Sigma-Aldrich, cat no. A7164, 1:10,0000 dilution,) followed by 1-step Ultra TMB and sulfuric acid. For both HER2- and PEG-specific ELISAs, total and nonspecific binding was measured and dissociation constants (K_D) were determined using nonlinear regression analysis for saturation binding with GraphPad Prism software.

4.2.4 Polystyrene nanoparticle synthesis and characterization

Carboxylate-modified green fluorescent polystyrene (PS) beads with mean diameter of 100 nm (Thermo Fisher Scientific) were PEGylated using methoxy polyethylene amine (MW 5000 g/mol, JenKem Technology) and EDC coupling. The PEG density on PS beads was indirectly quantified using fluorogenic 1-pyrenyldiazomethane, as previously described.[32] Hydrodynamic size and zeta potential of synthesized nanoparticles was determined by using dynamic light scattering and laser Doppler anemometry, respectively, using a Zetasizer Nano (Malvern, U.K.)

4.2.5 Cell uptake assay

Cells were seeded at $5x10^4$ cells/well into 96-well plates. Next day, the cells were incubated with 10 nM monoclonal antibody controls or bsAb for 4 h at 37°C. After washing to remove unbound Ab, the cells were then incubated with fluorescent, PEGylated polystyrene beads ($1:10^4$ cell:bead ratio) for 12 h at 37°C. Cells were washed to remove unbound beads and flow cytometry was performed using iQue Screener PLUS (Intellicyt, Albuquerque, NM). Data were analyzed using ForeCyt and BD FACSDiva software.

To determine if bsAb remained on the surface of cells 24 h after bsAb incubation, cells were treated using extended uptake conditions. After cells were treated with 10 nM mAb or bsAb for 4 h at 37°C, cells were washed and incubated in fresh media for 24 h at 37°C. Then, cells were washed and incubated with fluorescent, PEGylated polystyrene beads ($1:10^4$ cell:bead ratio) for 4 h at 37°C. Unbound beads were removed through washing, and cell-associated fluorescence was analyzed via flow cytometry.

4.2.6 Pharmacokinetics of bispecific antibody in the presence and absence of high dose IVIg

Female athymic nude mice either received a single intravenous injection of 30 μg bispecific Fab-IgG_1 or two intravenous injections separated by 15 minutes of 30 μg bispecific Fab-IgG_1 and 30 mg human intravenous immune globulin (IVIg, Provigen) via tail vein. Blood was collected from mice at different time points (5 min, 1 h, 3 h, 5 h, 7 h, 24 h, 48 h, 72 h; n = 8 mice per treatment group, n = 4 mice per time point). Whole blood was stored undisturbed at room temperature for 20 min to allow clotting. Samples were then centrifuged at 2,000 xg in a refrigerated centrifuge for 15 min to isolate serum. PEG-specific ELISAs[31] were used to quantify the serum concentration of bispecific Fab-$IgG_1^{HER2xPEG}$ at various time points by detecting antibody with goat anti-human IgG $F(ab)'_2$ (Rockland Immunochemicals, cat no. 209-1304, 1:10,000 dilution). PK analysis of the blood concentration of bispecific antibodies was conducted using PKSolver with a two-compartment model.[33]

4.2.7 Biodistribution of pretargeted PLD in tumor-bearing mice

Female athymic nude (nu/nu) mice received a subcutaneous implantation of a single 60-day, 0.36 mg 17β-estradiol pellet six days prior to left mammary pad injection of BT474 cells ($4x10^6$ cells in total volume of 100 μl 1:1 Matrigel/PBS). Once tumors were ≥ 100 mm^3, mice were randomized into antibody treatment groups. PBS, bsAb (30 μg Fab-IgG_1), and bsAb + IVIg (30 μg Fab-IgG_1 with 30 mg IVIg) were administered i.v., followed by generic PEGylated liposomal doxorubicin (PLD, 3 mg/kg i.v.) 24 h after Ab dose (n = 4 mice per group). Due to limitations in concentrating bsAb, the bsAb + IVIg dose was separated into two injections separated by 4 h (1^{st} injection: 30 μg Fab-IgG_1 + 10 mg IVIg; 2^{nd} injection: 20 mg IVIg).

Forty-eight hours after PLD dose, mice were sacrificed, and tissues (heart, liver, kidneys, spleen, lungs, tumor) and blood via cardiac puncture were collected. Total doxorubicin concentration in serum and tissue homogenate was quantified using HPLC. Generic PLD (Sun Pharmaceutical Industries Ltd.), comparable to Doxil® liposome, was gifted by the Zamboni lab at UNC-CH and purchased through UNC Shared Services Center Pharmacy.

4.2.8 Statistical analysis

All data are presented as mean ± SD. All graphs and statistical tests were performed using GraphPad Prism 8 software. Group comparisons were analyzed using two-way ANOVA and *post hoc* multiple comparisons Tukey's test unless specified as one-way ANOVA with *post-hoc* Tukey's. A p-value <0.05 was considered to indicate statistical significance.

4.3 Results

4.3.1 OrthoMab platform preserves antigen binding affinity

We engineered monoclonal IgG_1^{PEG}, IgG_1^{HER2}, and bsAb in Fab-IgG_1 and tandem Fab formats by merging human IgG_1 backbones with HER2- and PEG-binding V_H and V_L domains previously isolated from mouse IgG.[29,30] Purified Ab from the culture supernatant displayed the expected molecular weights as visualized on non-reduced and reduced 4-12% bis-tris protein gels (Thermo Fisher Scientific) (Figure 4.1A, 1B). We next evaluated specific binding to both HER2 and PEG using antigen-specific ELISA assays. Both bsAb possessed similar binding affinities to the monoclonal IgG_1 against HER2: the K_D for IgG_1^{HER2}, tandem $Fab^{HER2xPEG}$, and Fab-$IgG_1^{HER2xPEG}$ against HER2 proteins were 0.76 ± 0.11 nM, 2.76 ± 0.18 nM, and 1.20 ± 0.13 nM, respectively (Figure 4.1C). In contrast, Ab with bivalent Fabs possessed comparable binding

affinity for PEG (K_D for IgG_1^{PEG} and Fab-IgG_1 against PEG were 4.24 ± 0.48 nM and 4.16 ± 0.60 nM respectively), while tandem $Fab^{HER2xPEG}$, with one PEG-binding Fab, had markedly weaker affinity with K_D ~ 1166 ± 182.4 nM. All three mAb constructs bound PEG specifically, as incubation with excess free PEG_{8K} completely eliminated their binding signal (Figure 4.1D).

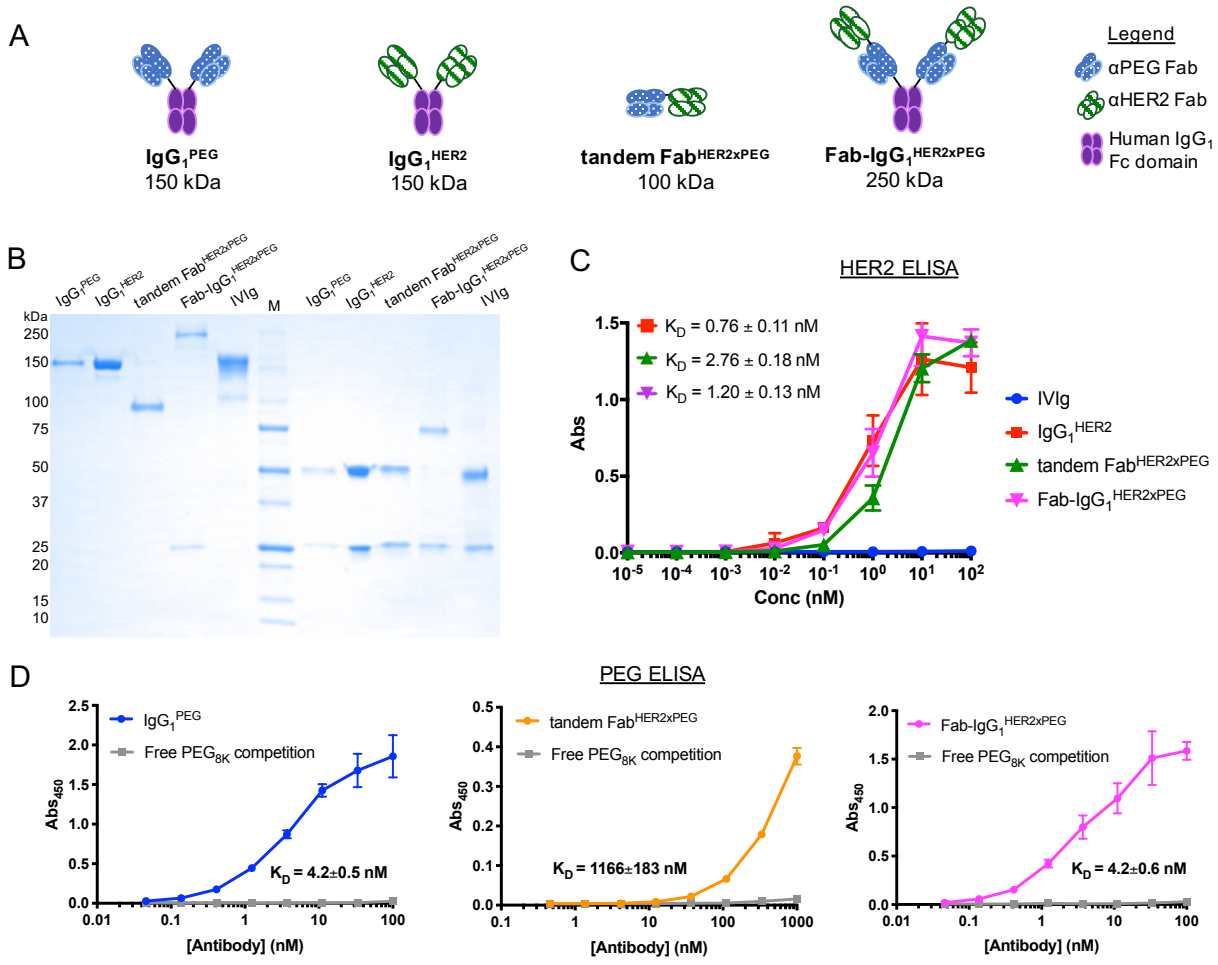

Figure 4.1. Characterization of monospecific and bispecific antibodies (Ab). A) Schematic illustrating differences in size and number of antigen-binding domains for each Ab. The theoretical molecular weight of bispecific Fab-IgG_1 and tandem Fab are ~250 kDa and ~100 kDa, respectively. **B**) Nonreducing (left) and reducing (right) protein gel showing Coomassie blue staining of IgG_1^{PEG}, IgG_1^{HER2}, tandem $Fab^{HER2xPEG}$, Fab-$IgG_1^{HER2xPEG}$, and non-specific IVIg. **C**) Binding affinity of IgG_1^{HER2}, tandem $Fab^{HER2xPEG}$, and Fab-$IgG_1^{HER2xPEG}$ to HER2-Fc chimera analyzed by ELISA (n=2). **D**) Binding affinity of IgG_1^{PEG} (left), tandem $Fab^{HER2xPEG}$ (middle), and Fab-$IgG_1^{HER2xPEG}$ (right) to DSPE-PEG_{5k} in the presence and absence of free PEG_{8K} competition analyzed by ELISA (n=2).

Altogether, these results confirmed that we were able to produce functional bsAb, and that the orthogonal mutations introduced at the heavy and light chain interface did not impair the binding to either HER2 or PEG compared to their respective parent monospecific IgGs.

4.3.2 Pretargeted delivery of PEGylated nanocarriers in vitro

We next assessed the pretargeting efficiencies of the different bsAb by measuring the cellular association of fluorescent PEG beads in both SKBR3 ($HER2^+$) and A2780 ($HER2^-$) cells pretargeted with Fab-IgG_1, tandem Fab, or combination of the parent mAbs (IgG_1^{HER2} and IgG_1^{PEG}. We observed minimal fluorescence in A2780 cells across all conditions, irrespective of the specific bsAb or mAb used (Figure 4.2). The mean fluorescence intensity (MFI) of PEG beads pretargeted with Fab-IgG_1 was 25-fold higher in $HER2^+$ SKBR3 cells compared to both monoclonal IgG controls and tandem Fab ($p<0.0001$), and also to A2780 cells pretargeted with the Fab-IgG_1 (Figure 4.2C). Similarly, the percentage of GFP positive cells for PEG beads pretargeted with Fab-IgG_1 was 20-fold higher in $HER2^+$ SKBR3 cells compared to all other conditions ($p<0.0001$; Figure 4.2B). These results not only validated the specificity of Fab-IgG_1 to both HER2 and PEG, but also underscored that pretargeting effectiveness can be influenced by the Fab valency on the bsAb. The results also confirmed that pretargeting molecules must be bispecific, as defined by a covalent linkage between anti-HER2 and anti-PEG binding domains, in order to enhance nanoparticle delivery to target cells.

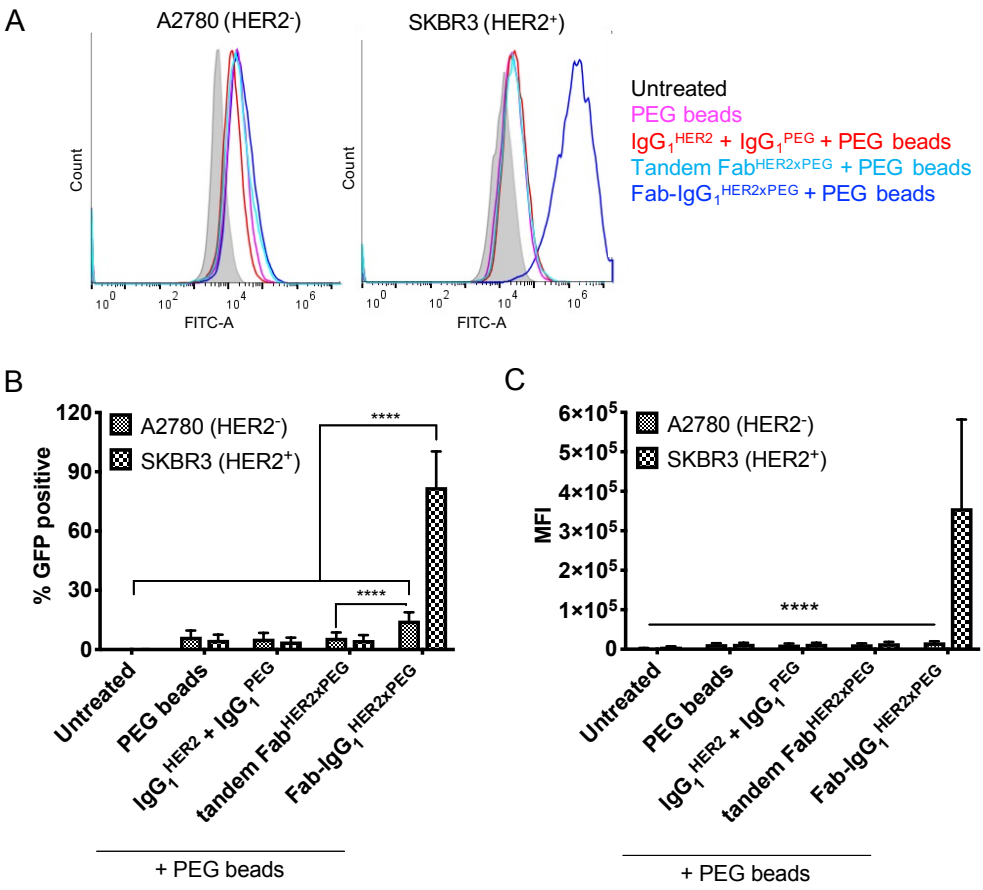

Figure 4.2. Pretargeted delivery of PEGylated nanoparticles to HER2$^+$ vs HER2$^-$ cells. A) Distribution of fluorescence in HER2$^-$ and HER2$^+$ cells upon incubation with monospecific and bispecific Ab followed by 100 nm fluorescent PEGylated polystyrene beads measured by flow cytometry. **B**) Percentage of GFP positive cells and (**C**) mean fluorescence intensity (MFI) and of cell-associated fluorescent PEG beads. The data represents n ≥ 2 independent experiments performed with ten replicates. **** indicates p<0.0001 vs bispecific Fab-IgG$_1$ + PEG beads incubated on SKBR3 cells.

To minimize the fraction of free pretargeting molecules in the circulation at the time of nanoparticle dosing, we must afford sufficient time for them to be eliminated by natural renal clearance. We thus tested next the pretargeting effectiveness following an extended lag time (ie. 24 h) between Ab and PEG bead incubations compared to the 4 h duration in the above study to determine if Fab-IgG$_1$ could remain on target cell surface over the entire duration. We observed a ~2-fold reduction in MFI of cells pretargeted with Fab-IgG$_1$ under the extended uptake (4 h

incubation, wash, wait) condition compared to the standard uptake condition (4 h incubation only; $p<0.0001$; Figure 4.3B). However, the fraction of cells taking up nanoparticles remained unchanged largely (>80%), and was markedly higher than all other tested conditions ($p<0.0001$; Figure 4.3A). These results suggest that Fab-IgG_1 can facilitate effective pretargeting even when introduced up to 24 h in advance. Due to its superior pretargeting efficiency *in vitro*, we advanced the Fab-IgG_1 for mouse studies.

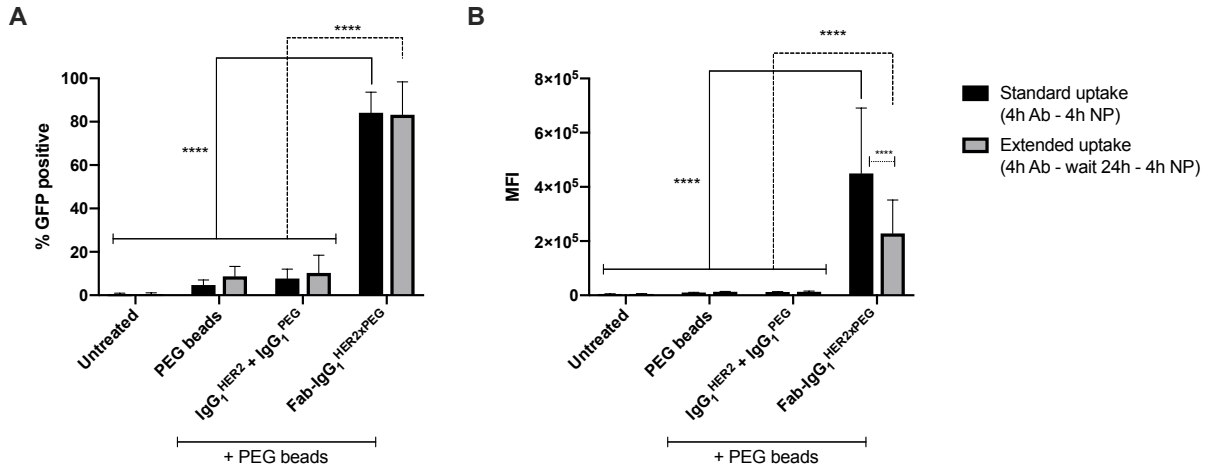

Figure 4.3. Fab-$IgG_1^{HER2xPEG}$ remained on the surface of cells 24h after Ab incubation for enhanced cellular association of PEG beads. SKBR3 cells were either immediately incubated with fluorescent PEG beads following bsAb incubation (standard uptake) or incubated with cell media for 24h prior to PEG beads (extended uptake). **A**) Percentage of GFP positive cells and **B**) mean fluorescence intensity (MFI) of cell-associated fluorescent PEG beads. The data represents n = 2 independent experiments performed with six replicates (**** $p<0.0001$).

4.3.3 Multivalent Fab-IgG_1 circulation kinetics was reduced in the presence of high dose IVIg

We evaluated the pharmacokinetics (PK) of Fab-IgG_1 following intravenous administration, and found that the half-life of Fab-IgG_1 was ~22 hours (Figure 4.4A), likely due to the Fc domain of the Fab-IgG_1 engaging neonatal Fc receptors (FcRn) resulting in their recycling. To validate the role of FcRn recycling on Fab-IgG_1 PK, we administered a high dose of human intravenous immune globulin (i.e. 30 mg IVIg) prior to dosing with Fab-IgG_1, given

the effectiveness of IVIg replacement therapy in accelerating catabolism of autoantibodies in patients with autoimmune diseases.[34,35] We observed a 3-fold reduction in serum half-life of Fab-IgG_1 when administered with high dose IVIg ($t_{1/2}$ ~ 7.2 h, Figure 4.4B), implicating FcRn for the prolonged circulation of Fab-IgG_1.

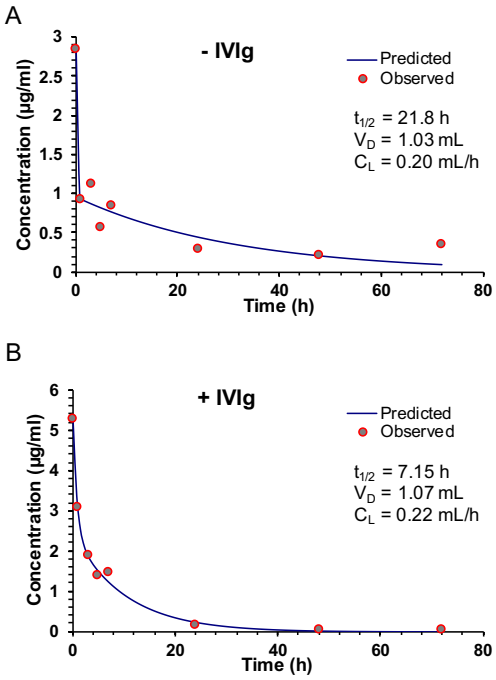

Figure 4.4. High dose IVIg reduces the circulation kinetics of bispecific Ab by 3-fold. A) The serum circulation profile of bispecific Fab-IgG_1 (30 µg) in athymic nude mice (n = 8 total mice, 4 mice per time point). **B**) The serum circulation profile of bispecific Fab-IgG_1 (30 µg) in the presence of high dose IVIg (30 mg) in athymic nude mice (n = 8 total mice, 4 mice per time point). The solid line for both figures represents the predicted fit for a two-compartment model used to calculate the elimination half-life ($t_{1/2}$), volume of distribution (V_D), and clearance (C_L).

4.3.4 Biodistribution and tumor accumulation of pretargeted PLD in tumor-bearing mouse model

Next, we evaluated the pretargeting effectiveness of Fab-IgG_1 in an orthotopic breast cancer mouse model with estradiol supplementation to better represent the tumor physiology and

stromal microenvironment of human breast cancer. Compared to mice receiving PEGylated liposomal doxorubicin (PLD) (i.e. passive targeting only), pretargeting with Fab-IgG$_1$ lacking FcRn recycling increased the concentration of doxorubicin in tumors by 3-fold (p = 0.0124, Figure 4.5B).

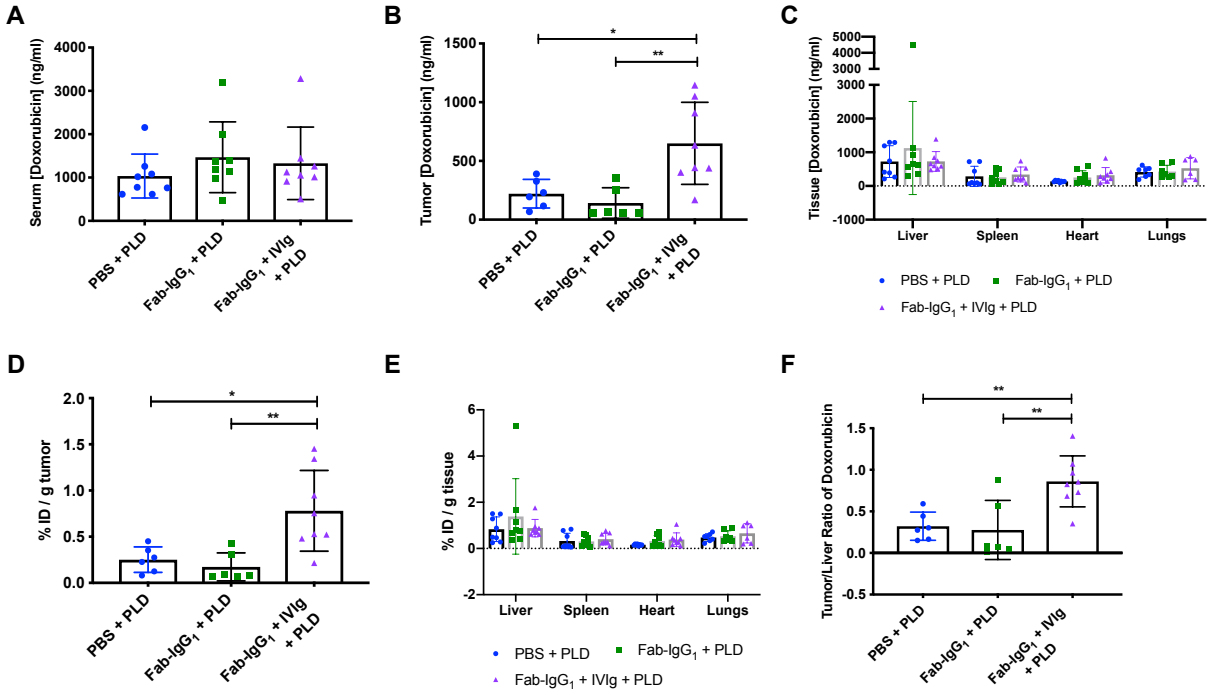

Figure 4.5. Biodistribution of passively targeted and pretargeted PEGylated liposomal doxorubicin (PLD) at 48 h post-PLD dose. Tumor-bearing mice received PBS or pretargeting antibody treatment 24 h prior to PLD (n = 6-8 mice per treatment group). **A**) Concentration of doxorubicin in mouse serum. **B**) Concentration of doxorubicin in homogenized tumors (one-way ANOVA and *post-hoc* Tukey test; * p = 0.0124, ** p=0.0035). **C**) Concentration of doxorubicin in homogenized non-targeted tissues: liver, spleen, heart, and lungs. **D**) Percent injected dose per gram of tumor (one-way ANOVA and *post-hoc* Tukey's test; * p = 0.0125, ** p = 0.0045). **E**) Percent injected dose per gram of tissue. **F**) Ratio of doxorubicin concentration in tumor to liver (one-way ANOVA and *post-hoc* Tukey's test; ** p = 0.0083, ** p = 0.0046). Means ± SD are shown, and all biodistribution data is representative of n = 2 independent experiments. Doxorubicin concentration in serum and homogenized tissues was quantified by HPLC, and was used to quantify tissue injected dose/g (%ID/g).

Pretargeting efficiency appears to be critically dependent on minimizing the serum levels of the Fab-IgG$_1$ at the time of PLD dosing: there was ~5-fold greater doxorubicin in tumors of mice

where Fc-FcRn binding was blocked with excess IVIg compared to tumors with normal Fc-FcRn binding ($p = 0.0035$, Figure 4.5B, D). At the time of PLD dose, we detected a higher concentration of Fab-IgG_1 molecules in the serum of mice treated with Fab-IgG with normal Fc-FcRn binding (without IVIg) than mice treated with PLD alone or Fab-IgG_1 with blocked Fc-FcRn binding (with IVIg) (Figure 4.6). Having residual pretargeting molecules present in the circulation at the time of nanoparticle dosing actually led to less effective nanoparticle delivery to tumors compared to passive targeting alone.

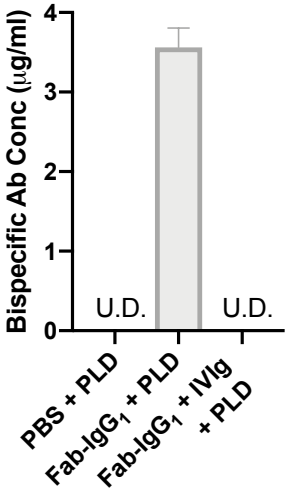

Figure 4.6. Minimal circulating bispecific Fab-IgG_1 antibodies were detected at the time of PLD dose using PEG-specific ELISA. Serum was collected from mice (n = 3-4 per group) prior to administering PLD for biodistribution study. U.D., undetected. LOQ = 0.026 ng/ml, LOD = 0.005 ng/ml. Data represents n = 1 experiment performed in duplicates.

Across treatment groups, there were no statistical differences in the serum doxorubicin concentration 48 h post-PLD dose (Figure 4.5A). There were also no statistical differences in the concentration of doxorubicin in non-targeted organs (liver, spleen, heart, and lungs) across treatment groups (Figure 4.5C, 4.5E). This is particularly important for the accumulation of doxorubicin in the heart because it is a major site of doxorubicin toxicity. The lack of increase in

liver accumulation means that the ratio of doxorubicin concentration in the tumor to liver was ~3-fold higher in mice treated with a pretargeting dose of bsAb + IVIg compared to mice treated with either PLD alone or pretargeting dose of bsAb (Figure 4.5F). Altogether, our data suggest that eliminating FcRn recycling of bispecific molecules maximizes pretargeted delivery of nanocarriers to tumors.

4.4 Discussion

Pretargeting is a promising strategy that can combine the benefits of both passive targeting (longer particle circulation increases the fraction of particles that can extravasate at target tissue) and active targeting (cell-specific binding and uptake of particles to target cells/tissues). By eliminating the need to conjugate ligands onto the particles, particles can maximize prolonged circulation afforded by "stealth" polymer coating. Extravasated particles can be more efficiently internalized and retained at target sites by cell-bound pretargeting molecules. Here, we systemically evaluated how the format of bsAb-based pretargeting molecule may influence the pretargeting efficiency of PEGylated nanoparticles to tumors. We found that increasing Fab valency and eliminating FcRn-mediated prolonged circulation are both important to maximize pretargeting efficiency. Our findings lay down the blueprint for how to engineer bsAb-based pretargeting molecules that maximizes pretargeting efficiencies.

Pretargeting molecules present in the circulation can accumulate on injected nanoparticles before the particles have the opportunity to extravasate at target tissues; this would effectively be no different that injecting actively-targeted nanoparticles. Thus, we postulate that the ideal pretargeting molecules should have a relatively short serum half-life such that any unbound pretargeting molecules are quickly cleared from systemic circulation prior to nanocarrier dosing.

BsAb molecules possessing Fc domain engage with neonatal Fc receptors (FcRn) for extended serum half-life. To evaluate the impact of prolong circulation due to FcRn-mediated recycling, we administered a high dose IVIg together with the Fab-IgG_1 to reduce FcRn-mediated recycling of the Fab-IgG_1. In good agreement with our expectation, the consequent shorter serum half-life of Fab-IgG_1 led to a 5-fold more PLD accumulated in the tumor compared to pretargeting with Fab-IgG_1 alone. To translate these insights forward, it is possible to eliminate Fc-Fcγ and Fc-FcRn interactions for bsAb-based pretargeting molecules by incorporating mutations to Fc that attenuate native binding to Fcγ receptors or FcRn. For instance, LALA-PG mutations in the C_H2 domain of pretargeting molecules very likely eliminate complement and Fcγ receptor binding while maintaining antibody stability and antigen specificity.[36] There are a number of approaches to abrogate FcRn recycling. This includes point mutations in the Fc amino acids directly involved in binding to FcRn (I253A/ H310A/H435A; IHH) ,[37] or point mutations in C_H3 domain (H433K/N434F; HN).[37,38] Similarly, MST-HN Fc mutations in human IgG_1 (M252Y/S254T/T256E/H433K/N434F) can inhibit FcRn function. [39]

The valency of pretargeting molecules also plays an important role in pretargeting efficiency. Specifically, multivalency - increasing the number of antigen-binding domains per pretargeting molecule - enhances the affinity to the particle, decreases dissociation rates when bound to cell-surface antigens, and maximizes tumor uptake and retention.[40] Harwood *et al* engineered a tetravalent T-cell recruiting bsAb composed of three EGFR-binding domains and a single CD3-binding domain, and a tandem bispecific with one EGFR-binding domain and a single CD3-binding domain.[41] The multivalent bsAb was 15- to 20-fold more potent at redirecting human T cells to lyse EGFR-expressing cells *in vitro* compared to bivalent bsAb. This result is consistent

with our findings that tetravalent bsAb are more potent at enabling pretargeted delivery of nanoparticles to tumors than bivalent bsAb.

Biodistribution studies comparing drug/particle accumulation in tumors of mice treated with nontargeted particles (ie. passive targeting) versus targeted particles (ie. active targeting) have produced variable results. Several studies reported active targeting improved tumor drug accumulation 3-4-fold compared to passive targeting.[10,42–44] However, other studies reported that actively targeted nanoparticles did not improve particle delivery to tumors compared to passively targeted nanoparticles.[16–18,45] Variations in therapeutic efficiency and drug accumulation in tumor for actively targeted versus nontargeted nanoparticles may be attributed in part to differences in the functionalization of particles. A narrow window of targeting ligand density exists that maximizes both tumor targeting and stealth properties,[10] which likely varies based on the specific ligand used. Further, the local biodistribution of actively targeted nanoparticles may differ from passively targeted particles, leading to differences in therapeutic benefit.[16] For instance, both Kirpotin *et al*[16] and Zahmatkeshan *et al*[46] found that nontargeted drug-loaded nanoparticles predominantly accumulated in tumor extracellular space while targeted nanoparticles were efficiently internalized by tumor cells, which correlated with superior antitumor activity. These results underscore the importance of cell-specific delivery, a feature preserved with pretargeted nanoparticle delivery.

Across tumor models (ie. target cell receptor, tumor type) and particle formulation (ie. chemotherapeutic drug-loaded nanoparticles, radiolabeled effector molecules and particles) pretargeting demonstrated therapeutic benefit to tumor-bearing mice as indicated by suppressed tumor growth and extended survival.[21,25,47–49] Consistent with this body of literature, we showed that bsAb-based pretargeting markedly improved tumor accumulation and tumor-to-non-target

organ ratio. Our results are similar to the work by Rauscher *et al*, which reported a 2-fold increase in specific tumor uptake of radiolabeled PEGylated liposomes with bsAb pre-injection and without bsAb pre-injection in two separate studies.[47,48] Both studies displayed ~8% ID/g in tumor for pretargeting formulations compared to nontargeted formulations (~4% ID/g). Other studies report much greater tumor uptake with pretargeting compared to passively targeted effector molecules, in large part due to very low baseline tumor uptake for passively targeted effector molecules: 30-fold increase (0.8± 0.02% ID/g vs 0.03± 0.01% ID/g)[49] and 100-fold improvement (7.58±0.78% ID/g vs 0.07±0.01% ID/g).[25] Although we saw less total accumulation and lower improvement than some of the studies, it is important to note that nearly all prior studies utilized subcutaneous xenograft models. Compared to subcutaneous xenograft models, the stromal microenvironment and tumor physiology of orthotopic breast tumor models likely limit EPR effects for reduced particle extravasation and tumor retention. Several other factors may contribute to differences in fold change of effector accumulation in tumors across studies, including choice of radiolabel and effector formulation, antigen density on target cells, dosing concentration of pretargeting and effector molecules, anatomical location of tumor xenograft, blood vessel density, and stromal content.

With at least 15 PEGylated therapeutics currently in clinical trials, we anticipate that more patients will be prescribed PEGylated therapeutics. The modular nature of our bsAb-based pretargeting enables facile targeting of the same nanocarrier to diverse tissues/cells simply by modifying the cell-binding Fab. Combining multiple pretargeting molecules as a cocktail may enhance delivery of PLD to diverse cell types within the tumor for greater drug exposure and better distribution throughout tumor. By maintaining the anti-PEG Fab binding domain on the pretargeting molecule, we can instantly enable cell-specific delivery of FDA approved

PEGylated therapeutics, providing an opportunity to further improve the efficacies of these therapeutics.

4.5 Conclusions

A major challenge in targeted drug delivery for cancer therapy is the balance between prolonged circulation afforded by "stealth" polymers versus cell-specificity provided by antibodies and targeting moieties. Using bivalent (tandem Fab) and tetravalent (Fab-IgG_1) bsAb against HER2 and PEG, we showed that multivalency and presence of Fc domain can influence the pretargeted delivery of PEGylated nanocarriers to orthotopic tumors. Our findings support pretargeting as a strategy to enhance PEGylated nanoparticle delivery to target cells/tissues, and further investigations into the use of Fc-attenuated multivalent pretargeting molecules for maximizing pretargeting efficiency.

REFERENCES

1. Fang, J., Nakamura, H. & Maeda, H. The EPR effect: Unique features of tumor blood vessels for drug delivery, factors involved, and limitations and augmentation of the effect. *Adv. Drug Deliv. Rev.* **63,** 136–151 (2011).

2. Kobayashi, H., Watanabe, R. & Choyke, P. L. Improving Conventional Enhanced Permeability and Retention (EPR) Effects; What Is the Appropriate Target? *Theranostics* **4,** 81–89 (2014).

3. Torchilin, V. Tumor delivery of macromolecular drugs based on the EPR effect. *Adv. Drug Deliv. Rev.* **63,** 131–135 (2011).

4. Bertrand, N., Wu, J., Xu, X., Kamaly, N. & Farokhzad, O. C. Cancer nanotechnology: The impact of passive and active targeting in the era of modern cancer biology. *Adv. Drug Deliv. Rev.* **66,** 2–25 (2014).

5. Torchilin, V. P. in *Handbook of Experimental Pharmacology* 3–53 (Springer, Berlin, Heidelberg, 2010). doi:10.1007/978-3-642-00477-3_1

6. Bazak, R., Houri, M., El Achy, S., Kamel, S. & Refaat, T. Cancer active targeting by nanoparticles: a comprehensive review of literature. *J. Cancer Res. Clin. Oncol.* **141,** 769–784 (2015).

7. Allen, T. M. Ligand-targeted therapeutics in anticancer therapy. *Nat. Rev. Cancer* **2,** 750–763 (2002).

8. Reuter, K. G. *et al.* Targeted PRINT Hydrogels: The Role of Nanoparticle Size and Ligand Density on Cell Association, Biodistribution, and Tumor Accumulation. *Nano Lett.* **15,** 6371–6378 (2015).

9. Elias, D. R., Poloukhtine, A., Popik, V. & Tsourkas, A. Effect of ligand density, receptor density, and nanoparticle size on cell targeting. *Nanomedicine Nanotechnology, Biol. Med.* **9,** 194–201 (2013).

10. Gu, F. *et al.* Precise engineering of targeted nanoparticles by using self-assembled biointegrated block copolymers. *PNAS* **105,** 2586–2591 (2008).

11. Beech, J. R., Shin, S. J., Smith, J. A. & Kelly, K. A. Mechanisms for targeted delivery of nanoparticles in cancer. *Curr. Pharm. Des.* **19,** 6560–6574 (2013).

12. Fakhari, A., Baoum, A., Siahaan, T. J., Le, K. B. & Berkland, C. Controlling Ligand Surface Density Optimizes Nanoparticle Binding to ICAM-1. *J. Pharm. Sci.* **100,** 1045–1056 (2011).

13. Moradi, E., Vllasaliu, D., Garnett, M., Falcone, F. & Stolnik, S. Ligand density and clustering effects on endocytosis of folate modified nanoparticles. *RSC Adv.* **2,** 3025–3033 (2012).

14. Cheng, Z., Al Zaki, A., Hui, J. Z., Muzykantov, V. R. & Tsourkas, A. Multifunctional nanoparticles: cost versus benefit of adding targeting and imaging capabilities. *Science* **338,** 903–910 (2012).

15. Yang, Q., Parker, C. L., McCallen, J. D. & Lai, S. K. Addressing challenges of heterogeneous tumor treatment through bispecific protein-mediated pretargeted drug delivery. *J. Control. Release* **220,** 715–726 (2015).

16. Kirpotin, D. B. *et al.* Antibody targeting of long-circulating lipidic nanoparticles does not increase tumor localization but does increase internalization in animal models. *Cancer Res.* **66,** 6732–6740 (2006).

17. Bae, Y. H. & Park, K. Targeted drug delivery to tumors: Myths, reality and possibility. *J. Control. Release* **153,** 198–205 (2011).

18. Leamon, C. P., Cooper, S. R. & Hardee, G. E. Folate-Liposome-Mediated Antisense Oligodeoxynucleotide Targeting to Cancer Cells: Evaluation in Vitro and in Vivo. *Bioconjug. Chem.* **14,** 738–747 (2003).

19. Patra, M., Zarschler, K., Pietzsch, H.-J., Stephan, H. & Gasser, G. New insights into the pretargeting approach to image and treat tumours. *Chem. Soc. Rev.* **45,** 6415–6431 (2016).

20. Larson, S. M., Carrasquillo, J. A., Cheung, N.-K. V. & Press, O. W. Radioimmunotherapy of human tumours. *Nat. Rev. Cancer* **15,** 347–360 (2015).

21. Su, Y.-C. *et al.* Conditional internalization of PEGylated nanomedicines by PEG engagers for triple negative breast cancer therapy. *Nat. Commun.* **8,** 15507 (2017).

22. Tung, H.-Y. *et al.* Selective Delivery of PEGylated Compounds to Tumor Cells by Anti-PEG Hybrid Antibodies. *Mol Cancer Ther* **14,** 1317–26

23. Khaw, B.-A. *et al.* Bispecific antibody complex pre-targeting and targeted delivery of polymer drug conjugates for imaging and therapy in dual human mammary cancer xenografts. *Eur. J. Nucl. Med. Mol. Imaging* **41,** 1603–1616 (2014).

24. Goldenberg, D. M., Chatal, J.-F., Barbet, J., Boerman, O. & Sharkey, R. M. Cancer Imaging and Therapy with Bispecific Antibody Pretargeting.

25. Cheal, S. M. *et al.* Theranostic pretargeted radioimmunotherapy of internalizing solid tumor antigens in human tumor xenografts in mice: Curative treatment of HER2-positive breast carcinoma. *Theranostics* **8,** 5106–5125 (2018).

26. Cheal, S. M. *et al.* Curative Multicycle Radioimmunotherapy Monitored by Quantitative SPECT/CT-Based Theranostics, Using Bispecific Antibody Pretargeting Strategy in Colorectal Cancer. *J. Nucl. Med.* **58,** 1735–1742 (2017).

27. Yang, Q. *et al.* Pretargeting with bispecific fusion proteins facilitates delivery of nanoparticles to tumor cells with distinct surface antigens. *J. Control. Release* **255,** 73–80 (2017).

28. Lewis, S. M. *et al.* Generation of bispecific IgG antibodies by structure-based design of an orthogonal Fab interface. *Nat. Biotechnol.* **32,** (2014).

29. Cheng, T. L., Roffler, S. R., Chuang, K. H. & Lu, S. J. Anti-polyethylene glycol antibody expressing cell quantify any free polyethylene glycol and polyethylene glycol-derivatized molecules. *U.S. Appl. 20120015380A1* (2012).

30. Breece, T. N. *et al.* Protein Purification. *Pat. No. US 6,870,034 B2* (2005).

31. Yang, Q. *et al.* Analysis of Pre-existing IgG and IgM Antibodies against Polyethylene Glycol (PEG) in the General Population. *Anal. Chem.* **88,** 11804–11812 (2016).

32. Yang, Q. *et al.* Evading immune cell uptake and clearance requires PEG grafting at densities substantially exceeding the minimum for brush conformation. *Mol. Pharm.* **11,** 1250–1258 (2014).

33. Zhang, Y., Huo, M., Zhou, J. & Xie, S. PKSolver: An add-in program for pharmacokinetic and pharmacodynamic data analysis in Microsoft Excel. *Comput. Methods Programs Biomed.* **99,** 306–314 (2010).

34. Bleeker, W. K., Teeling, J. L. & Erik Hack, C. Accelerated autoantibody clearance by intravenous immunoglobulin therapy: Studies in experimental models to determine the magnitude and time course of the effect. *Blood* (2001). doi:10.1182/blood.V98.10.3136

35. Jacob, S. & Rajabally, Y. A. Current proposed mechanisms of action of intravenous immunoglobulins in inflammatory neuropathies. *Curr. Neuropharmacol.* **7,** 337–342 (2009).

36. Lo, M. *et al.* Effector-attenuating Substitutions That Maintain Antibody Stability and Reduce Toxicity in Mice. *J. Biol. Chem.* **292,** 3900–3908 (2017).

37. Grevys, A. *et al.* Fc Engineering of Human IgG1 for Altered Binding to the Neonatal Fc Receptor Affects Fc Effector Functions. *J. Immunol.* **194,** 5497–5508 (2015).

38. Vaccaro, C., Bawdon, R., Ober, R. J., Wanjie, S. & Ward, E. S. Divergent activities of an engineered antibody in murine and human systems have implications for therapeutic antibodies. *PNAS* **103,** 18709–18714 (2006).

39. Vaccaro, C., Zhou, J., Ober, R. J. & Ward, E. S. Engineering the Fc region of immunoglobulin G to modulate in vivo antibody levels. *Nat. Biotechnol.* **23,** 1283–1288 (2005).

40. Cuesta, Á. M., Sainz-Pastor, N., Bonet, J., Oliva, B. & Álvarez-Vallina, L. Multivalent antibodies: When design surpasses evolution. *Trends Biotechnol.* **28,** 355–362 (2010).

41. Harwood, S. L. *et al.* ATTACK, a novel bispecific T cell-recruiting antibody with trivalent EGFR binding and monovalent CD3 binding for cancer immunotherapy. *Oncoimmunology* **7,** e1377874 (2017).

42. Su, C.-Y. *et al.* Bispecific antibodies (anti-mPEG/anti-HER2) for active tumor targeting of docetaxel (DTX)-loaded mPEGylated nanocarriers to enhance the chemotherapeutic efficacy of HER2-overexpressing tumors. *Drug Deliv.* **25,** 1066–1079 (2018).

43. Kao, C. H. *et al.* One-step mixing with humanized anti-mPEG bispecific antibody enhances tumor accumulation and therapeutic efficacy of mPEGylated nanoparticles. *Biomaterials* **35,** 9930–9940 (2014).

44. Zhao, Y. *et al.* therapeutic evaluation of polymeric nanomedicines: effect of different targeting peptides on therapeutic efficacy against breast cancer. *Nanotheranostics* **2,** 360–370 (2018).

45. Cui, J. *et al.* Modulating Targeting of Poly(ethylene glycol) Particles to Tumor Cells Using Bispecific Antibodies. *Adv. Healthc. Mater.* **1801607,** 1801607 (2019).

46. Zahmatkeshan, M., Gheybi, F., Rezayat, S. M. & Jaafari, M. R. Improved drug delivery and therapeutic efficacy of PEgylated liposomal doxorubicin by targeting anti-HER2 peptide in murine breast tumor model. *Eur. J. Pharm. Sci.* **86,** 125–135 (2016).

47. Rauscher, A. *et al.* Influence of pegylation and hapten location at the surface of radiolabelled liposomes on tumour immunotargeting using bispecific antibody. *Nucl. Med. Biol.* **41,** e66–e74 (2014).

48. Rauscher, A. *et al.* Improvement of the Targeting of Radiolabeled and Functionalized Liposomes with a Two-Step System Using a Bispecific Monoclonal Antibody (Anti-CEA × Anti-DTPA–In). *Front. Med.* **2,** (2015).

49. Westerlund, K. *et al.* Site-specific conjugation of recognition tags to trastuzumab for peptide nucleic acid-mediated radionuclide HER2 pretargeting. *Biomaterials* **203,** 73–85 (2019).

CHAPTER 5: EFFICIENT AND HIGHLY SPECIFIC GENE TRANSFER USING MUTATED LENTIVIRAL VECTORS REDIRECTED WITH BISPECIFIC ANTIBODIES

5.1 Introduction

Selective transduction of only target cells and tissues represents a major goal of therapeutic gene delivery. To do so, gene vectors must avoid binding to off-target cells while quickly binding target cells with high specificity, and efficiently deliver DNA to the nucleus following cell entry. Among common viral vectors, lentivirus (LV) is the among the most efficient gene transduction system for stable, long-term transgene expression. Importantly, the safety of LV has greatly improved since adverse effects were first observed in patients with X-clinical severe combined immunodeficiency (SCID) who underwent retrovirus-mediated gene therapy. That landmark gene therapy trial saw four cases of T-cell leukemia caused by insertional mutagenesis of the retroviral vectors leading to activation of proto-oncogenes and uncontrolled proliferation of mature T cells.[1–5] To reduce the risk of oncogenesis, lentiviral vector design has significantly improved by creating self-inactivating (SIN) vectors with transcriptionally inactive LTRs that reduce the transactivation potential of the vector; an internal promoter is included to drive transgene expression in the absence of LTR promoter activity. As a result, LV vectors are now routinely used in CAR T-cell therapies for B-cell malignancies where cells are selected, transduced with LV vectors, expanded, and reinfused into patients; two such therapies have received regulatory approval.

Despite the routine *in vivo* delivery of cells transduced with LV vectors *ex vivo*, LV vectors are rarely used directly for *in vivo* gene therapy. This is because common LV vectors

lack cell specificity: wildtype LV envelope proteins generally bind proteins present on the surface of most cells, leading to significant off-target effects. Strategies to alter or restrict the natural tropism of LV vectors include either pseudotyping LV with different viral envelope proteins for altered tropism and biodistribution,[6,7] or genetically inserting ligands, peptides, and single-chain antibodies into viral envelope glycoprotein domains to confer new cellular specificity.[8–14] A major drawback of the latter strategy is the need to generate new viral envelopes for each cellular target. Additionally, introducing large proteins can be deleterious to the structure of viral proteins, impede proper folding of incorporated peptide for diminished cell binding, and may hinder viral infectivity by altering normal functions of viral attachment proteins or preventing conformational changes necessary for fusion.[6] The success of this strategy critically depends on the size, structure, and binding activity of ligand. Frequently, such modified vectors generally suffers from inconsistent specificity, reduced fusion activity, and low viral titers.[12,15]

To enable highly specific transduction, we believe we must confer cell-specific receptor binding while simultaneously minimizing off-target binding. With wildtype viral vectors that are either pseudotyped with Ab or mixed with adaptor molecules, the resulting vectors can still bind and transduce off-target cells/tissues via the native viral Env. We thus hypothesized we can further improve viral vector specificity by first minimizing non-specific binding of LV to off-target cells. Previous work has shown that mutations in the receptor-binding domain (E2) of the Sindbis glycoprotein structure (mSindbis) eliminated its natural tropism for the liver and spleen, without affecting virus assembly or its high titer production.[8] These mutations specifically targeted regions within the E2 domain known to alter binding to target cells, block epitopes for neutralizing antibodies, and function in WT Sindbis tropism.[8] mSindbis-pseudotyped LV,

combined with bispecific antibodies (bsAb) that bind both mSindbis and specific cell receptors, thus provide a platform to evaluate our hypothesis. Here, we report the development of a potent and versatile gene carrier system, based on combining bsAb with LV, for highly specific gene delivery to select cells and tissues both *in vitro* and *in vivo*.

5.2 Materials and methods

5.2.1 Cell lines

293T cells were cultured in DMEM containing 10% FBS. Human SKBR3 cells were purchased from the University of North Carolina at Chapel Hill (UNC-CH) Tissue Culture Facility, and A2780 cells were provided by Michael Jay (UNC-CH). SKBR3 cells were cultured in McCoy's medium containing 15% fetal bovine serum (FBS), and A2780 cells were cultured in RPMI 1640 containing 10% FBS and 1% L-glutamine. For co-culture studies, SKBR3 and A2780 cells were both cultured in McCoy's medium with 15% FBS. All cells were maintained at 37°C and 5% CO_2.

5.2.2 Preparation and characterization of fluorescent Sindbis pseudotyped lentivirus

WT Sindbis and mSindbis pseudotyped lentiviruses (LV) were internally labeled with a GFP reporter gene. Particles were prepared by transfecting 293T cells with packaging plasmids pMDLg/pRRE and pRSV-Rev, transfer plasmid eGFP, and WT Sindbis or mSindbis envelope plasmid at a 1:1:1:1 ratio in media without serum. The cell supernatant was collected 48 h later, and fluorescently tagged lentiviruses from cell supernatant were purified by ultracentrifugation through 25% (w/v) sucrose in HEPES-NaCl buffer. Lentiviruses were resuspended in 10% sucrose in HEPES-NaCl buffer, divided into aliquots, and stored at -80°C. Viral titer was

quantified by qPCR-based lentivirus titration kit according to manufacturer's protocol (Applied Biological Materials, Inc., Richmond, British Columbia, Canada). Packaging plasmids pMDLg/pRRE (Addgene plasmid # 12251) and pRSV-Rev (Addgene plasmid # 12253) were provided by Didier Trono.[16]

5.2.3 Bispecific antibody construction and characterization

Sequences for chimeric anti-Sindbis E1 or E2 and anti-HER2 antibodies (Ab) were generated by combining the V_H/V_L regions of commercially available humanized anti-HER2 (Trastuzumab)[17] and murine anti-Sindbis with the C_H1/C_L and Fc regions of human IgG_1 Ab. Mouse anti-Sindbis E1 and E2 V_H/V_L sequences were provided by Diane Griffin (Johns Hopkins University). To generate bispecific IgG antibodies ($bsIgG_1$) that recognized both Sindbis E1 or E2 and anti-HER2, separate orthogonal mutation sets were incorporated into anti-HER2 and anti-Sindbis Fab domains.[18] Orthogonal mutation sets provided high fidelity pairing of heavy and light chains; this technology was licensed through a partnership between Dualogics and UNC-CH. These mutations were also incorporated into the chimeric monoclonal antibody, IgG_1^{HER2}.

Plasmids encoding chimeric heavy and light chains were cotransfected into Expi293F cells (Thermo Fisher Scientific, Grand Island, NY) and grown for 72h. IgG_1^{HER2}, $bsIgG_1^{E2xHER2}$, and $bsIgG_1^{E1xHER2}$ were purified from expression supernatant using protein A agarose (Thermo Fisher Scientific). $BsIgG_1$ antibodies were separated via size exclusion chromatography (ENnrich SEC 650 10 x 300 column, Bio-Rad Laboratories, Inc., Hercules, CA). The tandem Fab was designed to include a polyhistidine tag on its C-terminus and was purified from expression supernatant using Ni-NTA agarose (Qiagen Inc, Germantown, MD). All purified antibodies were concentrated (MWCO 10K, Amicon Ultra), buffer exchanged into PBS,

concentration determined using A280 (NanoDrop One/One), and assessed for size and purity by sodium dodecyl sulfate polyacrylamide gel electrophoresis (SDS-PAGE).

5.2.4 Antibody binding affinity characterization

HER2-specific ELISAs were performed to confirm binding of purified antibodies to HER2 as well as compare dissociation constants of bispecific antibodies relative to parental monoclonal control, IgG_1^{HER2}. Briefly, recombinant human ErbB2/HER2 Fc chimera protein (R&D Systems, cat no. 1129-ER, Minneapolis, MN) was coated onto high-binding half-area 96-well Costar plates (Corning) at 1 μg/ml in bicarbonate buffer overnight at 4°C. After blocking plate with 5% nonfat milk in PBS with 0.05% Tween (PBST), purified antibody samples were diluted in 1% nonfat milk in PBST at various concentrations and incubated for 1 h, followed by washes with PBST. Bound antibodies were detected using goat anti-human kappa light chain HRP (Sigma-Aldrich, cat no. A7164, 1:10,0000 dilution) for 1 h followed by 1-step Ultra TMB (Thermo Fisher Scientific). After stopping the HRP reaction with 2N sulfuric acid, the absorbance at 450 nm and 570 nm was measured using a Spectramax M2 plate reader (Molecular Devices).

To evaluate Sindbis specific binding, whole lentivirus (WT Sindbis, mSindbis, and no envelope control) was blotted onto nitrocellulose membrane. Bound bispecific antibodies were detected using goat anti-human kappa light chain HRP (Sigma-Aldrich, cat no. A7164, 1:10,000 dilution), followed by chemiluminescent detection using ECL reagents (Bio-Rad Laboratories, Inc).

5.2.5 Viral infectivity assay

SKBR3 ($HER2^+$) and A2780 ($HER2^-$) cells were seeded at $3x10^4$ cells per well in 96-well tissue culture treated plate. Sindbis pseudotyped lentiviruses (multiplicity of infection, MOI = 3) were premixed with antibodies at 1 nM concentration for 1 h at room temperature, and then incubated with cells at 37°C in 5% CO_2. Twenty-four hours later, the transduction mixture was removed from cells and cells were washed three times with PBS. Cells were allowed to grow for 72 h in fresh cell culture media at 37°C in 5% CO2. Cells were washed and the percentage of transduced cells (GFP^+) in each well was quantified using iQue Screener PLUS flow cytometer (Intellicyt, Albuquerque, NM). Additionally, to confirm that viral infectivity was dependent upon HER2 specificity of the bsAb, the viral infectivity assay was repeated with increasing concentrations of $bsIgG_1^{E2xHER2}$ in the presence and absence of excess IgG_1^{HER2} (0.1 μM).

To test the selectivity of targeted viral systems for $HER2^+$ cells, we established a co-culture model of SKBR3 and A2780 cells that were maintained in McCoy's 5A medium supplemented with 15% FBS. Cells in the co-culture were infected with nontargeted and targeted LV vectors as described above. Seventy-two hours post-infection, treated cells were washed and labeled with IgG_1^{HER2} followed by goat anti-human IgG-Alexa Fluor 594 (Thermo Fisher Scientific) to generate two key cell populations: cells double positive for GFP and HER2 expression and cells double negative for GFP and HER2 expression. The percentages of GFP^+ cells of all $HER2^+$ cells and GFP^+ cells of all $HER2^-$ cells in each well were quantified using iQue Screener PLUS flow cytometer. Data were analyzed using ForeCyt software and BD FACSDiva software.

5.2.6 Viral infectivity assay in the presence of exogenous mouse serum

The infectivity assay was also performed in the presence of exogenous mouse serum to determine whether mouse serum proteins could inhibit bsAb-mediated viral infectivity. Compared to the standard infectivity assay, SKBR3 cells were *pre-incubated* with undiluted BALB/c mouse serum (50 μl/well; BioVT, Westbury, NY) for 1 h. Then, serum was replaced with transduction mixture for 24 h, and the percentage of GFP^+ cells was quantified and compared to SKBR3 treated in the absence of mouse serum. To further investigate the effect of mouse serum on viral infectivity of targeted LV, transduction mixtures were also *co-incubated* with increasing amounts of mouse serum for 1 h prior to incubating with cells. The total volume of transduction mixture remained constant as the percentage of mouse serum increased.

5.2.7 Statistical analysis

All data are presented as mean ± SD. All graphs and statistical tests were performed using GraphPad Prism 7 software. Group comparisons were analyzed using two-way ANOVA and *post hoc* Tukey's test. A p-value <0.05 was considered to indicate statistical significance.

5.3 Results

5.3.1 OrthoMab-based bsAb preserves specificity and affinity to antigens

We engineered chimeric bsAb against both HER2 overexpressed on breast cancer cells and Sindbis Env glycoproteins displayed on LV, based on merging human IgG_1 backbones with HER2- and Sindbis envelope-binding V_H and V_L domains previously isolated from mouse IgG. We prepared bsAb that bound either Sindbis Env glycoprotein E1 (responsible for pH-dependent endo-lysosomal membrane fusion and escape) or E2 domain (responsible for binding high-

affinity laminin receptors[19] and heparin sulfate[20] and mediates entry) (Figure 5.1A). Purified Ab were separated via size exclusion chromatography, and exhibited the expected molecular sizes as visualized on non-reduced and reduced protein gels (Figure 5.1B-C).

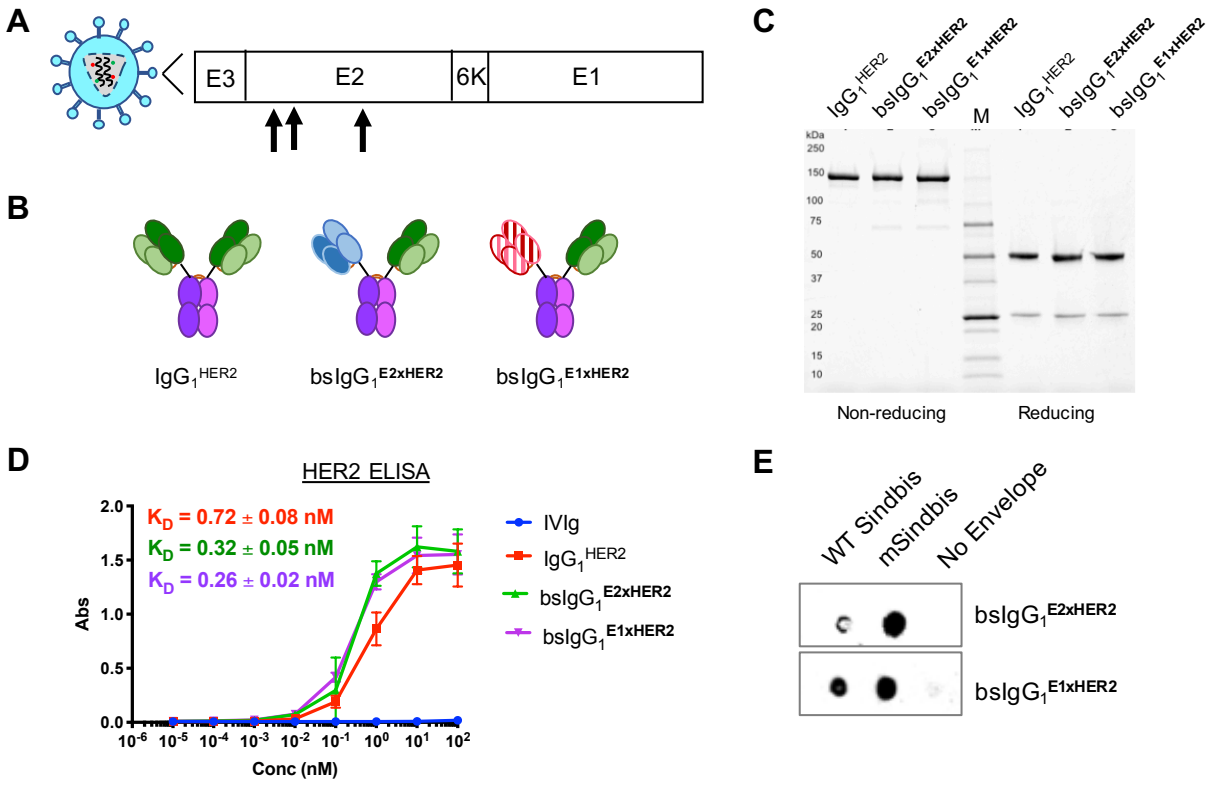

Figure 5.1. **Characterization of control and bispecific antibodies (bsAb). A**) Schematic representation of Sindbis glycoprotein domains E1 and E2. Mutated Sindbis envelope glycoprotein (mSindbis) contains mutations in the E2 domain (indicated by arrows) that ablate native receptor binding. E1 remains unchanged in both WT and mSindbis lentiviruses, and forms a heterodimer with E2. E3 is a signal sequence peptide for E2 protein. **B**) Schematic of control and bispecific Ab illustrating size and key design features. **C**) Nonreducing (left) and reducing (right) protein gel showing Coomassie blue staining of control and bispecific Ab. **D**) Binding affinity of control and bispecific Ab to HER2-Fc chimera analyzed by ELISA (n = 2). **E**) Selective binding of αE2 and αE1 bispecific Ab to Sindbis pseudotyped lentiviruses and no binding to negative control (no envelope lentivirus) as visualized by dot blot.

We next confirmed specificity and affinity of the monoclonal and bsAb using antigen-specific ELISAs against HER2, and found that bispecific bsIgG$_1^{E2xHER2}$ and bsIgG$_1^{E1xHER2}$ both

possessed similar binding affinities to HER2 as the monoclonal anti-HER2 IgG_1 (Trastuzumab; IgG_1^{HER2} control). The K_D for $bsIgG_1^{E2xHER2}$, $bsIgG_1^{E1xHER2}$, and IgG_1^{HER2} were 0.32 ± 0.05 nM, 0.26 ± 0.02 nM, and 0.72 ± 0.08 nM, respectively (Figure 5.1D). We also confirmed the binding of our bsAb to WT- and mSindbis pseudotyped LV using dot blot. Both bsAb bound WT and mSindbis Env pseudotyped LV, and did not bind to LV without an envelope (i.e. negative control) (Figure 1E). IgG_1^{HER2} also did not bind to WT Sindbis, mSindbis, or the non-enveloped LV control. Altogether, these results confirmed that we prepared functional bsAb, and that the orthogonal mutations introduced at the heavy and light chain interface did not impair binding to either HER2 or Sindbis envelope.

5.3.2 $bsIgG_1^{E2xHER2}$ enhanced viral infectivity compared to virus alone

Using flow cytometry, we first measured the transduction efficiency of nontargeted WT- and mSindbis lentiviruses expressing GFP in $HER2^+$ SKBR3 cells using a low vector-to-cell ratio (MOI) of three. As expected, mSindbis had markedly lower transduction efficiency compared to WT Sindbis, transducing only 1% of target $HER2^+$ cells vs 4% for WT Sindbis, with two-fold lower mean fluorescence intensity (MFI) than WT Sindbis (Figure 5.2A, B). The infectivity of both WT and mSindbis LV were substantially enhanced when pre-mixed with 1 nM of E2-bindig $bsIgG_1^{E2xHER2}$, transducing ~18% and 12% of $HER2^+$ cells at the same MOI, respectively (Figure 5.2A, B). Compared to non-targeted WT Sindbis, targeted WT Sindbis transduced 5-fold more target cells, with 5-fold greater MFI, whereas targeted mSindbis transduced 10-fold more target cells than mSindbis alone, with 8-fold greater MFI. These results indicate that bsAb can indeed confer greater cell binding of LV, with more pronounced

improvement of mSindbis versus WT Sindbis, most likely due to the exceedingly limited potency of mSindbis LV alone.

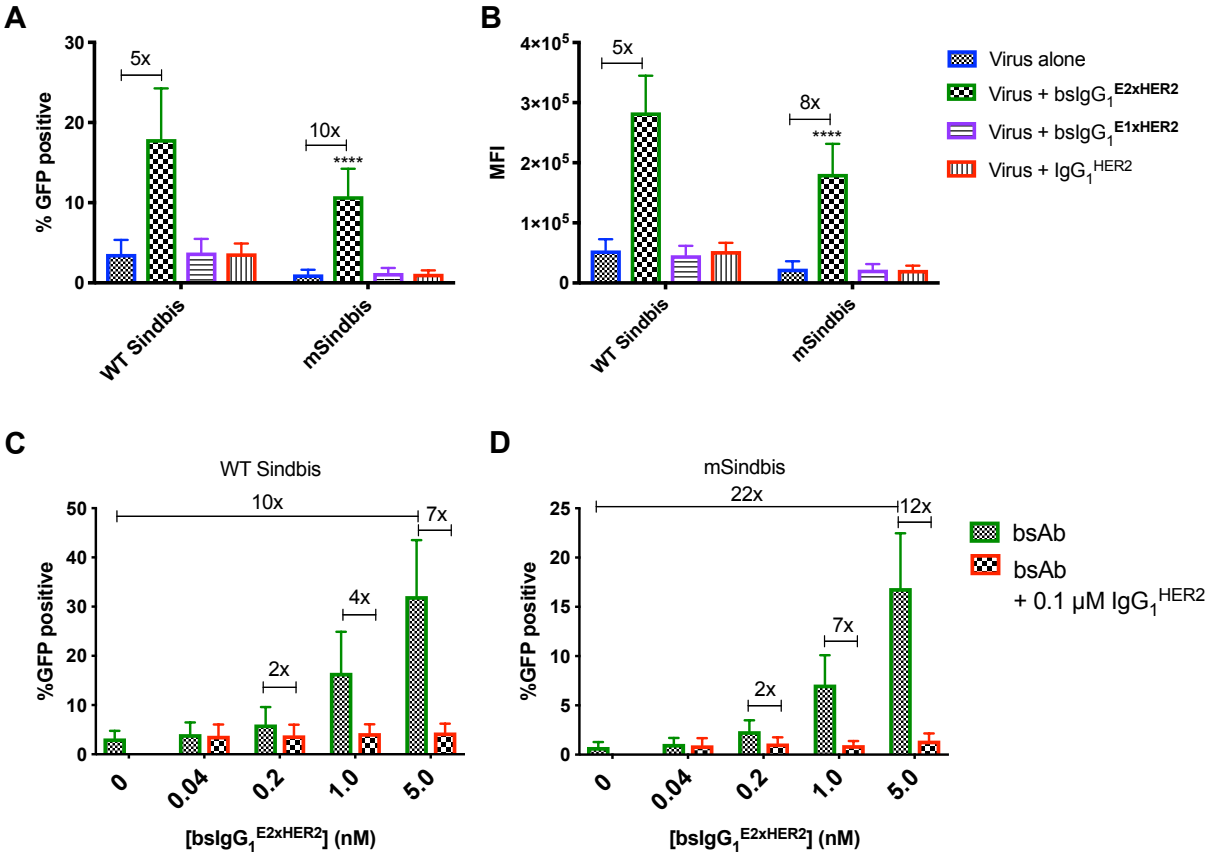

Figure 5.2. BsIgG$_1^{E2xHER2}$ enhanced transduction by WT Sindbis and mSindbis pseudotyped lentiviral vectors against HER2$^+$ SKBR3 cells compared to either virus alone. bsAb-mediated viral infectivity was measured by flow cytometry as **A**) percentage of GFP positive cells and **B**) mean fluorescence intensity, MFI. Data represents n = 5 independent experiments performed in duplicates, MOI = 3, and antibody concentration = 1 nM (two-way ANOVA *post-hoc* Tukey's test, **** indicates $p<0.0001$ vs all conditions). (**C, D**) Targeted lentiviral infectivity is dependent upon HER2 specificity of bsAb. At all tested concentrations of bsAb, excess Trastuzumab (IgG$_1^{HER2}$) effectively blocked viral infectivity of both targeted lentiviruses, suggesting that the infectivity was mediated specifically via binding to HER2 receptor and not due to differences between lentiviruses. Data represents n = 3 independent experiments performed in duplicates and MOI = 3.

We next assessed whether increasing the concentration of bsIgG$_1^{E2xHER2}$ could further enhance the transduction efficiency of both targeted LV. At the highest bsIgG$_1^{E2xHER2}$

concentration tested, targeted WT Sindbis and mSindbis LV increased the fraction of GFP^+ SKBR3 cells by ~10-fold and ~22-fold, respectively, compared to their corresponding nontargeted LVs (Figure 5.2C, D). $BsIgG_1^{E2xHER2}$ redirection were highly specific to HER2, as incubation with excess IgG_1^{HER2} control effectively blocked infectivity, reducing the percentage of GFP^+ at each tested bsAb concentration to the same level as non-targeted LVs (Figure 5.3C, D).

5.3.3 Effectiveness of bsAb retargeting depends on binding epitope on Sindbis Env

To assess whether bsIgG simply need to engage the LV or if efficient transduction is dependent on bsIgG binding to specific epitopes, we in parallel evaluated the transduction potencies of LVs pre-mixed with $bsIgG_1^{E1xHER2}$. Interestingly, $bsIgG_1^{E1xHER2}$ did not improve the transduction efficiency of either LV, with comparable percentages of GFP^+ cells and MFI of transduced cells to that of nontargeted LV alone (Figure 5.2A, 2B). Nontargeted WT Sindbis, WT Sindbis mixed with $bsIgG_1^{E1xHER2}$, and WT Sindbis mixed with IgG_1^{HER2} control all transduced ~4% of $HER2^+$ cells. Similarly, nontargeted mSindbis, targeted mSindbis mixed with $bsIgG_1^{E1xHER2}$, and targeted mSindbis mixed with IgG_1^{HER2} control all transduced ~1% of $HER2^+$ cells. These results indicate bsAb-mediated gene transfer is critically dependent on binding specific epitopes on the Sindbis Env-binding domain.

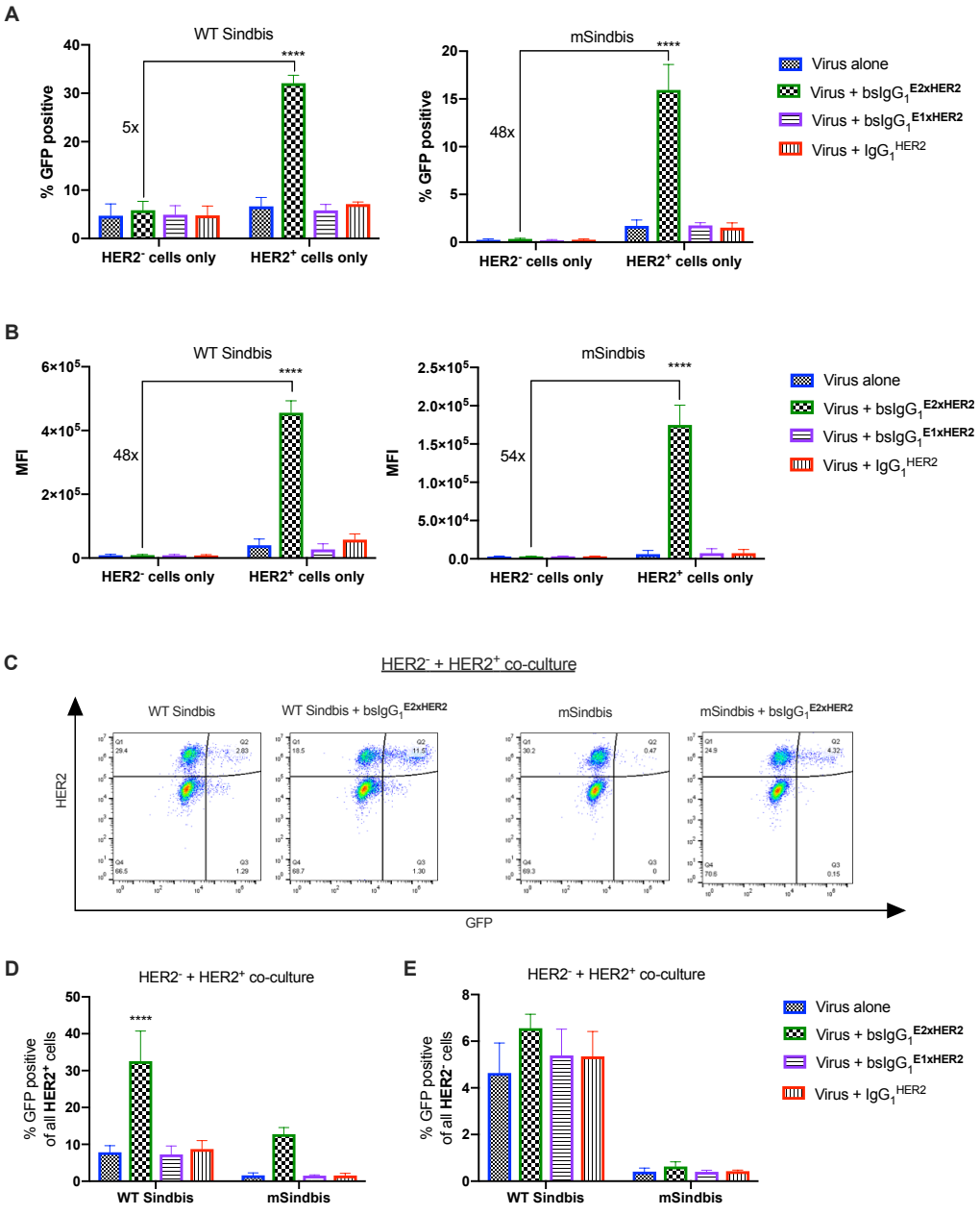

Figure 5.3. Specific infection of HER2$^+$ cells in a mixed cell population. (A-B) Targeted WT and mSindbis substantially enhanced viral infectivity in HER2$^+$ cells compared to control HER2$^-$ cells. Viral infectivity was measured by flow cytometry as **A**) percentage of GFP positive cells and **B**) mean fluorescence intensity, MFI. **C**) A2780 (HER2$^-$) cells were mixed with SKBR3 (HER2$^+$) to create a mixed cell population. Both targeted lentiviruses demonstrated selectivity for **D**) HER2$^+$ cells compared to **E**) HER2$^-$ cells as indicated by the substantial increase in percentage of GFP positive cells. Data represents 2 independent experiment performed in duplicates, MOI 3, [Ab] = 1 nM (two-way ANOVA with *post-hoc* Tukey's test, **** $p<0.0001$ vs all conditions).

5.3.4 Targeted LV vectors preferentially transduced target HER2$^+$ cells

To evaluate the specificity of bsAb-mediated LV for target cells relative to off-target cells, we compared viral potencies on HER2$^+$ (SKBR3) and HER2$^-$ (A2780) cells, where A2780 represented a nonspecific cell control with little to no HER2 expression. We observed minimal transduction of HER2$^-$ A2780 cells with WT and mSindbis LV alone (5% and 0.2% of A2780 cells, respectively; Figure 5.3A). In contrast, nontargeted WT Sindbis infected 7% of HER2$^+$ cells while nontargeted mSindbis infected 1.7% of HER2$^+$ cells (Figure 5.3A). Pre-mixing LV with bsIgG$_1^{E2xHER2}$ did not appreciably increase transduction of HER2$^-$ cells, with 6% and 0.3% of A2780 cells transduced with WT and mSindbis LV (Figure 5.3A). Both targeted LVs demonstrated greater selectivity for HER2$^+$ cells over HER2$^-$ cells, with targeted mSindbis LV substantially exceeding the specificity of targeted WT Sindbis LV. WT Sindbis LV mixed with bsIgG$_1^{E2xHER2}$ enhanced the percentage of GFP$^+$ cells 5-fold (Figure 5.3A) and MFI 48-fold (Figure 3B) in HER2$^+$ SKBR3 cells compared to HER2- A2780 cells, whereas targeted mSindbis LV transduced 48 times more SKBR3 cells than A2780 cells, with 54-fold higher MFI.

To further assess the specificity of gene transfer, we evaluated bsIgG$_1^{E2xHER2}$-targeted LV to selectively transduce HER2$^+$ cells in co-cultures of both HER2$^+$ and HER2$^-$ cells. In good agreement with its broad transduction nature, nontargeted WT Sindbis had very poor selectivity, transducing ~8% of HER2$^+$ cells (Figure 5.3D) and ~5% of HER2$^-$ cells (Figure 5.3E). Nontargeted mSindbis LV also had relatively limited selectivity, transducing ~2% of HER2$^+$ cells (Figure 3D) and ~0.4% of HER2$^-$ cells (Figure 5.3E).

Pre-mixing WT Sindbis LV with bsIgG$_1^{E2xHER2}$ modestly increased both the potencies and specificity: targeted WT Sindbis LV exhibited a ~5x selectivity towards HER2$^+$ cells, transducing ~33% of SKBR3 cells vs ~7% of A2780 cells (Figure 5.3D, E). Surprisingly,

combining bsAb-based redirecting with ablation of native receptor binding synergistically enhanced targeting efficiencies, with a 20x selectivity towards $HER2^+$ than $HER2^-$ cells (~13% of SKBR3 cells vs ~0.6% of A2780 cells). Overall, compared to WT Sindbis LV, targeted mSindbis LV were ~2-fold more efficient in transducing SKBR3 cells, while reducing non-specific gene transfer by ~22-fold (~13% of $HER2^+$ cells vs ~0.6% of $HER2^-$ cells). These results underscore the enhanced selectivity and potent gene transfer using mSindbis LV + $bsIgG_1^{E2xHER2}$.

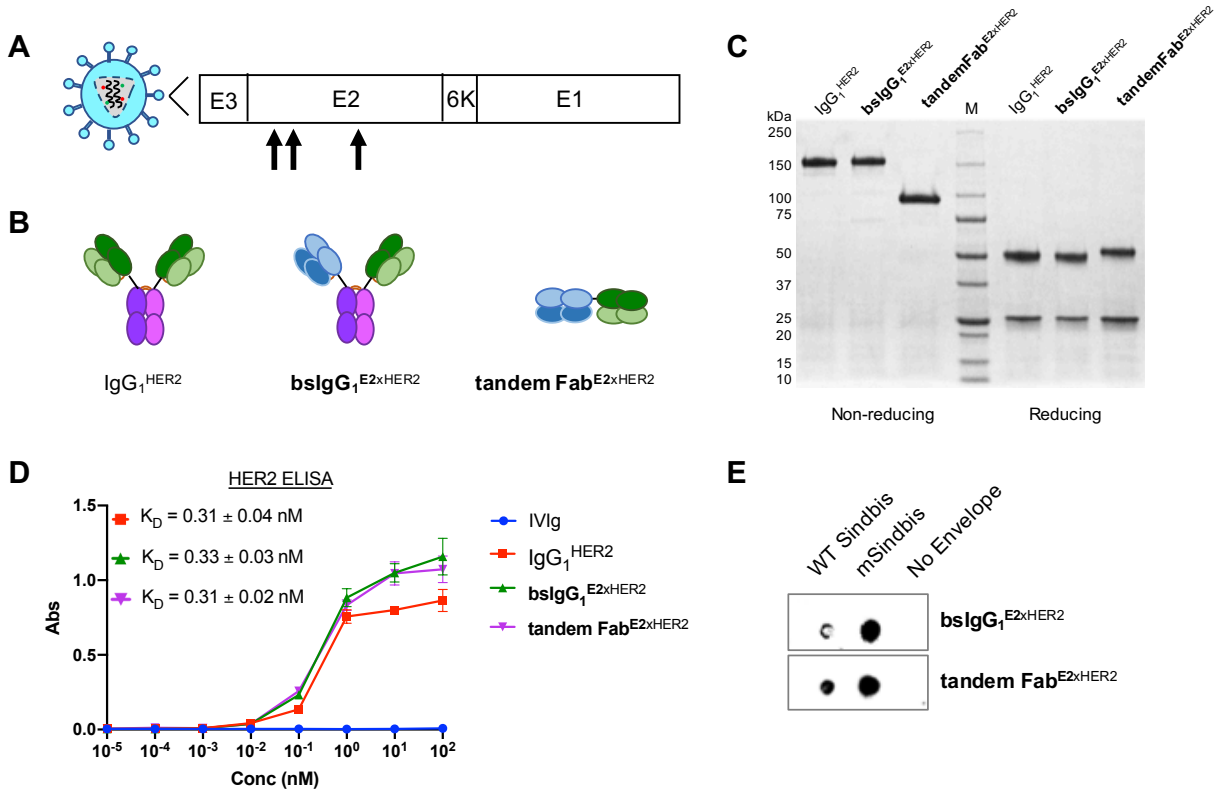

Figure 5.4. Characterization of bispecific tandem Fab. A) Schematic representation of Sindbis glycoprotein domains E1 and E2. Mutated Sindbis envelope glycoprotein (mSindbis) contains mutations in the E2 domain (indicated by arrows) that ablate native receptor binding. E1 remains unchanged in both WT and mSindbis lentiviruses, and forms a heterodimer with E2. E3 is a signal sequence peptide for E2 protein. **B**) Schematic of control and bispecific Ab illustrating size and key design features between $bsIgG_1$ and tandem Fab. **C**) Nonreducing (left) and reducing (right) protein gel showing Coomassie blue staining of control and bispecific Ab. **D**) Binding affinity of control and bispecific Ab to HER2-Fc chimera analyzed by ELISA. **E**) Selective binding of bispecific Ab ($bsIgG_1$ and tandem Fab) to Sindbis pseudotyped lentiviruses and no binding to negative control (no envelope lentivirus) as visualized by dot blot.

Because bsIgG$_1^{E2xHER2}$ outperformed bsIgG$_1^{E1xHER2}$, bsIgG$_1^{E2xHER2}$ became our lead bsAb. However, FcRn recycling and non-specific uptake by Fc receptors on immune cells present a challenge for *in vivo* efficiency of targeted viral vectors via systemic administration. We thus proceeded with a Fc-free tandem Fab that similarly binds Sindbis E2 and HER2 (Figure 5.4) for *in vivo* studies; this tandem Fab facilitated similar transduction effectiveness as bsIgG$_1$ (Figure 5.5).

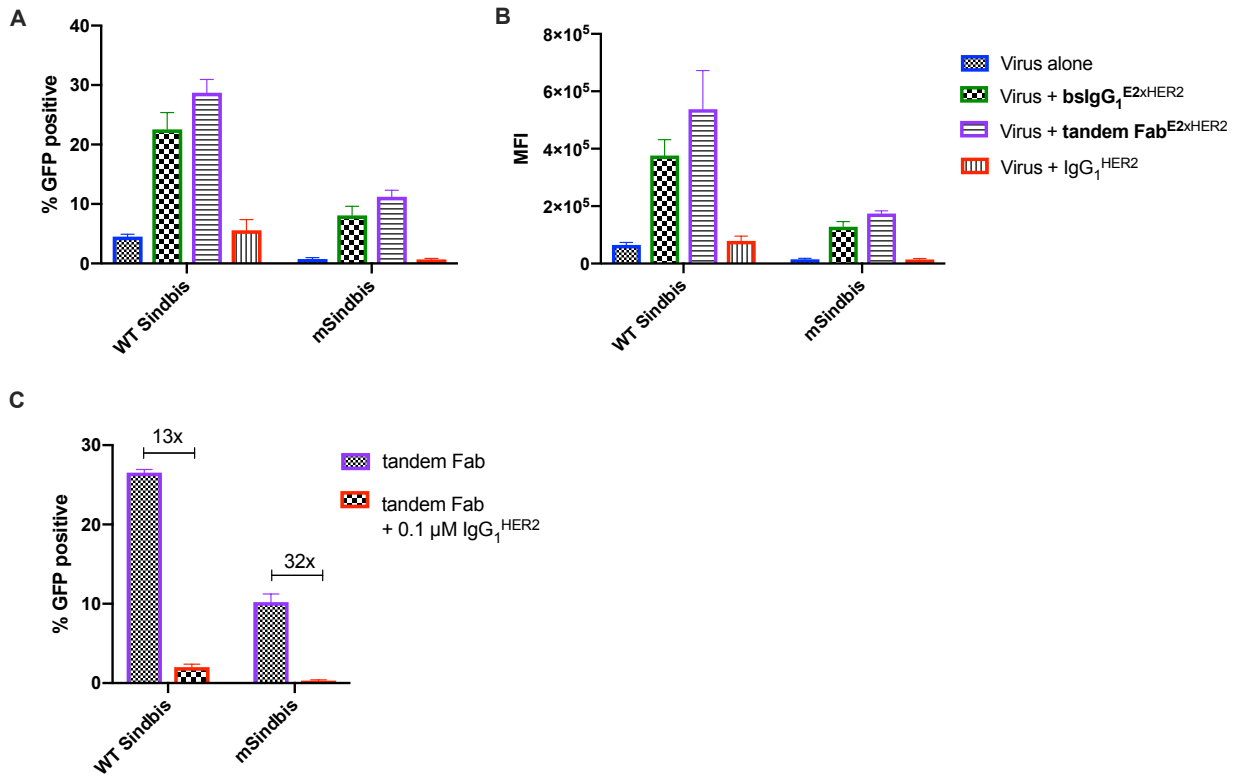

Figure 5.5. Comparable transduction efficiency of targeted viruses coated with bsIgG$_1^{E2xHER2}$ and tandem Fab^{E2xHER2} in target HER2$^+$ cells. Viral infectivity was measured by flow cytometry as **A**) percentage of GFP positive cells and **B**) mean fluorescence intensity, MFI. **C**) Targeted lentiviral infectivity is dependent upon HER2 specificity of bispecific antibody. Excess Trastuzumab (IgG$_1^{HER2}$) substantially reduced viral infectivity of both targeted lentiviruses. All data represents n = 2 independent experiments, MOI = 3, [bsIgG$_1^{E2xHER2}$] = 1 nM, [tandem Fab^{E2xHER2}] = 5nM, and [IgG$_1^{HER2}$] = 1nM.

5.3.5 Exogenous mouse serum reduced targeted viral infectivity at the viral level

To be effective *in vivo*, targeted viral systems must mediate efficient gene transfer in the presence of serum opsonizing proteins. We thus evaluated the transduction efficiency of targeted LV vectors in the presence of increasing mouse serum content (Figure 5.6A). Transduction efficiencies decreased substantially when observed serum content was increased beyond the 15% baseline, with a greater decrease observed with mSindbis than WT Sindbis LV, suggesting that mouse serum does not affect infectivity at the cellular level. Instead, it is likely that the stability of the bsAb/LV complexes is reduced by increasing serum content in the media. We found no drop in transduction efficiencies when SKBR3 cells were first incubated with undiluted mouse serum (Figure 5.6B).

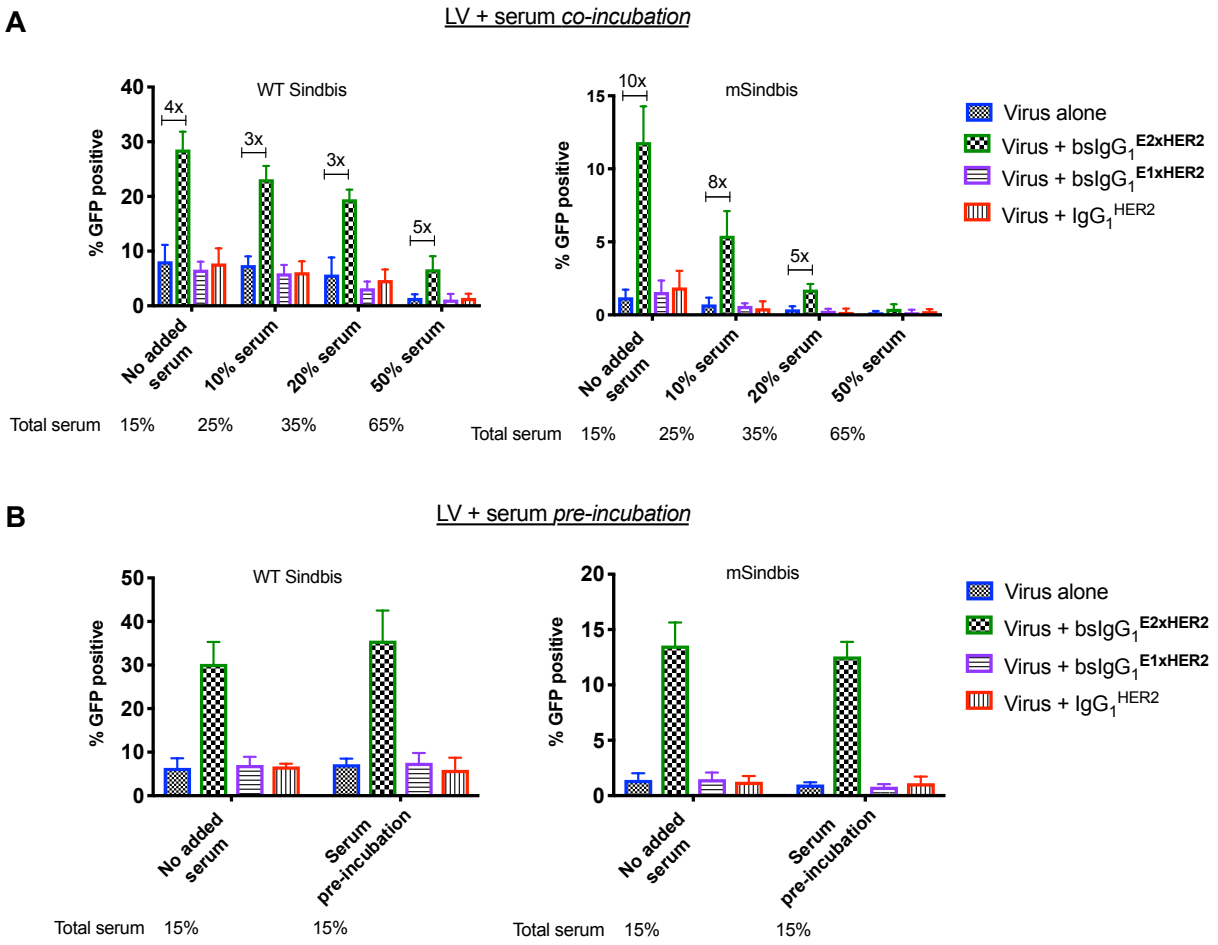

Figure 5.6. Serum affects targeted viral infectivity at the viral level not the cellular level. A) Viral infectivity was substantially reduced when cells were *co-incubated* with transduction mixture and increasing percentages of mouse serum. **B**) BsAb-mediated viral infectivity was maintained when cells were *pre-incubated* with undiluted mouse serum. Serum was removed from cells prior to incubation with transduction mixture. All data represents n = 2 independent experiments, MOI = 3, and [Ab] = 1nM.

5.4 Discussion

Efficient and highly specific gene delivery *in vivo* continues to be a major challenge in human gene therapy. Despite their exceptional potencies, the use of LV vectors *in vivo* remains very limited due to their poor cell and tissue specificity. WT Sindbis virus binds to high-affinity laminin receptors[19] and heparin sulfate[20] for wide distribution throughout the body, therefore making it an ineffective viral vector for targeted gene delivery *in vivo* via systemic

administration. In turn, this broad native tropism of LV vectors has restricted the use of LV to *ex vivo* transduction, selection, and reinfusion into patients. Introducing attenuating mutations into the receptor binding domain (E2) of Sindbis envelope glycoprotein structure drastically reduced its background level of infectivity in both target $HER2^+$ and off-target $HER2^-$ cells. Here, by combining bsAb that bind cell-specific receptors with abrogating the native tropism of the LV vectors, we substantially improved the specificity of LV vectors, culminating in a system that is 48-times more selective for $HER2^+$ cells over $HER2^-$ cells.

Reducing native binding for greater selectivity has been observed in other fields. For example, Slaga *et al* developed bsAb based on the avidity of two low-affinity anti-HER2 Fab domains to improve the selectively of T cell-recruiting bispecific antibodies for HER2-overexpressing cancer cells and tumors and not to cells with low HER2 expression.[21] The engineered bsAb were highly potent *in vitro* and their *in vivo* selectivity to HER2-overexpressing tumors was improved more than 100-fold for greater therapeutic index and mitigated adverse effects. Simnick *et al* engineered a highly specific, targeted delivery system that possessed low affinity for its target on off-target cells, but transformed into a high affinity, multivalent nanoparticle at target cells upon increased temperature.[22] Elastin-like polymers with RGD peptide in its low affinity, monovalent state demonstrated poor binding and uptake by both $\alpha_v\beta_3^+$ and $\alpha_v\beta_3^-$ cells. In contrast, the multivalent presentation of RGD peptide by self-assembled elastin-like polymer nanoparticles facilitated enhanced binding and uptake only to cells that overexpressed $\alpha_v\beta_3$ integrin.

The envelope of alphavirus Sindbis, capable of pseudotyping lentiviruses, contains two integral membrane glycoproteins, E1 and E2. While the E1 domain mediates endo-lysosomal membrane fusion and escape at low pH, the E2 domain is responsible for binding to host cell

receptor. Because receptor binding (attachment) and fusion (endosomal escape) are independent functions for Sindbis virus, it is possible to manipulate binding specificity without hindering fusion. We found that bsAb against Sindbis Env E2 domain were much more effective at transducing target cells than bispecific antibodies against Sindbis Env E1 domain. Since E1-binding bsAb was able to bind WT and mSindbis LV, we hypothesize that $bsIgG_1^{E1xHER2}$ failed to mediate efficient transduction possibly due to interference with the efficiencies of E1-mediated membrane fusion.

Multiple strategies have been implemented to confer new targeting specificity of mutated Sindbis pseudotyped lentiviruses using adaptors and antibodies.[8,12,13,23–27] The ZZ domain of protein A was genetically incorporated into the Sindbis Env protein, such that any targeting monoclonal antibody (mAb) with Fc region could redirect the virus to target cells.[8,23,24] Morizono *et al* demonstrated ~15-fold selectivity towards $CD4^+$ cells over $CD4^-$ cells using ZZ Sindbis pseudotyped lentivirus mixed with anti-CD4 mAb, [24] which is three times less selective than our bsAb-mSindbis LV system. Moreover, the ZZ Sindbis-mAb system is vulnerable to circulating serum immunoglobulins due to the reversible interaction between ZZ domain and Fc domain of mAb (K_D of streptavidin-biotin = 10^{-15} M is $10^{7–8}$ less than K_D of ZZ-Fc),[25] thereby making ZZ Sindbis pseudotype a poor choice for *in vivo* gene delivery. More recently, Chen and colleagues transitioned to a *covalent* interaction between Sindbis pseudotyped lentiviruses and cell-specific DARPin adaptors. Relying on the high affinity, covalent pairing of SpyTag/SpyCatcher, Kasaraneni *et al* engineered Sindbis pseudotyped lentivirus with Spy Tag and αHER2 DARPin-SpyCatcherΔ for significantly reduced nonspecific cell-binding and 7-fold selectivity towards $HER2^+$ cells over $HER2^-$ cells; notably, the transduction efficiency of this system was not altered in the presence of human serum.[26] This group also pursued a similar

approach by exploiting a disulfide bond-forming protein-peptide pair PDZ1 and its pentapeptide ligand (TEFCA) to engineer a covalent pairing between PSZI-Sindbis pseudotyped lentivirus and αHER2 DARPin-TEFCA. This stable targeting system was ~10-fold selective towards $HER2^+$ cells over $HER2^-$ cells, and maintained its transduction efficiency in the presence of human serum.[27] While our bsAb-mSindbis LV system exhibited greater targeting selectivity compared to the previous studies, we observed reduced transduction efficiency as the serum content was increased beyond the 15% baseline. Using phage display technology, we can engineer bsAb with higher affinity for mSindbis Env for more stability and resistance to serum sensitivity.

Adeno-associated virus (AAV) vectors are also used in targeted gene delivery methods, including in human patients, due to their simple binding and entry mechanisms, medium- to long-term gene expression depending on transduced cell type, and no risk of insertional mutagenesis. Gigout *et al* incorporated the immunoglobulin-binding Z34C fragment of protein A into AAV2 capsid to engineer a modified AAV2 that transduced target cells when mixed with targeting mAb.[28] Using exceedingly high MOIs of 10,000 and 40,000, modified AAV2 exhibited high level of background infectivity, so the inclusion of targeting mAb showed only a modest improvement of 2-4 fold increase. To effectively reduce WT tropism of modified AAV2, the group incorporated additional amino acid changes into the capsid. When mixed with bsAb, the engineered AAV2 with ablated WT tropism transduced 5-20% of target cells whereas the vector alone had very low background infectivity. Similar to our approach, Bartlett *et al* used a bsAb to redirect AAV to target $\alpha_{IIb}\beta_3^+$ cells and found a 70-fold improvement vs. WT AAV alone.[29] However, targeted bsAb-AAV system transduced off-target $\alpha_{IIb}\beta_3^-$ cells to levels comparable to $\alpha_{IIb}\beta_3^+$ cells, indicating a lack of targeting specificity and a poor choice for targeted gene delivery *in vivo*.

Challenges associated with targeted AAV gene delivery include lack of efficient transduction, natural tropism to liver for off-target effects, and need to use very high MOI for infectivity. These challenges are further exacerbated by the vector's high immunogenicity, such that pre-existing and neutralizing antibodies can prevent initial or repeated administration of gene therapy treatment respectively. In contrast, the general population is less likely to have pre-existing Ab against lentiviral vectors, thereby making it advantageous over AAV.[30] An added benefit of our approach is the use of human-based Fabs to redirect mSindbis LV to target cells; the "shield" of human Fab molecules around the mSindbis LV will likely block any induced Ab and prevent premature clearance from the circulation.

Lentiviral based gene therapy has long suffered from the misconception of poor safety arising from insertional mutagenesis that triggers carcinogenesis. This stemmed from the seminal French gene therapy clinical trials that restored the immune system in patients with X-linked SCID by transducing autologous hematopoietic stem cells *ex vivo* using γ-retroviral vectors.[31,32] Despite curing the disease, investigators observed serious adverse effects: leukemia caused by vector insertional mutagenesis.[1–5] Extensive work has been done since then to improve the safety of gene therapy vectors, in particular by removing unnecessary viral genome accessory genes, separating viral packaging genes into different plasmids to reduce replication competent viruses, and modifying viral envelopes for selective tropism.[33] Lentiviral safety has been further improved by the use of self-inactivating (SIN) lentiviral vectors and internal promoters for transgene expression.[33] Finally, extensive monitoring procedures have been implemented to evaluate patients who receive gene therapy treatments over time. Current lentiviral vectors display a more favorable integration pattern than γ-retroviral vectors used in the French clinical trials[30,33] with ~3-fold fewer "hot spots" for viral insertions, which are not enriched in loci

affecting proto-oncogenes and growth controlling genes unlike γ-retroviral vectors.[34] Clinical data of newer generations of LV vectors strongly suggests reduced risks of insertional mutagenesis because no vector-associated safety concerns have been observed in the thousands of patients treated with CAR T-cells,[30] and two CAR T-cell therapies engineered using lentiviruses are FDA approved. These advances highlight the improved safety and efficacy of lentiviral vectors, and underscore the potential use *in vivo*. LV-mediated gene delivery appears to be particularly suitable for treatment of chronic diseases, such as congenital genetic deficiencies, chronic acquired infections, and malignant diseases where sustained transgene expression is desired.[25]

5.5 Conclusions

A key challenge in gene therapy continues to be a potent yet highly selective gene vector system for select transduction of only targeted cells and tissues. By exploiting specificity and ease of bsAb production with a mutated Sindbis pseudotyped LV vector that abrogates its native tropism, we have developed a system that is both efficient and specific. We showed that coupling bsAb with reduction of native tropism synergistically enhanced the selectivity of our targeted system. Our findings support bsAb-mSindbis LV vectors as a promising platform to enhance gene delivery to target cells/tissues *in vivo.*

REFERENCES

1. Check, E. Gene therapy: A tragic setback. *Nature* **420,** 116–118 (2002).

2. Hacein-Bey-Abina, S. *et al.* LMO2-associated clonal T cell proliferation in two patients after gene therapy for SCID-X1. *Science (80-.).* **302,** 415–419 (2003).

3. Check, E. Regulators split on gene therapy as patient shows signs of cancer. *Nature* **419,** 545–546 (2002).

4. Hacein-Bey-Abina, S. *et al.* Insertional oncogenesis in 4 patients after retrovirus-mediated gene therapy of SCID-X1. *J. Clin. Invest.* **118,** 3132–3142 (2008).

5. McCormack, M. P. & Rabbitts, T. H. Activation of the T-Cell Oncogene LMO2 after Gene Therapy for X-Linked Severe Combined Immunodeficiency. *N. Engl. J. Med.* **350,** 913–922 (2004).

6. Waehler, R., Russell, S. J. & Curiel, D. T. Engineering targeted viral vectors for gene therapy. *Nat. Rev. Genet.* **8,** 573–587 (2007).

7. Cronin, J., Zhang, X.-Y. & Reiser, J. Altering the tropism of lentiviral vectors through pseudotyping. *Curr. Gene Ther.* **5,** 387–398 (2005).

8. Morizono, K. *et al.* Lentiviral vector retargeting to P-glycoprotein on metastatic melanoma through intravenous injection. *Nat. Med.* **11,** 346–352 (2005).

9. Jiang, A., Dornburg, R. & Dornburg, R. In vivo cell type-specific gene delivery with retroviral vectors that display single chain antibodies. *Gene Ther.* **6,** 1982–1987 (1999).

10. Han, X., Kasahara, N. & Kan, Y. W. Ligand-directed retroviral targeting of human breast cancer cells. *PNAS* **92,** 9747–9751 (1995).

11. Marin, M. *et al. Targeted Infection of Human Cells via Major Histocompatibility Complex Class I Molecules by Moloney Murine Leukemia Virus-Derived Viruses Displaying Single-Chain Antibody Fragment-Envelope Fusion Proteins*. *Journal of Virology* **70,** (1996).

12. Yang, L., Bailey, L., Baltimore, D. & Wang, P. Targeting lentiviral vectors to specific cell types in vivo. *PNAS* **103,** 11479–11484 (2006).

13. Morizono, K., Pariente, N., Xie, Y. & Chen, I. S. Y. Redirecting lentiviral vectors by insertion of integrin-tageting peptides into envelope proteins. *J Gene Med* **11,** 549–58 (2009).

14. Situ, K., Chua, B. A., Bae, S. Y., Meyer, A. S. & Morizono, K. Versatile targeting system for lentiviral vectors involving biotinylated targeting molecules. *Virology* **525,** 170–181 (2018).

15. Morizono, K., Bristol, G., Xie, Y. M., Kung, S. K. & Chen, I. S. Antibody-directed targeting of retroviral vectors via cell surface antigens. *J. Virol.* **75,** 8016–8020 (2001).

16. Dull, T. *et al.* A third-generation lentivirus vector with a conditional packaging system. *J. Virol.* **72,** 8463–8471 (1998).

17. Breece, T. N. *et al.* Protein Purification. *Pat. No. US 6,870,034 B2* (2005).

18. Lewis, S. M. *et al.* Generation of bispecific IgG antibodies by structure-based design of an orthogonal Fab interface. *Nat. Biotechnol.* (2014). doi:10.1038/nbt.2797

19. Wang, K. S., Kuhn, R. J., Strauss, E. G., Ou, S. & Strauss, J. H. High-affinity laminin receptor is a receptor for Sindbis virus in mammalian cells. *J. Virol.* **66,** 4992–5001 (1992).

20. Klimstra, W. B., Ryman, K. D. & Johnston, R. E. Adaptation of Sindbis virus to BHK cells selects for use of heparan sulfate as an attachment receptor. *J. Virol.* **72,** 7357–7366 (1998).

21. Slaga, D. *et al.* Avidity-based binding to HER2 results in selective killing of HER2-overexpressing cells by anti-HER2/CD3. *Sci. Transl. Med.* **10,** eaat5775 (2018).

22. Simnick, A. J., Valencia, A., Liu, R. & Chilkoti, A. Morphing low affinity ligands into high avidity nanoparticles by thermally triggered self-assembly of a genetically encoded polymer. *ACS Nano* **4,** 2217–2227 (2010).

23. Ohno, K., Sawai, K., Lijima, Y., Levin, B. & Meruelo, D. Cell-specific targeting of Sindbis virus vectors displaying IgG-binding domains of protein A. *Nat. Biotechnol.* **15,** 763–767 (1997).

24. Morizono, K., Bristol, G., Xie, Y. M., Kung, S. K. & Chen, I. S. Antibody-directed targeting of retroviral vectors via cell surface antigens. *J. Virol.* **75,** 8016–8020 (2001).

25. Morizono, K. *et al.* A versatile targeting system with lentiviral vectors bearing the biotin-adaptor peptide. *J Gene Med* **11,** 655–663 (2009).

26. Kasaraneni, N., Chamoun-Emanuelli, A. M., Wright, G. & Chen, Z. Retargeting lentiviruses via SpyCatcher-SpyTag chemistry for gene delivery into specific cell types. *MBio* **8,** e01860-17 (2017).

27. Kasaraneni, N., Chamoun-Emanuelli, A. M., Wright, G. A. & Chen, Z. A simple strategy for retargeting lentiviral vectors to desired cell types via a disulfide-bond-forming protein-peptide pair. *Sci. Rep.* **8,** 10990 (2018).

28. Gigout, L. *et al.* Altering AAV tropism with mosaic viral capsids. *Mol. Ther.* **11,** 856–865 (2005).

29. Bartlett, J. S., Kleinschmidt, J., Boucher, R. C. & Samulski, R. J. Targeted adeno-associated virus vector transduction of nonpermissive cells mediated by a bispecific F(ab'gamma)2 antibody. *Nat. Biotechnol.* **17,** 181–186 (1999).

30. Mátrai, J., Chuah, M. K. L. & VandenDriessche, T. Recent advances in lentiviral vector development and applications. *Mol. Ther.* **18,** 477–490 (2010).

31. Cavazzana-Calvo, M. *et al.* Gene therapy of human severe combined immunodeficiency (SCID)-X1 disease. *Science (80-.).* **288,** 669–672 (2000).

32. Hacein-Bey-Abina, S. *et al. Sustained correction of X-linked severe combined immunodeficiency by ex vivo gene therapy*. *N Engl J Med* **346,** (2002).

33. Milone, M. C. & O'Doherty, U. Clinical use of lentiviral vectors. *Leukemia* **32,** 1529–1541 (2018).

34. Oldham, R. A. A., Berinstein, E. M. & Medin, J. A. Lentiviral vectors in cancer immunotherapy. *Immunotherapy* **7,** 271–284 (2015).

CHAPTER 6: CONCLUSIONS & PERSPECTIVES

In this dissertation, I systemically investigated the use of bispecific antibodies (bsAb) and bispecific fusion proteins (BFP) to enhance cell-specific delivery of drug and gene carriers to tumor cells *in vitro* and *in vivo*. To overcome challenges associated with passive and active targeting, I explored a two-step targeting approach called pretargeting that relies on bsAb to home nanoparticles to tumor cells. By carefully tuning BFP dose at cell surface, I showed that pretargeting can facilitate intracellular delivery. I also increased cell-specific targeting of nanoparticles to tumors using multivalent, pretargeting bsAb without FcRn recycling. Finally, I showed efficient targeted gene delivery by coupling bsAb with engineered lentiviral vectors that exhibited minimal off-target binding.

Pretargeting is a well-established strategy for enhancing delivery of effector molecules to target cells yet remains underexplored for use in improving targeting of nanoparticles. The success of the pretargeting approach relies on BFP binding to target cell receptors and remaining on cell surface until nanoparticles can extravasate from the circulation and reach target cells. I found that multivalent interactions between streptavidin-based pretargeting BFP and biotin-functionalized polymeric nanoparticles hindered nanoparticle internalization, but carefully tuning interactions between BFP and nanoparticles on the cell surface can indeed facilitate intracellular delivery.

Despite the high affinity between streptavidin and biotin ($K_D \sim 10^{-15}$ M), this binding pair is not an ideal choice for *in vivo* or clinical use because streptavidin-based BFP are immunogenic.[1–3] High levels of endogenous biotin can bind to cell-bound or circulating BFP,

ultimately reducing the fraction of extravasated biotinylated nanoparticles at the target site. Moreover, biotin-functionalization of polymeric nanoparticles actually compromised its stealth properties, resulting in an exceedingly short half-life of 40 minutes.[4] These disadvantages as well as my thesis laboratory's interest in polymer- and virus-binding antibodies afforded me the opportunity to explore other binding pairs, including anti-PEG/PEG and anti-viral envelope/viral envelope glycoprotein.

I found that multivalency and elimination of FcRn recycling of bsAb-based pretargeting molecules are both critical in maximizing pretargeted efficiency. My bsAb-based pretargeting system increased tumor accumulation of PEGylated liposomal doxorubicin (PLD) 3-fold versus passively targeted PLD alone, and 5-fold compared to bsAb with FcRn recycling. However, I observed less total accumulation (<1% ID/g tumor) and a smaller improvement than previous studies comparing pretargeting and passive targeting.[5–9] I evaluated pretargeting in an orthotopic xenograft tumor model while nearly all prior studies utilized subcutaneous xenograft models. Compared to subcutaneous xenograft models, it is possible that the stromal microenvironment and tumor physiology of orthoptic breast tumor models likely limit EPR effects for reduced particle extravasation and retention.

Given the challenges associated with pretargeted delivery to orthotopic tumors, it is critically important to identify strategies that increase extravasation and retention of nanoparticles in tumors. External stimuli can be applied to alter tumor physiological condition for increased permeability of nanoparticles into tumors, leading to improved EPR effect.[10,11] Nagamitsu *et al* used angiotensin II to transiently induce systemic hypertension in patients with solid tumors, resulting in increased nanoparticle tumor accumulation and improved therapeutic response with reduced toxicity.[12] However, systemic hypertension can affect the entire body,

which is likely not feasible for the majority of patients who are currently taking antihypertensive medication. Coupling mild hyperthermia with nanoparticle delivery enhances nanoparticle extravasation by increasing tumor blood flow and tumor microvascular pore size.[13,14] Microbubbles are an alternative strategy that bypasses the EPR effect to effectively deliver drug to tumors. Huynh *et al* applied ultrasound to convert porphyrin microbubbles into porphyrin nanoparticles that effectively accumulated in the tumor for multimodality imaging.[15,16] For any combination approach, it is imperative to evaluate the pharmacokinetics and pharmacodynamics of each therapeutic component for optimal drug delivery to target site and minimal adverse effects.

A major goal of therapeutic gene delivery is efficient and selective gene transfer in target cells/tissues. To reduce off-target binding, I introduced known mutations into the Sindbis viral envelope receptor binding (E2) domain to produce a mutated Sindbis (mSindbis) pseudotyped LV vector.[17] By coupling mSindbis LV with bsAb that binds both LV and cell-specific receptors, I found that bsAb and reduction of native tropism synergistically enhanced the selectivity of the targeting system. This viral targeting platform is applicable for gene therapy of malignant diseases and hereditary and chronic disorders, including lysosomal storage disorders. The platform may also be applicable for adoptive T-cell therapies where targeted LV specifically deliver tumor-specific T cell receptor (TCR) or chimeric antigen receptor (CAR) to T cells via a single intravenous injection of pre-mixed bsAb and mSindbis LV. *In vivo* delivery of CARs and TCRs is an alternative to *ex vivo* CAR T cell engineering, *ex vivo* tumor-specific TCR T cell engineering, and *in situ* secretion of T cell-redirecting bsAbs (STAb) from genetically modified immune cells.[18–20]

Despite its potency, off-target gene transfer was not completely abrogated because

bsIgG$_1^{E2xHER2}$-mSindbis LV infected ~0.6% of HER2$^-$ cells. Multiple strategies are available to further improve upon the bsAb-mSindbis LV targeting system, including transcriptional targeting, bsAb engineering, and inclusion of additional safety elements. To reduce off-target binding and enhance the specificity of the viral targeting system, the constitutive promoter used here to drive GFP gene expression could be replaced with a tissue-specific promoter that is only active in target mammary cells. A better understanding of the functions of the amino acids present in Sindbis Env E2 domain may identify more potent amino acid mutations that would effectively ablate native receptor binding. Also, phage display technologies can be used to engineer anti-Sindbis E2 Fab with higher affinity for Sindbis E2 domain, potentially making the binding pair less sensitive to serum. Although bsIgG$_1^{E2xHER2}$ and tandem Fab^{E2xHER2} exhibit monovalent binding for HER2 and E2, mixing the bsAb with mSindbis LV actually yields multivalent binding to HER2 receptors on cell surface. Previous work has shown that multivalent bsAb engineered with low affinity towards HER2 dramatically enhanced selectivity towards HER2-overexpressing cells and not to cells with low HER2 expression *in vitro* and *in vivo* for greater therapeutic benefit and reduced off-target effects.[21] Additional studies can compare the transduction efficiency of mSindbis LV pre-mixed with current bsAb with high-affinity for HER2 versus bsAb with low-affinity towards HER2. Finally, to effectively minimize off-target binding, an alternative viral envelope with no human tropism may be utilized for *in vivo* gene delivery. The Eilat virus, an alphavirus like Sindbis virus, cannot infect mammalian or avian cells.[22] Similar to Sindbis Env, optimization will be needed to produce stable, functional, high titer Eilat pseudotyped LV, and to identify antibodies against Eilat Env glycoproteins for bsAb development.

In general, LV-based gene delivery has suffered from the risk of insertional mutagenesis

despite no current reports of vector-associated safety concerns in recent clinical data. LV vectors can be further engineered to selectively eradicate transduced tumor cells causing adverse side effects and to lower risk of insertional mutagenesis. Suicide gene safety elements can be included in transgene cassette to mitigate potential adverse effects.[23] Upon administering prodrug, transduced cells will be selectively killed, thereby haltering undesired side effects of gene therapy. Additionally, non-integrating LV vectors (NILV) are integrase-deficient and the transgene plasmid remains in nucleus episomally like AAV. Yet, NILV have a much larger transgene capacity than AAV, enabling the inclusion of genetic machinery such as zinc finger nucleases and CRISPR/Cas system.[23] NILV with genetic machinery enable targeted gene correction with no risk of insertional mutagenesis and reduced off-target gene editing because the editing machinery is only temporarily expressed.

Tumors are frequently characterized by genetically and phenotypically distinct cell populations within the same tumor lesions, a phenomenon termed *tumor heterogeneity*. [24,25] Tumor heterogeneity can result in variable EPR effects within different regions of the same tumor.[11] More importantly, variable target receptor expression in heterogeneous tumors presents a critical challenge in the efficacy of targeted delivery of anti-cancer agents. The modular nature of our bsAb-based pretargeting enables facile targeting of the same nanoparticle to diverse cell/tissues simply by changing the cell-binding Fab. Combining multiple pretargeting bsAb as a cocktail may enhance nanoparticle delivery to multiple tumor subpopulations for greater drug exposure and better distribution throughout the tumor. We have focused on understanding the fundamentals of pretargeting and have not explored pretargeting to heterogeneous tumors in detail yet. However, we have shown in a dual-tumor mouse model that a cocktail of pretargeting bsAb against two distinct surface antigens, CD20 and TAG-72, markedly increased nanoparticle

accumulation to both tumor types compared to animals dosed with nanoparticles alone.[4] An obvious next step is to validate the pretargeting efficiency of bsAb cocktail in a heterogenous tumor model.

Overall, the specificity and modular nature of bsAb enables facile targeting of nanoparticles and gene carriers to diverse cell types within the target site (ie. tumor). Careful consideration must be given to the choice of target receptors, affinity, avidity, format, and inclusion or exclusion of Fc domain on bsAb for effective nanoparticle and viral targeting strategies.

REFERENCES

1. Forero, A. *et al.* Phase 1 trial of a novel anti-CD20 fusion protein in pretargeted radioimmunotherapy for B-cell non-Hodgkin lymphoma. *Blood* **104,** 227–236 (2004).

2. Weiden, P. L. *et al.* Pretargeted Radioimmunotherapy (PRIT^{TM}) for Treatment of Non-Hodgkin's Lymphoma (NHL): Initial Phase I/II Study Results. *Cancer Biother. Radiopharm.* **15,** 15–29 (2000).

3. Weiden, P. L. & Breitz, H. B. Pretargeted radioimmunotherapy (PRIT^{TM}) for treatment of non-Hodgkin's lymphoma (NHL). *Crit. Rev. Oncol. Hematol.* **40,** 37–51 (2001).

4. Yang, Q. *et al.* Pretargeting with bispecific fusion proteins facilitates delivery of nanoparticles to tumor cells with distinct surface antigens. *J. Control. Release* **255,** 73–80 (2017).

5. Su, Y.-C. *et al.* Conditional internalization of PEGylated nanomedicines by PEG engagers for triple negative breast cancer therapy. *Nat. Commun.* **8,** 15507 (2017).

6. Cheal, S. M. *et al.* Theranostic pretargeted radioimmunotherapy of internalizing solid tumor antigens in human tumor xenografts in mice: Curative treatment of HER2-positive breast carcinoma. *Theranostics* **8,** 5106–5125 (2018).

7. Rauscher, A. *et al.* Influence of pegylation and hapten location at the surface of radiolabelled liposomes on tumour immunotargeting using bispecific antibody. *Nucl. Med. Biol.* **41,** e66–e74 (2014).

8. Rauscher, A. *et al.* Improvement of the Targeting of Radiolabeled and Functionalized Liposomes with a Two-Step System Using a Bispecific Monoclonal Antibody (Anti-CEA × Anti-DTPA–In). *Front. Med.* **2,** (2015).

9. Westerlund, K. *et al.* Site-specific conjugation of recognition tags to trastuzumab for peptide nucleic acid-mediated radionuclide HER2 pretargeting. *Biomaterials* **203,** 73–85 (2019).

10. Nehoff, H., Parayath, N., Domanovitch, L., Taurin, S. & Greish, K. Nanomedicine for drug targeting: strategies beyond the enhanced permeability and retention effect. *Int. J. Nanomedicine* **9,** 2539–2555 (2014).

11. Huynh, E. & Zheng, G. Cancer nanomedicine: addressing the dark side of the enhanced permeability and retention effect. *Nanomedicine* **10,** 1993–1995 (2015).

12. Nagamitsu, A., Greish, K. & Maeda, H. Elevating blood pressure as a strategy to increase tumor-targeted delivery of macromolecular drug SMANCS: Cases of advanced solid tumors. *Jpn. J. Clin. Oncol.* **39,** 756–766 (2009).

13. Kong, G., Braun, R. D. & Dewhirst, M. W. Hyperthermia enables tumor-specific nanoparticle delivery: Effect of particle size. *Cancer Res.* **60,** 4440–4445 (2000).

14. Kong, G., Braun, R. D. & Dewhirst, M. W. Characterization of the Effect of Hyperthermia on Nanoparticle Extravasation from. *Cancer Res.* **61,** 3027–3032 (2001).

15. Huynh, E. *et al.* In situ conversion of porphyrin microbubbles to nanoparticles for multimodality imaging. *Nat. Nanotechnol.* **10,** 325–332 (2015).

16. Lanza, G. M. Theranostic agents: From micro to nano in seconds. *Nat. Nanotechnol.* **10,** 301–302 (2015).

17. Morizono, K. *et al.* Lentiviral vector retargeting to P-glycoprotein on metastatic melanoma through intravenous injection. *Nat. Med.* **11,** 346–352 (2005).

18. Blanco, B., Compte, M., Lykkemark, S., Sanz, L. & Alvarez-Vallina, L. T Cell-Redirecting Strategies to 'sTAb' Tumors: Beyond CARs and Bispecific Antibodies. *Trends Immunol.* **40,** 243–257 (2019).

19. Milone, M. C. & O'Doherty, U. Clinical use of lentiviral vectors. *Leukemia* **32,** 1529–1541 (2018).

20. Thakur, A. & Lum, L. G. "NextGen" Biologics: Bispecific Antibodies and Emerging Clinical Results. *Expert Opin. Biol. Ther.* **16,** 675–688 (2016).

21. Slaga, D. *et al.* Avidity-based binding to HER2 results in selective killing of HER2-overexpressing cells by anti-HER2/CD3. *Sci. Transl. Med.* **10,** eaat5775 (2018).

22. Nasar, F. *et al.* Eilat virus, a unique alphavirus with host range restricted to insects by RNA replication. *Proc. Natl. Acad. Sci.* **109,** 14622–14627 (2012).

23. Oldham, R. A. A., Berinstein, E. M. & Medin, J. A. Lentiviral vectors in cancer immunotherapy. *Immunotherapy* **7,** 271–284 (2015).

24. Bedard, P. L., Hansen, A. R., Ratain, M. J. & Siu, L. L. Tumour heterogeneity in the clinic. *Nature* **501,** 355–364 (2013).

25. Jamal-Hanjani, M., Quezada, S. A., Larkin, J. & Swanton, C. Translational implications of tumor heterogeneity. *Clin. Cancer Res.* **21,** 1258–1266 (2015).